Facile synthesis of ternary quantum dot bio-conjugates for the sensing of vascular endothelial growth factor

By

Nozikumbuzo Anati Vitshima

(212158295)

NDANCH, BTech (Cape Peninsula University of Technology)

Thesis submitted in fulfilment of the requirements for the degree

Master of Applied Sciences: Chemistry

Department of Chemistry

Faculty of Applied Sciences

Cape Peninsula University of Technology

Bellville, Cape Town

Supervisor: Dr Ncediwe Ndube – Tsolekile

Co-Supervisor: Prof. M. C. Matoetoe

December 2022

CPUT copyright information

The dissertation/thesis may not be published either in part (in scholarly, scientific, or technical journals), or (as a monograph), unless permission has been obtained from the University.

Declaration

I, Nozikumbuzo Anati Vitshima, declare that the contents of this project report represent my own unaided work, and that the thesis has not previously been submitted for academic examination towards any qualification. Furthermore, it represents my own opinions and not necessarily those of the Cape Peninsula University of Technology.

15 December 2022

Signed **Date**

Abstract

In nanotechnology, the synthesis of semiconductor nanoparticles known as quantum dots (QDs) has gained much interest due to their excellent optical and electronic properties compared to traditionally used organic dyes. In practice, quantum dots are usually prepared from toxic elements of group II-VI and group II-VI on the periodic table, including compounds such as PbTe, PbS, CdSe and CdTe. Their inherent toxicity and reported leakage of Cd^{2+} / Pb^{2+} ions from the core of QDs into their surrounding environment have limited the biological applications of these QDs. Modern research has therefore focused on developing less toxic QDs such as CuInS and AgInS/ZnS QDs. However, challenges with these QDs are their synthetic methods which have been mainly reported to be time-consuming, costly and, use harsh conditions such as high temperature and organic solvents, thus limiting their biological applications. Bio-conjugation, the chemical modification of biomolecules, has been reported to improve quantum dots' biocompatibility and biological targeting. Although bio-conjugation of Cd-free QDs has been reported, only some researchers have focused on their electrochemical characterization of ternary QDs. Electrochemical techniques play an essential role in studying electrons that may undergo quantum confinement effects, which are reflected in their electrochemical behaviour. This study synthesized water-soluble glutathione-capped AgInS core QDs and AgInS/ZnS core/shell QDs via the reflux, heat-up and mono-wave 50 synthesis methods. Various synthetic conditions such as reaction time, pH, Ag: In ratios, ZnS shell layers, capping agent, GSH concentration and stabilizing agent on the fluorescence properties of the ternary AgInS/ZnS based QDs were examined. Optimal conditions were obtained using the reflux method for AgInS core QDs synthesis at pH 7.58, Ag: In molar ratio of 1:4, and glutathione (GSH) concentration of 0.145 mmol after 45 min. FTIR analysis confirmed the formation of GSH capping on the QDs the via S-

metal bond. The successful passivation of AgInS core by ZnS shell resulted in a PLQY increase from 31.6 to 35.4% for AgInS core and AgInS/ZnS core/shell QDs, respectively. The as-synthesized QDs were conjugated to Bovine serum albumin (BSA) to form AgInS/ZnS-BSA bioconjugate. The fluorescence intensity was enhanced after the conjugation of QDs to BSA, indicating improved quality of the QDs. Electrochemical properties of AgInS core, AgInS/ZnS core/shell, QDs and AgInS/ZnS-BSA bioconjugate were evaluated using cyclic voltammetry (CV), differential pulse voltammetry (DPV), square wave voltammetry (SWV) and electrochemical impedance spectroscopy (EIS).

A comparative study of the electrochemical properties of AgInS QDs and AgInS/ZnS QDs showed that AgInS core QDs and AgInS/ZnS core/shell QDs exhibited chemical and electrochemical composition-dependent properties enabling the use of the materials in both electronics and bio-applications. Studies of the electrochemical properties of AgInS-BSA and AgInS/ZnS-BSA bioconjugates showed enhanced peak currents suggesting higher conductivity and electrical properties. EIS confirmed improved charge transfer resistance for AgInS/ZnS-BSA core/shell bioconjugate. Developing an immunosensor using AgInS/ZnS-BSA bioconjugate for electrochemical sensing of vascular endothelial growth factor (VEGF) was done using DPV. The immunosensor was tested against VEGF at different concentrations and had a satisfactory response. The method's linear range was from 0.003 to 0.017 μg/ml. The LOD and LOQ were determined to be 1.5×10^{-3} μg/ml and 5×10^{-3} μg/ml, respectively. The immunosensor showed improvement in stability over a period of five weeks.

Acknowledgements

I wish to thank: God, for his love, grace, and mercy.

I want to express my gratitude to my supervisor Dr Ncediwe Ndube -Tsolekile for being such a wonderful person to work with, for her guidance, availability, for her patience, help and support. Special thanks to my co-supervisor Prof. M. C. Matoetoe for her support and guidance. Also special thanks to Dr Bongiwe Silwana for her guidance and assistance. To the nanotechnology and electrochemistry lab team your support and motivation are highly appreciated. The staff of the Department of Chemistry, Cape Peninsula University of Technology and finally my family and friends for their support and encouragement. The financial assistance of the National Research Foundation towards this research is acknowledged.

Dedication

I dedicate this report to me and my family.

PREFACE

Objective and Overview of Thesis.

This thesis focuses on synthesizing and optimization of AgInS-based QDs and their bioconjugates. The study of the AgInS and AgInS/ZnS QDs focusing on their optical properties, electrochemical properties, and application in sensing vascular endothelial growth factor using electrochemistry. This study's primary objective was developing synthetic methods for ternary AgInS QDs and their bioconjugates for electrochemical applications.

RESEARCH OUTPUTS

1. Publications

i. **Vitshima, N.A.**, Silwana, B., Tsolekile, N. and Matoetoe, M.C., 2022. Effect of ZnS coating on the optoelectronic properties of aqueous glutathione capped AgInS quantum dots. Journal of Alloys and Compounds, 900, p.163386.

ii. Tsolekile, N., Mngcutsha, N. and **Vitshima, N**., 2022. Application of Quantum Dots in Lateral Flow Immunoassays: Non-Communicable and Communicable Diseases

2. Conference presentation

i. Anati Vitshima, Ncediwe Tsolekile, Mangaka Matoetoe. Synthesis of Fluorescent AgInS quantum dots using *Helichrysum Petiolare* for Amino Acid Detection. 10th Annual Nanosciences Young Researcher's Symposium (NYRS-2020/21), South Africa. 7-8 October 2021 (Oral presentation).

ii. Anati Vitshima, Ncediwe Tsolekile, Mangaka Matoetoe. Photocatalytic degradation of R6G dye in grey water using Cu-doped AgInS/ZnS QDs. National Young Chemists' Symposium 2022, South Africa. 3-4 October 2022 (Poster presentation).

iii. RSC/SACI western cape Young Chemists' Symposium 2022. South Africa. 9 September 2022 (Chair/organizing committee).

3. Awards & honours

i. Third prize award at 10th Annual Nanosciences Young Researcher's Symposium (NYRS-2020/21), South Africa. 7-8 October 2021 (Oral presentation).

Table of Contents

List of figures

List of tables

List of diagrams

Glossary

Terms/Abbreviations	Definition/Explanation
AIS	: AgInS
AIS/ZnS	: AgInS/ZnS
CDI	: Carbonylimidazole
EDC	:1-ethyl-3-(3-dimethylaminopropyl)-carbodiimide
EDS	: Energy dispersive x-ray
DDT	: Dodecanethiol
DNA	: Deoxyribonucleic acid
DPV	: Differential Pulse Voltammetry
DTG	: Dithioglycerol
ELISA	: Enzyme-Linked Immunosorbent Assay
FRET	: Fluorescence resonance energy transfer
FTIR	: Infrared spectroscopy
GCE	: Glassy carbon electrode
GSH	: Glutathione
IBP	: Ibuprofen
LOD	: Limit of Detection
LOQ	: Limit of Quantitation
MPA	: Mercapto-propanoic acid
NMs	: Nanomaterials

NPs	: Nanoparticles
ODE	: Octadecene
OLA	: Oleylamine
PL	: photoluminescence spectroscopy
QD’s	: Quantum dots
SPCE	: Screen-printed carbon electrode
SWV	: Square wave voltammetry
TBP	: 2,4,6-Tri-tert-butylphenol
TCE	: Tetrachloroethylene
TEM	: Transmission electron microscope
TGA	: Thioglycolic acid
TGL	: Thioglycerol
TOP	: Trioctylphosphine
UV-vis spectroscopy	: UV–Visible spectroscopy
VEGF	: Vascular endothelial growth factor
XRD	: X-ray diffraction

Chapter 1

Introduction

1.1. Background

1.1.1. Vascular endothelial growth factor

Vascular endothelial growth factor (VEGF) is a mammalian antibody that has four different isomers, one of which, $VEGF_{165}$, is associated with the growth and metastasis of several malignancies. VEGF overexpression is usually considered to be a sign of cancer (Şahin *et al.,* 2020). Therefore, identifying and detecting cancer-specific biomarkers is crucial for improving cancer patient survival rates and early cancer diagnosis (Xu *et al.,* 2017). Currently, VEGF and other biomarkers are analysed using various techniques including radioimmunoassay, Enzyme-Linked Immunosorbent Assay (ELISA) and immunohistochemistry. The drawbacks of these techniques, even though they provide adequate analytical performance, include the need for advanced instruments, complex protocols, labour-intensive, and complexity, cost, and time-consuming (Şahin *et al.,* 2020). Therefore, there is a need for the development of alternative methods for detection of VEGF for early diagnosis and evaluation recovery of patients (Xu *et al.,* 2017). Biosensors are possible methods that can overcome limitation of the current detection methods due to attributes such as excellent analytical specificity, efficiency, and sensitivity (Şahin *et al.,* 2020).

1.1.2. Biosensors

Biosensors refers to self-contained devices that can convert detected biological processes into measured signals using a transducer and a bio-receptor that are physically connected. Depending on the transducer system used, some common biosensors are electrochemical, optical, piezoelectric, and calorimetric (Nagraik *et al.,* 2021). Electrochemical biosensors make use of a three-electrode system such as the reference electrode, working electrode and counter electrode. These biosensors offer significant advantages compared to other analytical techniques due to their conversion of biological processes directly into a stable

electrical signal (Napi *et al.,* 2019). As such, electrochemical-based biosensors have been of great success, offering quicker, user-friendly, affordable instrumentation, precise, portable, and flexible for multiplexing and label-free sensing of various biomolecules, including proteins, enzymes, and nucleic acids (Dhara and Mahapatra, 2020). Recently nanomaterials have been of great interest for developing biosensors with different sizes, surface areas and electrolytic properties (Goud *et al.,* 2018). Some of the commonly used nanomaterials in biosensors include metallic sheets, graphene dots, carbon nanotubes, nanoparticles, and quantum dots (QDs) (Nagraik *et al.,* 2021).

1.1.3. Quantum dots

QDs are fluorescent semiconductors with three-dimensional motion controlled by their charge carriers (Tsolekile *et al.,* 2017). They are often synthesized using the groups II-VI and IV-VI elements of the periodic table and include compounds such as CdSe, ZnS, PbTe and PbS. However, because heavy metals like Cd and Pb are toxic in nature, recent research has focused on ternary QDs from the group I-III-VI. AgInSe, $CuInS_2$, and $AgInS_2$, are the ternary QDs that have been studied (Tsolekile *et al.*, 2017). The synthesis of ternary QDs can be a great challenge due to the properties of precursors such as Ag^+ and Cu^+, which are soft acids and In^{3+} a hard acid toward sulphur ions. They form binary products such as copper or indium sulphides (Aladesuyi and Oluwafemi 2020; Girma *et al.,* 2017). Another challenge is the formation of multiple peaks on PL spectra (May *et al*., 2022). However, this can be overcomed by using capping agents, stabilizing agents, and single precursors with dual properties (Aladesuyi and Oluwafemi 2020). Additionally, varying the synthetic conditions including cation and anion mole ratios, ligands, pH, temperature and reaction time during the synthetic process can produce the desired material. The application determines the synthetic method to be used for preparation of

QDs. Bio-conjugated QDs are effective for use in cancer diagnostics due to their steady emission and high fluorescence sensitivity (Nagraik *et al.,* 2021).

1.2.Problem statement

Since VEGF is an essential regulator of cancer angiogenesis, developing a technology intended for its sensitive detection is crucial. To date, numerous established detection and quantification techniques exist for the analysis of VEGF. However, these techniques are complicated, costly, time-consuming, and instrument-intensive to perform diagnostic tests. Therefore, there is a great need to establish detection approaches that are affordable, extremely sensitive, and highly specific for the detection of this biomarker (Şahin *et al.,* 2020). Recently, biomarkers have gained great attention in medicine and nanotechnology (Hasan *et al.,* 2014). Unlike traditional methods, biosensors are compact, portable, selective, sensitive, and require minimal sample pre-treatment (Sadighbayan *et al.,* 2019). To improve properties of biosensors and increase its electronic properties, metallic nanostructures such as carbon nanotubes, nanoparticles and quantum dots are used to modify the electrode. QDs have been used as an alternative to fluorophores, for the fabrication of optical biosensors to detect organic substances, pharmaceutical analytes, biomolecules, etc. Additionally, they have been utilized to identify cancer target sites in *vivo*. (Pandit *et al.,* 2016). However, compared to optical biosensors, QD-based photoelectrochemical biosensors are more simple and portable and can be measured using electronic output rather than expensive optical equipment (Ma and Zhang 2018). Photoelectrochemical biosensor are commonly modified using CdS and PbS QDs (Wang *et al.,* 2019; Ma *et al.,* 2015). However, the reported leakage of the heavy metals such as Cd^{2+} from the core of the QDs into its surroundings limits their biological application (Reshma and Mohanan, 2019). Moreover, in *vivo* and in *vitro* analyses have demonstrated Cd ion toxicity. Modern research has focused on synthesising QDs using less toxic

elements such as carbon, graphene, $AgInS_2/ZnS$, $CuInS_2$, and ZnO QDs (Ranibar-Navazi *et al.,* 2019). However, challenges with these QDs are that their current synthesis methods are time-consuming, using extreme conditions such as high temperatures and organic solvents, which limit their biological application (Mal *et al.,* 2016). Bio-conjugation refers to the chemical modification of biomolecules (Ducharme and Auclair, 2018) and has been reported to improve on the biocompatibility and biological targeting of QDs (Rosenthal *et al.,* 2011). Although bio-conjugation of Cd-free QDs have been reported, limited research has focused on their electrochemical characterization, which may assist in further understanding the material and their electrochemical applications as biosensors.

1.3.Aims and Objectives

The study aims to develop a method for synthesis of ternary quantum dots and their bio-conjugation for electrochemical sensing applications.

The specific objectives of the study include:

1.3.1. To synthesize core AgInS QDs and core/shell AgInS/ZnS QDs.

1.3.2. To optimize the synthetic methods used to synthesize the QDs.

1.3.3. The bio-conjugation of QDs to antibodies.

1.3.4. Characterization of the as-synthesized QDs

1.3.5. Electrochemical sensing of vascular endothelial growth factor using the as-synthesized QDs.

1.4.Research methodology

The synthesis AgInS/ZnS core/shell QDs capped with glutathione (GSH) using reflux approach along with the investigation of the effect of synthetic conditions including reaction time, pH, synthetic method, Ag: In precursor ratio, Zn/S shell layers, capping agent, GSH concentration and the stabilizing agent is explored. The AgInS/ZnS QDs is conjugated to Bovine serum albumin (BSA). The as-synthesised material is further used to develop a biosensor using BSA-AgInS/ZnS conjugate for detection of VEGF antibody.

1.5.Delimitations and ethics

The study focus is on synthesizing AgInS QDs and AgInS/ZnS QDs. While the Vascular endothelial growth factor antibodies will only be sensed using electroanalytical techniques.

1.6. Research structure

The problem statement aims and objectives, research methodology, and study structure are all included in the current chapter's introductory review of the research theme. The succeeding chapters will be as follows:

Chapter 2: Literature Review

This chapter provides the literature review, introducing vascular endothelial growth factor and the various detection methods. A detailed description of AgInS/ZnS QDs and their bioconjugates is outlined. Applications of quantum dots in biosensing as well as their electrochemical studies are included.

Chapter 3: *Synthesis, optimization, and characterization of AgInS QDs, AgInS/ZnS QDs and AgInS/ZnS bio-conjugates.*

This chapter covers the synthesis, optimization, and characterization of AgInS/ZnS core/shell QDs and their bioconjugates. It focuses on the general experimental procedure for synthesizing AgInS/ZnS core/shell QDs, AgInS/ZnS-bioconjugates and characterization using various techniques. Furthermore, it covers the results and discussion of the as-synthesized material.

Chapter 4: *Sensing of Vascular endothelial growth factor using AIS/ZnS QDs*

This chapter focuses on the optical, morphological, and electrochemical properties of the synthesized AgInS/ZnS QDs and their bioconjugates. Furthermore, it examines the application of AgInS/ZnS QDs bioconjugates for sensing vascular endothelial growth factors using electrochemistry.

Chapter 5: *Conclusion and recommendations*

The conclusions and recommendations from this study are outlined in this chapter.

1.7. References

Aladesuyi, O.A. and Oluwafemi, O.S., 2020. Synthesis strategies and application of ternary quantum dots—in cancer therapy. Nano-Structures & Nano-Objects, 24, p.100568.

Dhara, K. and Mahapatra, D.R., 2020. Review on electrochemical sensing strategies for C-reactive protein and cardiac troponin I detection. Microchemical Journal, 156, p.104857.

Ducharme, J. and Auclair, K., 2018. Use of bioconjugation with cytochrome P450 enzymes. Biochimica et Biophysica Acta (BBA)-Proteins and Proteomics, 1866(1), pp.32-51.

Girma, W.M., Fahmi, M.Z., Permadi, A., Abate, M.A. and Chang, J.Y., 2017. Synthetic strategies and biomedical applications of I–III–VI ternary quantum dots. Journal of Materials Chemistry B, 5(31), pp.6193-6216.

Goud, K.Y., Kailasa, S.K., Kumar, V., Tsang, Y.F., Gobi, K.V. and Kim, K.H., 2018. Progress on nanostructured electrochemical sensors and their recognition elements for detection of mycotoxins: A review. Biosensors and Bioelectronics, 121, pp.205-222.

Hasan, A., Nurunnabi, M., Morshed, M., Paul, A., Polini, A., Kuila, T., Al Hariri, M., Lee, Y.K. and Jaffa, A.A., 2014. Recent advances in application of biosensors in tissue engineering. BioMed research international, 2014.

Ma, Z.Y., Ruan, Y.F., Zhang, N., Zhao, W.W., Xu, J.J. and Chen, H.Y., 2015. A new visible-light-driven photoelectrochemical biosensor for probing DNA–protein interactions. Chemical Communications, 51(39), pp.8381-8384.

Ma, F., Li, C.C. and Zhang, C.Y., 2018. Development of quantum dot-based biosensors: principles and applications. Journal of Materials Chemistry B, 6(39), pp.6173-6190.

May, B.M., Bambo, M.F., Hosseini, S.S., Sidwaba, U., Nxumalo, E.N. and Mishra, A.K., 2022. A review on I–III–VI ternary quantum dots for fluorescence detection of heavy metals ions in water: optical properties, synthesis and application. RSC advances, 12(18), pp.11216-11232.

Nagraik, R., Sharma, A., Kumar, D., Mukherjee, S., Sen, F. and Kumar, A.P., 2021. Amalgamation of biosensors and nanotechnology in disease diagnosis: mini-review. Sensors International, 2, p.100089.

Napi, MLM, Sultan, S.M., Ismail, R., How, KW and Ahmad, M.K., 2019. Electrochemical-based biosensors on different zinc oxide nanostructures: A review. Materials, 12(18), p.2985.

Pandit, S., Dasgupta, D., Dewan, N. and Prince, A., 2016. Nanotechnology based biosensors and its application. The Pharma Innovation, 5(6, Part A), p.18.

Reshma, V.G. and Mohanan, P.V., 2019. Quantum dots: Applications and safety consequences. Journal of Luminescence, 205, pp.287-298.

Rosenthal, S.J., Chang, J.C., Kovtun, O., McBride, J.R. and Tomlinson, I.D., 2011. Biocompatible quantum dots for biological applications. Chemistry & biology, 18(1), pp.10-24.

Sadighbayan, D., Sadighbayan, K., Tohid-Kia, M.R., Khosroushahi, A.Y. and Hasanzadeh, M., 2019. Development of electrochemical biosensors for tumor marker determination towards cancer diagnosis: Recent progress. TrAC Trends in Analytical Chemistry, 118, pp.73-88.

Şahin, S., Caglayan, M.O. and Üstündağ, Z., 2020. Recent advances in aptamer-based sensors for breast cancer diagnosis: special cases for nanomaterial-based VEGF, HER2, and MUC1 aptasensors. Microchimica Acta, 187(10), pp.1-27.

Tsolekile, N., Parani, S., Matoetoe, M.C., Songca, S.P. and Oluwafemi, O.S., 2017. Evolution of ternary I–III–VI QDs: synthesis, characterization and application. Nanostructures & Nano-Objects, 12, pp.46-56.

Wang, S.E., Huang, Y., Hu, K., Tian, J. and Zhao, S., 2014. A highly sensitive and selective aptasensor based on fluorescence polarization for the rapid determination of oncoprotein vascular endothelial growth factor (VEGF). Analytical Methods, 6(1), pp.62-66.

Wang, P., Cao, L., Chen, Y., Wu, Y. and Di, J., 2019. Photoelectrochemical biosensor based on Co3O4 nanoenzyme coupled with PbS quantum dots for hydrogen peroxide detection. ACS Applied Nano Materials, 2(4), pp.2204-2211.

Xu, H., Kou, F., Ye, H., Wang, Z., Huang, S., Liu, X., Zhu, X., Lin, Z. and Chen, G., 2017. Highly sensitive antibody-aptamer sensor for vascular endothelial growth factor based on hybridization chain reaction and pH meter/indicator. Talanta, 175, pp.177-182.

Chapter 2

Literature review

2.1. Introduction

This chapter covers a detailed background on nanomaterials with a specific focus on quantum dots (QDs). This is followed by a description of ternary QDs, different methods used to synthesize QDs and their bio-conjugates. Also, a detailed description on AgInS/ZnS core/shell QDs and the effects of experimental parameters (i.e., reaction time, pH of the reaction solution, the concentration of precursors, molar ratios, reaction time and capping agents) will be covered. Furthermore, detailed literature on vascular endothelial growth factor (VEGF) and its detection methods will be covered. Then a brief description of electrochemistry and various electrochemical studies will be covered. Lastly, QDs and their bioconjugates and characterization techniques will be discussed.

2.2. Nanomaterials

Nanomaterials are materials with less than 100 nm size at least in one dimension (Kolahalam *et al.,* 2019). They have excellent high-contrast signal-generating devices, however, most molecular imaging, diagnostic, or sensing applications may require conjugation with functional molecules (Kairdolf *et al.,* 2017). Integrating nanomaterials with sensing devices as active elements in nanotechnology has advanced stable sensing probes, improved detection signals in small sample quantities, and systems for multiplex detection (Yüce and Kurt 2017). Based on chemical composition, nanomaterials are divided into three categories: organic polymeric nanomaterials, carbon allotrope-based and inorganic nanomaterials made of metallic or non-metallic components like gold nanoparticles, silver nanoparticles, SiO_2, and QDs (Pirzada and Altintas 2019).

2.3. Quantum dots (QDs)

Quantum dots (QDs) are semiconductor nanoparticles with size-dependent optical and electronic properties (Girma *et al.,* 2017). The structure of QDs is composed of a semiconductor core and a core/shell as shown in diagram 1. The core of QDs is the most reactive yet unstable layer, and carries the optical properties of the QDs. In the fabrication and design of QDs, the core is essential. (Vitshima *et al.,* 2022). The shell (e.g., ZnSe, ZnS, etc.) improves the quantum quality and yield while protecting the core from oxidation. QDs have better photo-physical properties than traditionally used organic fluorescent dyes and proteins. The inherent properties of QDs (i.e., significant stocks shift (≤100 nm), broad excitation spectra, narrow and sharp emission spectra with an approximately gaussian shape) offer great possibilities for multiplexed analysis and multicolor imaging (Bilan *et al.,* 2015). According to Ranibar-Navazi *et al.,* 2019, in biological applications, the most fundamental parameter is the cytotoxicity and biocompatibility of any nanocarrier thus, there is an urgent need for producing relatively harmless QDs. In practice, group II-VI elements like CdSe, CdTe, and CdS and group IV-VI elements like PbTe, PbS in the periodic table are typically used to prepare QDs (Tsolekile *et al.,* 2017). The use of group IV-VI and II-VI QDs possess limitations because of the presence of carcinogenic heavy metals such as Cd and Pb, which are harmful to the biological and environmental systems. QDs of group II-VI elements have been used in bio-imaging and therapeutics due to their excellent optical properties (Ranibar-Navazi *et al.,* 2019). The reported leakage of heavy metals such as Cd^{2+} from the core of the QDs into their surroundings limits their biological application (Reshma and Mohanan, 2019). Moreover, it has been demonstrated in-*vitro* and in *vivo* that Cd ions are carcinogenic. Due to toxic heavy metals such as Cd and Pb, recent researchers have drawn interest in ternary QDs (Tsolekile *et al.,* 2017).

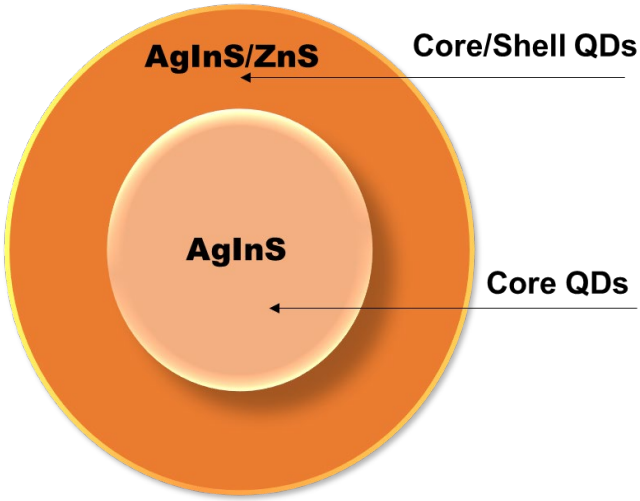

Figure 2.1. Schematic diagram of quantum dots

2.4. Ternary Quantum dots

Ternary QDs from group I–III–VI (I = Cu, Ag; III = In, Sn, Ga, Al and VI = S, Se, Te) contain less harmful elements and are free of Cd and Hg, therefore, are ideal candidates to develop economically friendly QDs. Different types of ternary QDs including $CuInS_2$, $CuInSe_2$, $AgInS_2$, $AgInSe_2$ have been used in biosensors, bioimaging and drug delivery (Girma *et al.,* 2017). Among the studied ternary QDs, AgInS QDs have attracted more attention in the past few years (Mao *et al.,* 2011). AgInS QDs exhibit excellent potential for light absorption and emission. AgInS-based QDs possess long photoluminescence (PL) and large stokes shifts, which minimize the impacts of self-absorption in light-emitting and bioimaging applications (Soheyli *et al.,* 2020). Numerous studies have been conducted on synthesizing AgInS QDs with size and composition-dependent physical characteristics (Jiao *et al.,* 2020). Alloying ZnS in AgInS core QDs results in a blueshift of the absorption and emission with an enhancement in the PL quantum yield (QY) (Kobosko *et al.,* 2017). Methodologies for synthesizing QDs have thus progressed significantly in the past two decades and a variety of synthetic strategies, from liquid phase

techniques to vapour phase nucleation and growth have been developed for the Synthesis of QDs (Pu *et al.,* 2018).

2.4.1. Synthesis of ternary quantum dots

Synthetic methods used in synthesizing QDs include solvothermal, thermolysis, hot injection, and heating-up methods. The selection of synthetic methods depends on the application in which the QDs will be used (Tsolekile *et al.,* 2017). The use of organic ligands in synthesizing QDs is required to coat the nanoparticle surface to prevent aggregation and convert the material to be water soluble (Pu *et al.,* 2018). Some of the widely used ligands include mono-thiolated ligands, including Glutathione (GSH), 3-Mercaptopropionic acid (MPA) and Mercaptoacetic acid etc. (Girma *et al.,* 2017). These ligands enable the solubilization of QDs, enabling conjugation to biomolecules like proteins, oligonucleotides, immunoglobulins, and aptamers, among others (Foubert *et al.,* 2016).

The synthesis method for core/shell material involves two steps: initially synthesizing core QDs followed by shell growth (Girma *et al.,* 2017). Usually, core QDs exhibit surface defects and low quantum yield, this is due to the high surface-to-volume ratio and small size. Thus, the core is coated with shell materials (i.e., ZnS and CdS) that have a wider band gap to increase quantum yield, assure stability, and minimize or remove surface defects (Aladesuyi and Oluwafemi 2020). ZnS is the semiconductor shell material mainly used for ternary QDs due to its higher band gap, low toxicity and low lattice mismatch compared to other passivating reagents (Vitshima *et al.,* 2022).

The synthesis of ternary QDs is a significant challenge due to complex chemistry because of the chemical properties of the precursor cations (Aladesuyi and Oluwafemi 2020). As a result of Cu^{+} and Ag^{+} being soft Lewis acids and In^{3+} a hard Lewis acid, their reactivity

towards sulphur compounds differs (soft Lewis bases). As a result, the unbalanced cationic precursors often lead to the formation of binary side products (i.e., copper sulphides, silver sulphides or indium sulphides) rather than the growth of ternary QDs (Girma *et al.,* 2017). This can be regulated using capping agents and single precursors with dual properties, which refers to substances that can act as stabilizing agents and reducing agents in order to control the reactivity of cations (Jose Varghese and Oluwafemi 2020; Aladesuyi and Oluwafemi 2020). Hu *et al.,* 2018 synthesized highly luminescent AgInS QDs via a synthetic hydrothermal method. The group used GSH and sodium citrate as ligands. The luminescent properties of the QDs, including Ag: In molar ratio, reaction temperature, and reaction time were studied. The as-synthesized QDs exhibited high QY reaching 21.6 % and a PL lifetime of up to 414 nS. Furthermore, Chen *et al.,* 2019 synthesized AgInS/ZnS core/shell QDs via the hydrothermal method using sodium citrate and GSH as stabilizing agent and ligands, respectively. In contrast to AgInS core QDs, the AgInS/ZnS core/shell QDs showed improved yellow to orange emission with long lifetimes and an increased QY from 21.6 % to 45.7 %.

2.4.2. Effect of synthetic parameters.

The most fundamental parameters considered during QDs preparation include injection temperature in hot-injection methods, reactivity and stoichiometric ratios of precursors, the solvent used, surfactants pH and reaction time etc. These parameters assist in adjusting size, composition, and quality of QDs (Girma *et al.,* 2017). The PL QY of semiconductor nanocrystals is affected by numerous parameters, including precursor concentration, reaction time, and ligands during the synthesis (Jiao *et al.,* 2020). The effects of various synthesis conditions on the characteristics of AgInS/ZnS QDs will be thoroughly examined in this section.

2.4.2.1. Effect of precursor ratios

Precursor concentration is one of the most important parameters in controlling the core or shell thickness. The formation of core/shell nanoparticles requires a low concentration of precursor at a slow reaction rate to generate a uniform-coated core/shell (Jain *et al.,* 2020). The equivalent component molar ratio $_X$Ag: $_X$In: $_X$S can be used to illustrate the AgInS QDs composition (Tong and Wang 2020). For AgInS QDs nanoparticles, chemical precursors that are more sensitive include In and S (Tsolekile *et al.,* 2017). Soheyli *et al.,* (2019) studied N-acetyl-L-cysteine-capped AgInS QDs with QY near 32% at 615 nm. They examined molar ratios of In: Na_2S, which was adjusted from 1: 0.5 to 1: 3. As the amount of sulphur precursor increased, a redshift in the UV-vis spectra were observed.

Furthermore, at the highest amount of sulphur precursor (In: Na_2S, 1:3) the colloidal QDs solution turned turbid, indicating aggregation of AgInS QDs. In the absorption spectra, this was indicated by absorption height at the long-wavelength side in support of their observation of the turbidity of the colloidal QDs solution. The best PL intensity was thus obtained at the In: Na_2S molar ratio of 1:2. Furthermore, Vitshima *et al.,* (2022) examined the effect of Ag: In precursor and observed that increasing the amount of In molar ratios from 1:1 to 1:16 gradually shifted to higher intensities. The highest intensity was observed at a 1:4 (Ag: In) molar ratio. The highest wavelength was at a ratio of 1:4 and the PL spectral position was tuned throughout a wide range from 558 to 582 nm. The UV spectra of the Ag: In ratios of 1:4, 1:6, 1:8, and 1:16 showed broad excitonic peaks with increasing In content.

2.4.2.2. Effect of pH

The influence of pH on particle size depends on the mechanism of reactions involved. and Reduction and precipitation reactions are greatly affected by changes in pH. In aqueous synthesis, pH directly affects the optical properties of the QDs (Jain *et al.,* 2020). Xiong *et al.,* (2013) studied the effects of pH on water-soluble $AgInS_2$/ZnS nanocrystals synthesized via a microwave-assisted approach. The results revealed that the pH value significantly affected the PL intensity of the $AgInS_2$ nanocrystals. As the pH value increased from 8.5 to 10.5 the PL intensity decreased gradually, and at pH values lower than 8.5 the solution turned turbid. These observations concluded that this could be due to the GSH pKa value being 8.7 and the GSH and $AgInS_2$ nanocrystals showing stronger bonding forces at this pH value. Xue *et al.,* studied the effect of pH on GSH-capped $AgInS_2$ QDs. The pH of the reaction solution had a significant impact on the fluorescence emission intensity of AgInS QDs. The fluorescence intensity increased with the increase in pH value ranging from 5.03 to 7.12 due to the deprotonation process of functional groups of the stabilizer. Further increase in pH from 7.12 to 10.02 resulted in decreased fluorescence intensity due to excess OH^- radicals in the reaction solution. Thus 7.12 was selected as the optimum pH.

2.4.2.3. Effect of reaction temperature and time

The growth of nanocrystals is ideally enhanced by increasing the reaction time and temperature, making reaction precursors more reactive. Long reaction times can lead to the aggregation of small crystals with a wide size distribution, which reduces the stability of QDs (Tsolekile *et al.,* 2017). To control the reaction kinetics for the formation of nanoparticles, the temperature is considered as one of the important parameters. In the case of core/shell formation, low temperatures are favoured for effective coating on the core rather than separating the nucleation of shell material (Jain *et al.,* 2020). Hu *et al.,*

2018 studied the effect of temperature on $AgInS_2$ QDs via the hydrothermal method. They observed that when the temperature reached 110 °C, the PL emission intensity increased and reached to its maximum. When the reaction temperature increased above 130 °C, phase separation of InS_3 caused a narrow peak to appear at roughly 432 nm, which significantly decreased the luminescence properties of AgInS QDs. In another study, Soarers *et al.,* 2020 assessed and modelled the synthesis of high-quality MPA-capped AgInS/ZnS QDs. The reaction temperature was kept constant at100 °C, while the reaction time was optimized. They discovered that the PL intensity increased with time while the wavelength of PL emission maximum remained unaffected. These studies highlight that temperature and time play a significant in adjusting the phase and composition of AgInS/ZnS core/shell QDs.

2.4.2.4. Effect of capping agent

Capping agents, such as surfactants, organic ligands, and polymers, help prevent particle agglomeration and achieve the appropriate nano-size (Subramanian *et al.,* 2020). Surface-modifying agents (i.e., 3-mercaptopropionic acid, thioglycolic acid or mercaptoacetic acid, glutathione and L-cysteine etc) are used in QDs synthesis as stabilizing agents and to coat the QDs for optimal optoelectronic properties (Masab *et al.,* 2018). Moreover, capping agents have advantages in reducing the core toxicity and increasing the quantum yield (Subramanian et al., 2020), thus assisting in producing high-quality material. Wonci *et al.,* 2022 studied the effects of different capping agents, such as mercapto-propanoic acid (MPA), glutathione (GSH) and L-Cysteine on Cu-In-S QDs. The absorption spectra exhibited broad absorption peaks for all capping agents centered around 415 nm, 419 nm and 421 nm for MPA, L-Cysteine and GSH, respectively. PL spectra of the QDs coated with these capping agents demonstrated QDs with two emission states. L-Cysteine and MPA had similar emission states, while GSH displayed higher luminescent intensities and

stability. This was accounted for by the long thiol alkyl chain of GSH better passivating the surface of QDs than L-Cysteine and MPA.

2.4.3. Synthesis of quantum dot bio-conjugates

Bruchez and Chan first discovered the ability to conjugate QDs to biomolecules in 1998, his work has since been applied in various biomedical applications such as bioimaging, immunoassays and deoxyribonucleic acid (DNA) sequencing techniques (Foubert *et al.,* 2016). QDs can form conjugates with several functional biomolecules such as proteins, oligonucleotides, antibodies and small molecule ligands to direct their *in vitro* and *in vivo* pathways to a particular target or an essential therapeutic function. Conjugation of biomolecules to the QD surface depends on the chemistry of the available ligands to provide functional groups suitable for covalent attachment or non-covalent binding (Wagner *et al.,* 2019). The quantity and orientation of biomolecules that can be attached to a QD surface depend on factors such as the size of QDs, properties of the QDs surface, nature of the biomolecule, stearic reasons and the technique used for bio-conjugation. The hydrophilic coating should also be considered as it determines the mechanism of bio-conjugation by providing the necessary active groups. Two main approaches to conjugating biomolecules on the QDs surface are covalent linking and non-covalent binding. Non-covalent binding is determined by hydrophobic, electrostatic or affinity interactions between biomolecules and the surface of QDs. Non-covalent binding is mainly based on electrostatic interaction between oppositely charged molecules and high-affinity secondary interactions such as biotin/ streptavidin (Foubert *et al.,* 2016). Covalent linkage is accomplished through different bio-conjugation methods using activated functional groups at the surface of QDs. Covalently linked QD bioconjugates are usually obtained using standard protein conjugation techniques. The most common method of covalent linkage involves binding primary amines of biomolecules such as 1-ethyl-3-(3-

dimethylaminopropyl)-carbodiimide (EDC) to activate the carboxylic acid groups on the surface of quantum dots (Bilan *et al.,* 2015). Figure 2.2 shows diagram depicting reaction steps between a carboxylic acid and an amine using EDC and NHS as coupling agents. N-hydroxysuccinimide (NHS) or sulfo-NHS are often used with water-soluble EDC. The reaction occurs via when the carboxylic acid's oxygen attacks the carbodiimide nucleophilically, resulting in the formation of the highly reactive intermediate known as O-acylisourea, which reacts with amines to produce an amide bond. The addition of NHS enables the formation of a second intermediate that is more soluble and stable, which reacts with the amine to yield the final product (Pereira *et al.,* 2019).

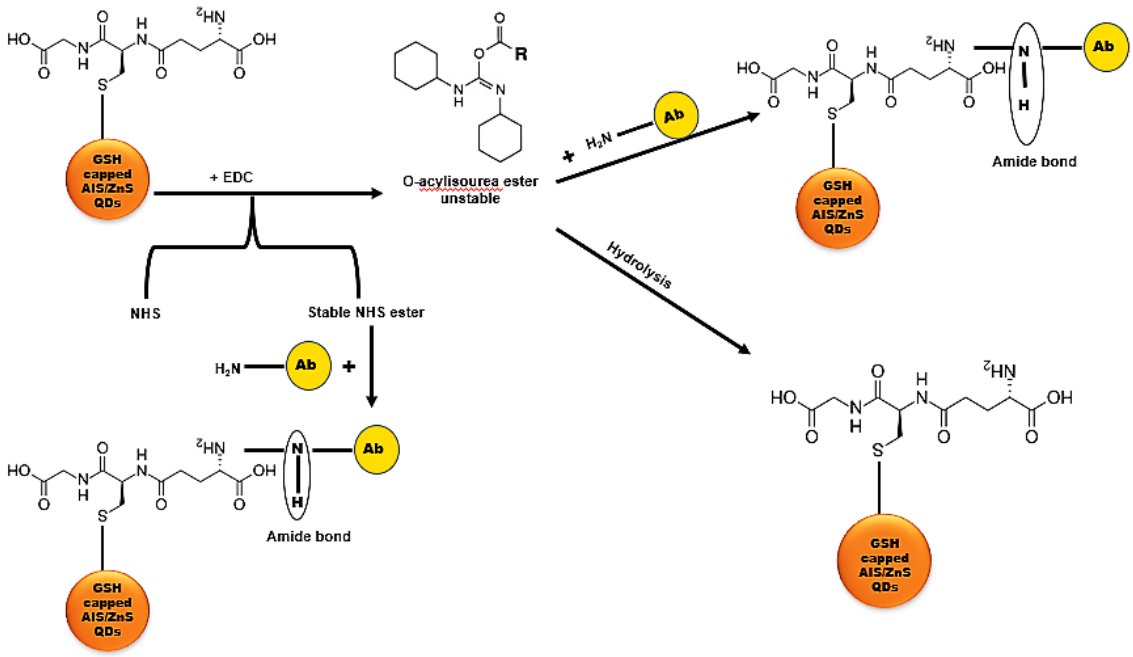

Figure 2.2: Diagram depicting reaction between a carboxylic acid and an amine using EDC and NHS as coupling agents.

Serum albumins are applied as protein models for various biochemical and physicochemical research, including conjugation with nanomaterials, due to their inherent function as carrier biomolecules in proximal biological fluids. Serum albumins, the most abundant proteins in mammalian fluids such as plasma, have been used as protein models for conjugation with nanomaterials due to their inherent function as carrier biomolecules

(Barba-Vicente *et al.,* 2020). One of the most commonly used serum albumins in the conjugation of QDs is Bovine serum albumin (BSA). BSA, which has an isoelectric point (pI) of 4.7 and a molecular weight of 67 kDa, is one of the most important globular proteins. BSA has 583 amino acid residues, 17 disulfide pairs and a substantial quantity of cysteine. Maintaining blood pressure balance and distributing medications throughout the body contributes to the movement of fatty acids, metal ions, and amino acids (Razavi *et al.,* 2021). For targeted cell imaging, Liu *et al.,* 2015, coated CuInS/ZnS QDs with an amphiphilic bioconjugate composed of bovine serum albumin (BSA)-poly(-caprolactone) (PCL). In a pH 7.4 PBS buffer, the CuInS/ZnS QD- BSA/PCL conjugate exhibited high stability.

2.4.4. Characterization of QDs

The optical, structural, and morphological characteristics of QDs have been studied using a variety of methods. These include photoluminescence (PL) which determines the change in intensity or peak shifts, UV-vis spectroscopy used to compare spectra of core and core/shell NPs and changes in peak shifts; Fourier transform infrared spectroscopy (FTIR) which determines functional groups. Transmission electron microscope (TEM) which studies morphological properties of NPs for understating their sizes, shape, dispersion, etc, Scanning electron microscope (SEM) which studies size and shape of QDs. Dynamic light scattering (DLS) which measures particle size in NPs suspension as well as shell thickness by comparing size of core and core/shell NPs and X-ray diffraction (XRD) which determines the crystallographic structure, identify unknown materials and orientation in powder solid samples (Mourdikoudis *et al.,* 2018).

2.5. Application of quantum dots and their bio-conjugates

Quantum dots are of great interest in biological applications compared to traditional organic dyes because of their well-known properties, such as stability, biocompatibility, water-dispersion properties, broad excitation spectra, and narrow emission spectra. These properties allow for long-term imaging with a long shelf-life and possess distinct photoelectrochemical activity (Bilan *et al.,* 2016; Ma *et al.,* 2015). In some instances, using these quantum dots to identify a specific molecule in a biological environment requires conjugation, which links quantum dots to the substrate of interest (Zhang *et al.,* 2019). As shown in figure 2.3 QDs have been applied in drug delivery and cancer therapy. Significant progress has been achieved in the design of QD-based drug delivery systems for cancer therapy. QDs conjugated with mutation-specific antibodies, for example, were recently used in the immunofluorescence histochemical detection of gene mutations in clinical samples of lung cancer. According to this theory, the use of specific antibodies against mutated proteins may be used in the future for lung cancer diagnosis and treatment (Mo *et al.,* 2017).

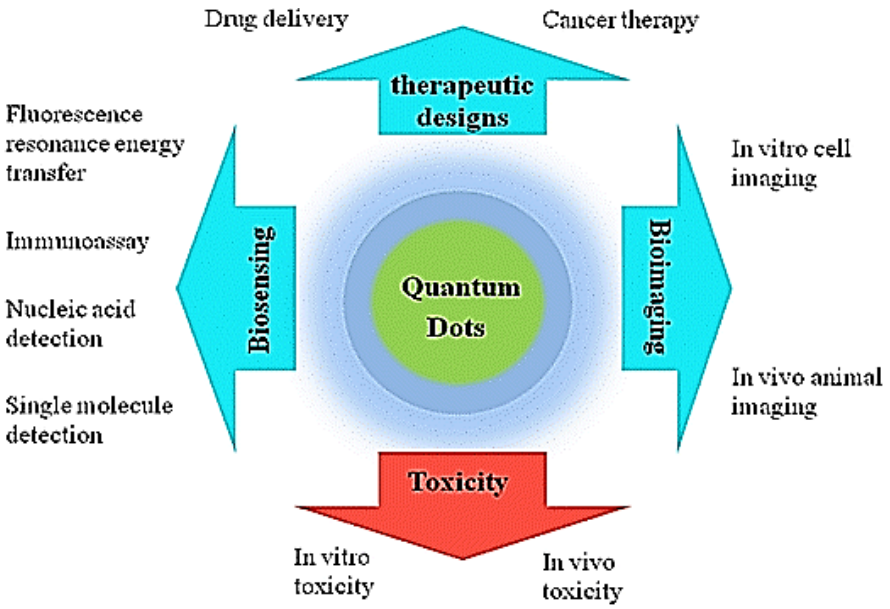

Figure 2.3: Various biological applications of quantum dots. Mo *et al.,* 2017 Applied Microbiology and Biotechnology 101(7). DOI:10.1007/s00253-017-8140-9.

2.6. Vascular endothelial growth factor (VEGF)

According to Hu and Olsen 2016, VEGF is one of the most crucial growth factors for regulating vascular formation and angiogenesis. It plays a crucial role as a signalling protein in pathological angiogenesis associated with many tumours. VEGF is one of six homodimeric proteins, along with VEGF-A and VEGF-B. VEGF-C, VEGF-D, VEGF-E, and placental growth factor (PLGF). PLGF is a crucial component of pathological angiogenesis, VEGF-B plays a function in embryonic angiogenesis, and VEGF-C and D are necessary for lymphangiogenesis (Hu and Olsen 2016). The VEGF-A commonly referred to as VEGF produces four distinct isoforms, including $VEGF_{121}$, $VEGF_{189}$, $VEGF_{165}$, and $VEGF_{206}$. $VEGF_{165}$ is a predominant isoform; it accounts for different human cancer developments and metastasis (Dehghani *et al.,* 2018). Also, this isoform is used to explore VEGF functions in animal models of bone healing and in vitro experiments and is bound to an extracellular matrix (ECM). VEGF consists of different types of receptors, which include $VEGFR_1$, $VEGFR_2$, $VEGFR_3$, Neuropilin 1(Npr_1) and Neuropilin 2 ((Npr_2). $VEGFR_2$ is considered the primary VEGF signalling receptor and is mainly expressed in endothelial cells to mediate angiogenesis and vasculogenesis, including promoting vessel permeability in response to VEGF while functions for $VEGFR_1$ are still debated (Hu and Olsen 2016). Overexpression of VEGF is a potential sign of cancers, particularly in developing independent blood supplies due to the requirement of oxygen and nutrients to initiate the metastasis process (Şahin *et al.,* 2020). VEGF has been utilized as a serum biomarker for several human disorders, including cancer, proliferative retinopathy, rheumatoid arthritis, psoriasis, and Parkinson's disease. Due to its importance as a biomarker, this biomolecule has attracted a lot of interest for sensing and detecting using analytical sensing devices (Dehghani *et al.,* 2018).

2.6.1. Detection methods of VEGF

Traditional VEGF isomer detection and quantification techniques include radioimmunoassay, mass spectrometry, and enzyme-linked immunosorbent assays (ELISA) (Dehghani *et al.,* 2018). However, although these methods are sensitive, accurate and precise, they pose some disadvantages as listed in table 2.1.

Table 2.1: List of traditional detection and quantification methods used to analyse biomarkers.

Technique	Principle	Disadvantages	Reference
ELISA	Techniques used in immunoassays that form immune complexes using radiolabeled substances.	•Requires trained personnel • Time-consuming • Expensive	Eftekhari *et al.,* 2019
Radioimmunoassay	An immunoassay that forms immune complexes step wise using radiolabeled substances.	• Costly •Radiolabelled chemicals only have a short shelf life. •Issues related to discarding of radioactive waste	Eftekhari *et al.,* 2019
Mass spectrometry	A technique for analysis that ionizes different chemical species and groups the ions according to their mass-to-charge ratios	•Unable to analyze mixtures •Having difficulty cleaning the instrument and being sensitive to contamination from previous samples	Eftekhari *et al.,* 2019

It is, therefore, essential to develop cost-effective, non-invasive, fast, user-friendly, highly sensitive and selective methods for detecting VEGF in blood serum for various human disorders. Recently, biosensors have been highly considered for detecting VEGF due to their exciting advantages such as cost-effectiveness, sensitivity and specificity, small target detection and non-toxicity.

2.6.2. Biosensors

Biosensors are chemical sensors that recognize systems that use biomedical mechanisms (Khanmohammadi *et al.,* 2020). They are composed of molecular sensing elements, a transducer that converts an obtained signal into a measurable physical signal and analytical devices from which the data is obtained (Şahin *et al.,* 2020). Biosensors are classified based on transducers used in the fabrication of cancer biosensors such as electrochemical, optical-electronic, piezoelectric, gravimetric and pyroelectric biosensors (Khanmohammadi *et al.,* 2020; Şahin *et al.,* 2020). Various approaches have been used to enhance the analytical performance of biosensors which includes incorporating nanomaterials (i.e., carbon nanotubes, graphene sheets, nanoparticles and QDs) in biosensing design to provide simpler, quicker, sensitive and hybrid nano-biosensor platforms with synergetic properties and functions (Şahin *et al.,* 2020; Pandit *et al.,* 2016). Furthermore, complexes of NPs with different bio-recognition elements, such as antibodies, peptides, polymers, and aptamers, can improve the performance of detection systems (Dehghani *et al.,* 2018).

2.6.2.1. Types of biosensors.

Optical biosensors (also known as fluorescent biosensors) are compact analytical devices that consist of a biorecognition sensing element. The sensing element produces a signal proportional to the desired analyte concentration that recognizes with an optical transducer system (Şahin *et al.,* 2020). QD-based fluorescent biosensors are developed due to their high sensitivity and excellent capability for multiplex analysis. Fluorescence resonance transfer (FRET) is mainly used for QD-based biosensors. Even though QD-based photoelectrochemical biosensors have emerged as optical biosensors, they have been developed due to their high sensitivity without the concern of using expensive instruments (Ma *et al.,* 2015). Electrochemical biosensors detect the generated electrical output signal

and then specifically bind surface-modifying biomaterials, such as aptamers, enzymes, antibodies, or nucleic acids to the electrode surface. In QD-based photoelectrochemical (PEC) biosensors, the QD is immobilized on the surface of the electrode, and a photocurrent signal is generated through the illumination of the electrode. The QDs may significantly promote photo-to-current conversion efficiency by enhancing the application of light energy and facilitating charge separation (Ma *et al.,* 2015). Electrochemical biosensors have been utilized for monitoring, early illness detection and biological analysis. Amperometric, potentiometric, and impedimetric electrochemical techniques, among others, have been employed for biosensing applications and offer significant potential for sensing low to high molecular mass analytes, such as protein markers (Dehghani *et al.,* 2018). Voltammetry is also an electro-analytical technique used in biosensing where the current is measured by sweeping the potential such as cyclic voltammetry (CV), differential pulse voltammetry (DPV), and square wave voltammetry (SWV) (Şahin et *al.,* 2020). Table 2.1 below summarises some of the electrochemical and optical biosensing techniques used for detecting VEGF that have been reviewed by (Dehghani *et al.,* 2018; Şahin *et al.,* 2020).

Table 2.2: Summary of various electrochemical and optical biosensing techniques that have been used for the detection of VEGF.

Technique	Method of detection	Bioreceptor	Biomarker	Lod	Range	References
Optical	Fluorescence	DNA aptamer	VEGF165	2.56 × 10−10 M	5 × 10−10–5 × 10−9 M	(Wang and Si 2013) (Dehghani *et al.,* 2018)
Electrochemical	nFIS EIS	Serum sample	VEGF	20 fM	250 fM–50 pM	(Qureshi et al., 2015) (Şahin *et al.,* 2020)
	CV	human serum samples	VEGF	4.6 pM	6–20 pM	(Fu *et al.,* 2016) (Şahin *et al.,* 2020)
	DPV		VEGF	1.85 pM	1.85 pM–3.7 nM	(Pan *et al.,* 2017) (Şahin *et al.,* 2020)
	SWV	3 different cancer cell lines	VEGF	7.5 pM	7.5 pM–5 nM	(Crulhas *et al.,* 2017) (Şahin *et al.,* 2020)

2.7. Conclusion

This literature review discussed a detailed background on properties and composition of ternary QDs mainly AgInS/ZnS core/shell QDs. The synthetic methods, factors affecting the synthesis of ternary QDs, bioconjugation and application of QD-bioconjugates in biosensing etc are described. Due to the underlying challenges on the synthesis and synthetic methods for the synthesis of ternary QDs, researchers should focus on designing and improving the existing synthetic strategies and various routes such as conjugation and encapsulation of QDs can be employed to produce QDs that are less toxic and applicable in biological analysis. Furthermore, a detailed background on VEGF and its detection methods was discussed. Therefore, the development of biosensors as detection methods that are user-friendly, cost-effective, sensitive and specific for detecting VEGF is of great importance. Few studies have applied ternary QD-bioconjugates as less toxic materials for developing biosensors and they possess excellent properties to be used in developing a biosensor for detecting VEGF.

2.8. References

Ahmad, S.A.A., Zaini, M.S. and Kamarudin, M.A., 2019. An electrochemical sandwich immunosensor for the detection of HER2 using antibody-conjugated PbS quantum dot as a label. Journal of pharmaceutical and biomedical analysis, 174, pp.608-617.

Aliofkhazraei, M. ed., 2016. *Handbook of nanoparticles*. Cham, Switzerland: Springer International Publishing.

Arshad, A., Akram, R., Iqbal, S., Batool, F., Iqbal, B., Khalid, B. and Khan, A.U., 2019. Aqueous Synthesis of tunable fluorescent, semiconductor CuInS2 quantum dots for bioimaging. *Arabian Journal of Chemistry*, *12*(8), pp.4840-4847.

Barba-Vicente, V., Parra, M.J.A., Boyero-Benito, J.F., Auría-Soro, C., Juanes-Velasco, P., Landeira-Viñuela, A., Furones-Cuadrado, Á., Hernández, Á.P., Manzano-Román, R. and Fuentes, M., 2020. Detection of human p53 in-vitro expressed in a transcription-translation cell-free system by a novel conjugate based on cadmium sulphide nanoparticles. Nanomaterials, 10(5), p.984.

Bilan, R., Fleury, F., Nabiev, I. and Sukhanova, A., 2015. Quantum dot surface chemistry and functionalization for cell targeting and imaging. Bioconjugate chemistry, 26(4), pp.609-624.

Crulhas, B.P., Karpik, A.E., Delella, F.K., Castro, G.R. and Pedrosa, V.A., 2017. Electrochemical aptamer-based biosensor developed to monitor PSA and VEGF released by prostate cancer cells. Analytical and bioanalytical chemistry, 409(29), pp.6771-6780.

Dehghani, S., Nosrati, R., Yousefi, M., Nezami, A., Soltani, F., Taghdisi, S.M., Abnous, K., Alibolandi, M. and Ramezani, M., 2018. Aptamer-based biosensors and nanosensors for the detection of vascular endothelial growth factor (VEGF): A review. Biosensors and Bioelectronics, 110, pp.23-37.

Eftekhari, A., Hasanzadeh, M., Sharifi, S., Dizaj, S.M., Khalilov, R. and Ahmadian, E., 2019. Bioassay of saliva proteins: The best alternative for conventional methods in non-invasive diagnosis of cancer. International journal of biological macromolecules, 124, pp.1246-1255.

Foubert, A., Beloglazova, N.V., Rajkovic, A., Sas, B., Madder, A., Goryacheva, I.Y. and De Saeger, S., 2016. Bioconjugation of quantum dots: Review & impact on future application. TrAC Trends in Analytical Chemistry, 83, pp.31-48.

Fu, X.M., Liu, Z.J., Cai, S.X., Zhao, Y.P., Wu, D.Z., Li, CY and Chen, J.H., 2016. Electrochemical aptasensor for the detection of vascular endothelial growth factor (VEGF) based on DNA-templated Ag/Pt bimetallic nanoclusters. Chinese Chemical Letters, 27(6), pp.920-926.

Ge, S., Zhang, C., Zhu, Y., Yu, J. and Zhang, S., 2010. BSA activated CdTe quantum dot nanosensor for antimony ion detection. Analyst, 135(1), pp.111-115.

Girma, W.M., Fahmi, M.Z., Permadi, A., Abate, M.A. and Chang, J.Y., 2017. Synthetic strategies and biomedical applications of I–III–VI ternary quantum dots. Journal of Materials Chemistry B, 5(31), pp.6193-6216.

Hu, K. and Olsen, B.R., 2016. The roles of vascular endothelial growth factor in bone repair and regeneration. Bone, 91, pp.30-38.

Hu, X., Chen, T., Xu, Y., Wang, M., Jiang, W. and Jiang, W., 2018. Hydrothermal Synthesis of bright and stable AgInS2 quantum dots with tunable visible emission. Journal of Luminescence, 200, pp.189-195.

Jain, S., Bharti, S., Bhullar, GK and Tripathi, S.K., 2020. I-III-VI core/shell QDs: Synthesis, characterizations and applications. Journal of Luminescence, 219, p.116912.

Jiao, M., Li, Y., Jia, Y., Li, C., Bian, H., Gao, L., Cai, P. and Luo, X., 2020. Strongly emitting and long-lived silver indium sulfide quantum dots for bioimaging: Insight into co-ligand effect on enhanced photoluminescence. Journal of colloid and interface science, 565, pp.35-42.

Kairdolf, B.A., Qian, X. and Nie, S., 2017. Bioconjugated nanoparticles for biosensing, in vivo imaging, and medical diagnostics. Analytical chemistry, 89(2), pp.1015-1031.

Kalnaitytė, A., Bagdonas, S. and Rotomskis, R., 2014. Effect of light on stability of thiol-capped CdSe/ZnS quantum dots in the presence of albumin. *Lithuanian Journal of Physics*, *54*(4).

Khanmohammadi, A., Aghaie, A., Vahedi, E., Qazvini, A., Ghanei, M., Afkhami, A., Hajian, A. and Bagheri, H., 2020. Electrochemical biosensors for the detection of lung cancer biomarkers: A review. Talanta, 206, p.120251.

Kobosko, S.M., Jara, D.H. and Kamat, P.V., 2017. AgInS2–ZnS quantum dots: excited state interactions with TiO2 and photovoltaic performance. ACS applied materials & interfaces, 9(39), pp.33379-33388.

Kolahalam, L.A., Viswanath, I.K., Diwakar, B.S., Govindh, B., Reddy, V. and Murthy, Y.L.N., 2019. Review on nanomaterials: Synthesis and applications. Materials Today: Proceedings, 18, pp.2182-2190.

Liu, Z., Chen, N., Dong, C., Li, W., Guo, W., Wang, H., Wang, S., Tan, J., Tu, Y. and Chang, J., 2015. Facile construction of near infrared fluorescence nanoprobe with amphiphilic protein-polymer bioconjugate for targeted cell imaging. ACS Applied Materials & Interfaces, 7(34), pp.18997-19005.

Mao, B., Chuang, C.H., Wang, J. and Burda, C., 2011. Synthesis and photo-physical properties of ternary I–III–VI AgInS2 nanocrystals: intrinsic versus surface states. The Journal of Physical Chemistry C, 115(18), pp.8945-8954.

Martynenko, I.V., Litvin, A.P., Purcell-Milton, F., Baranov, A.V., Fedorov, A.V. and Gun'Ko, Y.K., 2017. Application of semiconductor quantum dots in bioimaging and biosensing. *Journal of Materials Chemistry B*, *5*(33), pp.6701-6727.

Masab, M., Muhammad, H., Shah, F., Yasir, M. and Hanif, M., 2018. Facile Synthesis of CdZnS QDs: Effects of different capping agents on the photoluminescence properties. Materials Science in Semiconductor Processing, 81, pp.113-117.

Mohamed, W.A., Abd El-Gawad, H., Mekkey, S., Galal, H., Handal, H., Mousa, H. and Labib, A., 2021. Quantum dots synthetization and future prospect applications. Nanotechnology Reviews, 10(1), pp.1926-1940.

Mo, D., Hu, L., Zeng, G., Chen, G., Wan, J., Yu, Z., Huang, Z., He, K., Zhang, C. and Cheng, M., 2017. Cadmium-containing quantum dots: properties, applications, and toxicity. Applied Microbiology and Biotechnology, 101(7), pp.2713-2733.

Mourdikoudis, S., Pallares, R.M. and Thanh, N.T., 2018. Characterization techniques for nanoparticles: comparison and complementarity upon studying nanoparticle properties. Nanoscale, 10(27), pp.12871-12934.

Pan, L.H., Kuo, S.H., Lin, T.Y., Lin, C.W., Fang, P.Y. and Yang, H.W., 2017. An electrochemical biosensor to simultaneously detect VEGF and PSA for early prostate cancer diagnosis based on graphene oxide/ssDNA/PLLA nanoparticles. Biosensors and Bioelectronics, 89, pp.598-605.

Pandit, S., Dasgupta, D., Dewan, N. and Prince, A., 2016. Nanotechnology based biosensors and its application. The Pharma Innovation, 5(6, Part A), p.18.

Pereira, G., Monteiro, C.A., Albuquerque, G.M., Pereira, M.I., Cabrera, M.P., Cabral, P.E., Pereira, G.A., Fontesa, A. and Santos, B.S., 2019. (Bio) conjugation strategies applied to fluorescent semiconductor quantum dots. Journal of the Brazilian Chemical Society, 30, pp.2536-2561.

Pirzada, M. and Altintas, Z., 2019. Nanomaterials for healthcare biosensing applications. Sensors, 19(23), p.5311.

Pu, Y., Cai, F., Wang, D., Wang, J.X. and Chen, J.F., 2018. Colloidal Synthesis of semiconductor quantum dots toward large-scale production: a review. Industrial & Engineering Chemistry Research, 57(6), pp.1790-1802.

Qureshi, A., Gurbuz, Y. and Niazi, J.H., 2015. Capacitive aptamer–antibody based sandwich assay for the detection of VEGF cancer biomarker in serum. Sensors and actuators B: Chemical, 209, pp.645-651.

Razavi, M., Kompany-Zareh, M. and Khoshkam, M., 2021. PARAFAC study of L-cys@ CdTe QDs interaction to BSA, cytochrome c and trypsin: An approach through electrostatic and covalent bonds. Spectrochimica Acta Part A: Molecular and Biomolecular Spectroscopy, 246, p.119016.

Roushani, M. and Shahdost-fard, F., 2017. Ultra-sensitive detection of ibuprofen (IBP) by electrochemical aptasensor using the dendrimer-quantum dot (Den-QD) bioconjugate as an immobilization platform with special features. Materials Science and Engineering: C, 75, pp.1091-1096.

Roushani, M. and Shahdost-fard, F., 2019. Applicability of the Dendrimer-quantum Dot (Den-QD) Bioconjugate as a Novel Nanocomposite for Signal Amplification in the Fabrication of Cocaine Aptasensor. Analytical and Bioanalytical Chemistry Research, 6(1), pp.13-27.

Şahin, S., Caglayan, M.O. and Üstündağ, Z., 2020. Recent advances in aptamer-based sensors for breast cancer diagnosis: special cases for nanomaterial-based VEGF, HER2, and MUC1 aptasensors. Microchimica Acta, 187(10), pp.1-27.

Singh, S., Dhawan, A., Karhana, S., Bhat, M. and Dinda, A.K., 2020. Quantum dots: An emerging tool for point-of-care testing. Micromachines, 11(12), p.1058.

Soares, J.X., Wegner, K.D., Ribeiro, D.S., Melo, A., Häusler, I., Santos, J.L. and Resch-Genger, U., 2020. Rationally designed Synthesis of bright AgInS 2/ZnS quantum dots with emission control. Nano Research, 13(9), pp.2438-2450.

Soheyli, E., Azad, D., Sahraei, R., Hatamnia, A.A., Rostamzad, A. and Alinazari, M., 2019. Synthesis and optimization of emission characteristics of water-dispersible ag-in-s quantum dots and their bactericidal activity. Colloids and Surfaces B: Biointerfaces, 182, p.110389.

Soheyli, E., Ghaemi, B., Sahraei, R., Sabzevari, Z., Kharrazi, S. and Amani, A., 2020. Colloidal synthesis of tunably luminescent AgInS-based/ZnS core/shell quantum dots as biocompatible nano-probe for high-contrast fluorescence bioimaging. Materials Science and Engineering: C, 111, p.110807.

Subramanian, S., Ganapathy, S., Rajaram, M. and Ayyaswamy, A., 2020. Tuning the optical properties of colloidal Quantum Dots using thiol group capping agents and its comparison. Materials Chemistry and Physics, 249, p.123127.

Tong, X. and Wang, Z.M., 2020. Core/Shell Quantum Dots. Springer International Publishing.

Tsolekile, N., Parani, S., Matoetoe, M.C., Songca, S.P. and Oluwafemi, O.S., 2017. Evolution of ternary I–III–VI QDs: Synthesis, characterization and application. Nano-Structures & Nano-Objects, 12, pp.46-56.

Tsolekile, N., Parani, S., Vuyelwa, N., Maluleke, R., Matoetoe, M., Songca, S. and Oluwafemi, O.S., 2020. Synthesis, structural and fluorescence optimization of ternary Cu–In–S quantum dots passivated with ZnS. Journal of Luminescence, 227, p.117541.

Vitshima, N.A., Silwana, B., Tsolekile, N. and Matoetoe, M.C., 2022. Effect of ZnS coating on the optoelectronic properties of aqueous glutathione capped AgInS quantum dots. Journal of Alloys and Compounds, 900, p.163386.

Wagner, A.M., Knipe, J.M., Orive, G. and Peppas, NA, 2019. Quantum dots in biomedical applications. Acta biomaterialia, 94, pp.44-63.

Xu, Y., Chen, T., Hu, X., Jiang, W., Wang, L., Jiang, W. and Liu, J., 2017. The off-stoichiometry effect on the optical properties of water-soluble copper indium zinc sulfide quantum dots. Journal of colloid and interface science, 496, pp.479-486.

Xue, T., Shi, Y., Guo, J., Guo, M. and Yan, Y., 2021. Preparation of AgInS2 quantum dots and their application for Pb2+ detection based on fluorescence quenching effect. Vacuum, 193, p.110514.

Wonci, Z., Tsolekile, N. and Matoetoe, M.C., 2022. Polyvinylpyrrolidone as a polymer template for CuInS quantum dots: Effect on optical properties. Materials Today: Proceedings, 56, pp.1989-1994.

Yüce, M. and Kurt, H., 2017. How to make nanobiosensors: surface modification and characterization of nanomaterials for biosensing applications. RSC advances, 7(78), pp.49386-49403.

Zhang, C., Vinogradova, E.V., Spokoyny, A.M., Buchwald, S.L. and Pentelute, B.L., 2019. Arylation chemistry for bioconjugation. *Angewandte Chemie International Edition*, *58*(15), pp.4810-4839.

Chapter 3

Synthesis, optimization and characterization of AgInS QDs, AgInS/ZnS QDs and AgInS/ZnS bio-conjugates.

3.1. Introduction

Ternary QDs are of great interest for biosensors and chemotherapy applications etc. (Girma *et al.,* 2017). The synthesis of ternary QDs can be challenging, and their chemistry can be complex due to the chemical properties of precursor cations. However, using stabilizing agents and suitable capping agents can help overcome these challenges and achieve a good yield. Various synthetic methods have been reported to synthesize ternary QDs (Aladesuyi and Oluwafemi, 2020), while biomedical applications of QDs require surface modification and bioconjugation of QDs. This chapter will focus on the synthesis and optimization of AgInS core QDs and AgInS/ZnS core/shell QDs using three synthetic methods, namely, (i) Reflux method, (ii) heat-up method and (iii) monowave 50 method. The aqueous based reflux method is a technique that yields the desired product by varying reaction conditions (Aditha *et al.,* 2016). The reflux technique has advantages over hydrothermal techniques including easy operation, safety, and high yield (Xu et al., 2009). It has been used to synthesize various nanostructured materials, including nanoparticles, nanowires, nanorods, and core-shell nanostructures etc. In this method the reaction solution is heated over long period of time to provide the energy required for the reaction. The size, shape and crystallinity of materials can be regulated by optimizing parameters such as reaction time, precursor concentration and the type of solvent. To achieve the appropriate phase and morphology of the product using this method it is important to tune the following parameters: the sequence of precursor addition, the time of the reflux, and the cooling rate (Aditha *et al.,* 2016).

Heat-up methods for synthesizing QDs are well known, but they are far less popular than hot injection methods since most of them involve rapid heating to separate particle nucleation and growth to produce narrow size distributions. (Luo *et al.,* 2018). Heat-up methods are generally considered a more efficient for synthesizing nanocrystals because

they can be prepared in a single pot without the injection step (Sinatra and Pan 2017). Various heat-up methods explored in this chapter include open and closed beaker heat-up methods. A closed beaker heat-up method is more like a closed system whereby evaporation takes place, but the vapour encounters the surface of the glass covering the beaker, and it cools and condenses to form liquid water again. An open beaker heat-up method is like an open system whereby the liquid becomes vapour, and due to evaporation water level drops.

The Monowave 50 is an experimental synthesis reactor using conventional rather than microwave heating. Monowave 50 offers the performance of a microwave reactor at the cost of an autoclave, enabling synthesis at rates several times quicker than conventional stirrer hot-plate configurations. It is a relatively inexpensive and low scale (McGown *et al.,* 2022).

In a conventional aqueous synthesis of QDs, precursors are added at room temperature in the presence of stabilizing agents such as thiol groups (i.e., MPA, GSH and TGA) followed by heating under reflux. While synthesizing ternary QDs to balance the reactivities of anions (i.e., Ag^{2+} and In^{3+}), stabilizing agents such as GSH and sodium citrate are often used (Chen *et al.,* 2013). The optical and electronic properties of ternary QDs can be modified by adjusting the cation: anion ratio because they depend mainly on the amount of cation (i.e., Ag: In molar ratio during the synthesis).

Ag^{2+} and In^{3+} precursor cation and anion (S^{2-}) species were combined while being vigorously stirred magnetically to synthesize AgInS core QDs. Since In^{3+} is a hard acid and Ag^{+} is a soft Lewis acid, the reaction required careful balancing and control of the metal ions' reactivity. This was obtained by using a non-stoichiometric metal ion ratio (adding In^{3+} in four-fold excess), two stabilizing agents (mainly glutathione and sodium citrate as soft bases), and highly reactive Na_2S as a sulfur source (Hu *et al.,* 2018). GSH

was used as the thiol capping because of its biocompatibility. In addition, GSH is a tripeptide with several functional groups (such as amine and carboxylate), which allows additional structural modifications.

A variety of synthetic parameters, including reaction time, pH, synthetic method, Ag: In ratios, ZnS shell layers, capping agent, GSH content, and stabilizing agent, were evaluated to select the optimum reaction conditions. Zinc acetate and thiourea were introduced as ZnS shell precursors to the AgInS core QDs to form AgInS/ZnS core/shell QDs as shown in Scheme 3.1 below.

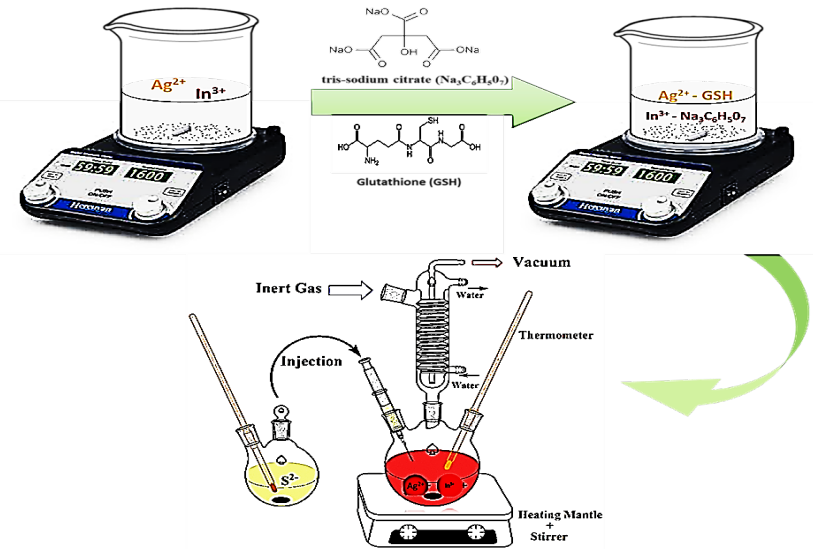

Diagram 3.1: Schematic representation of reflux synthesis.

To further enhance the optical properties of AgInS core QDs, the surface of the AgInS core QDs was coated with a ZnS shell. ZnS shell was selected because it is the most often employed passivating agent due to its high bandgap, low lattice mismatch, and low toxicity. In general, capping agents are used to control growth of materials. They can perform as stabilizers and passivate QDs to obtain desired optoelectronic characteristics (Masab *et al.,* 2018, Vitshima *et al.,* 2022). Furthermore, bioconjugation of AgInS/ZnS QDs using bovine serum albumin (BSA) is also reported in this chapter.

3.2. Materials and methodology

3.2.1. Chemicals.

Indium (III) chloride ($InCl_3$), L-Glutathione reduced (GSH), Silver nitrate ($AgNO_3$), tris-sodium citrate ($Na_3C_6H_5O_7$). $2H_2O$), Sodium hydroxide (NaOH) pellets, zinc acetate dihydrate ($Zn(O_2CCH_3)_2(H_2O)_2$), Hydrochloric acid 32% (HCl), sodium sulphide (Na_2S), thiourea (CH_4N_2S), ethanol (CH_3CH_2OH), Dimethylformamide (DMF), N,N′-Dicyclohexylcarbodiimide (DCC), ethyl (dimethylamino propyl) carbodiimide/N-hydroxysuccinimide (EDC/NHS) and BSA were bought from Sigma Aldrich, South Africa and used exactly as directed. The synthesis and analysis were performed using deionized water.

3.2.2. Effect of synthetic methods

3.2.2.1. Synthesis and optimization of AgInS/ZnS core/shell QDs via reflux.

AgInS core QDs was synthesized using a method by Tsolekile *et al.,* 2020 with modifications. Briefly, $AgNO_3$ (0.063 mmol; 0.0107 g), $InCl_3$ (0.25 mmol; 0.055 g), $Na_3C_6H_5O_7$ (1.00 mmol; 0.294 g) and GSH (0.145 mmol; 0.045 g) were combined into a three-neck flask with 100 ml of distilled water under magnetic stirring. The pH was adjusted to 7.58 by the addition of small amounts of NaOH (1.0 M) and HCl (1.0 M) using a pH meter before adding Na_2S (1.25 mmol; 0.0975 g in 10 ml). The mixture was refluxed at 95˚C for 60 minutes under stirring to obtain AgInS core QDs. Aliquots were taken every 15 minutes for analysis during the synthesis. Following the core synthesis thiourea (0.200 mmol; 0.015 g in 10 ml) and zinc acetate (0.200 mmol; 0.044 g in 10 ml) were added to the core solution, which was refluxed for 1 hour 20 min at 95˚C to form AgInS/ZnS core/shell QDs. The experiment was optimized by adjusting several synthetic factors such as reaction time, pH (3.58, 7.58, 9.58 and 11.58), In: Ag ratio (1:4, 1:2, 1:1, 1:8 and 1:16) and ZnS shell (layer 1, 2 and 3), capping agent (i.e., GSH and Glycine), stabilizing agents (i.e., dual, and single source) and GSH concentration (0.29, 0.145 and 0.58 mmol).

Ethanol (200 ml) was added to precipitate the obtained QDs, and the dispersion was centrifuged. The precipitate was collected and re-dispersed in water and the procedure was repeated twice. The obtained QDs were kept at room temperature and stored in amber glass vials.

3.2.2.2.Synthesis of AgInS core QDs via open and closed beaker method

AgInS core QDs were obtained with $AgNO_3$ (0.063 mmol; 0.0107 g), $InCl_3$ (0.25 mmol; 0.055 g), $Na_3C_6H_5O_7$ (1.00 mmol; 0.294 g), GSH (0.29 mmol; 0.09 g) and Na_2S (1.25 mmol; 0.0975 g in 10 ml). The precursors were dissolved sequentially in 100 ml of distilled water under magnetic stirring. The pH of the solution was adjusted to 7.58 before adding sodium sulphide. The solution was heated at 95˚C for 45 minutes under stirring to obtain AgInS core QDs. Aliquots were taken every 15 minutes for analysis during the synthesis.

3.2.2.3. Synthesis and optimization of AgInS/ZnS core/shell QDs via Monowave 50

A modified version of the previously published procedure was used to synthesize glutathione capped AgInS core QDs (Vitshima *et al.,* 2022). In a typical synthesis, $AgNO_3$ (1.1 mg), $InCl_3$ (5.5 mg), $Na_3C_6H_5O_7$ (29.4 mg), GSH (4.5 mg) were added to 10 mL of distilled water under magnetic stirring in a 50 ml beaker. The pH was adjusted to 7.58 by adding small amounts of NaOH (1.0 M) and HCl (0.1 M). Na_2S (9.8 mg) was added under vigorous magnetic stirring, and the resulting solution was poured into a reactor vial and placed in a Monowave at 95°C for 45 min to form AgInS core QDs. After this period, $Zn(O_2CCH_3)_2(H_2O)_2$ (4.5 mg) and CH_4N_2S (1.5 mg) were added to the reaction mixture and placed in a Monowave for 1 h 20 min at 95 °C to form AgInS/ZnS core/shell QDs. The experimental conditions for the synthesis of QDs were optimized by assessing the effect of reaction time, Ag: In molar ratio, temperature (95, 75,50 ℃) and capping agents

(L-serine, Methionine and Glycine). The QDs were precipitated as described in section 3.2.2.1.

3.2.3. Preparation of phosphate buffered saline (PBS) (pH 7) solution.

The fresh PBS solution was prepared as follows: ~8 g NaCl and 200 mg KCl were dissolved into 800 mL distilled water. Approximately 1.44 g $Na_2HPO_4 \cdot 12H_2O$ and 245 mg KH_2PO_4 were then dissolved into the solution. The pH was adjusted to 7.44 using 0.1 M HCl or 0.1 M NaOH solutions.

3.2.3.1. Preparation of 1 mg/ml BSA stock solution and standard solution.

About 5 mg of BSA was dissolved in 5 ml of PBS and mixed well until everything dissolved.

The stock solution prepared a series of 5 serial dilutions with final concentrations of 0.9, 0.70, 0.55 and 0.20 mg/ml by dissolving an appropriate amount of BSA in freshly prepared PBS buffer.

3.2.4.Synthesis of AgInS/BSA-ZnS and AgIn-BSA-S/ZnS bioconjugates

Effect of concentration

Following the synthesis of AgInS/ZnS core/shell as described in section 3.2.2.1, AgInS/BSA-ZnS QDs were prepared by adding different concentrations of BSA (i.e., 0.2, 0.55, 0.7 and 0.9 mg/ml) during ZnS passivation. While AgIn-BSA-S/ZnS were prepared by adding BSA after indium precursor, the core was synthesized for 45 min. Then ZnS was added, and the synthesis continued for 1hr 20 min via reflux.

Effect of Ratios of AgInS/ZnS: BSA

1:1 (2 ml AgInS/ZnS was mixed with 2 ml BSA (0.9 mg/ml), 1:2 (1ml AgInS/ZnS was mixed with 2 ml BSA (0.9 mg/ml), 1:3 (1ml AgInS/ZnS was mixed with 3 ml BSA (0.9

mg/ml) 1:4 (1ml AgInS/ZnS was mixed with 4ml BSA (0.9 mg/ml), 1:5 (1ml AgInS/ZnS was mixed with 5 ml BSA (0.9 mg/ml).

Effect of cross-linker (EDC/NHS) on AgInS/ZnS-BSA conjugation

About 5 mL of AgInS/ZnS was added to 10 mL DMF. DCC (0.47 g, 2.26 mmol) and NHS (0.25 g, 2.26 mmol) were added under magnetic stirring. 0.9 mg/ml BSA was added. The solution stirred for 2.5 hr. Aliquots were taken for analysis.

3.2.5. Characterization

Several techniques were used to characterize the AgInS core QDs and AgInS/ZnS core/shell QDs, including ultraviolet-visible spectrophotometry (UV–Vis) (Perkin Elmer UV–Vis Lambda 25 spectrometer, (UK); 1 nm slit width), Photoluminescence (PL) (RF-6000, Shimadzu, Japan), Fourier Transform Infrared spectroscopy (FT-IR) (Spectrum two UATR spectrometer, Perkin Elmer, UK), Transmission electron microscopy (TEM) and X-ray diffraction (XRD) patterns of the as-synthesized QDs were collected by Bruker D8. Advance diffractometer with monochromatic Cu-Kα1 radiation (λ = 1.5418 Å) at room temperature. Scanning Electron Microscope (SEM) measurements were carried out using JEOL 2010 operated at 200 kV. Dynamic light scattering (DLS).

The photoluminescence quantum yield (PLQY) of AgInS core QDs and AgInS/ZnS core-shell QDs was calculated using rhodamine 6 G (QY = 0.95, ethanol solution) as a reference standard and the equation below:

The PLQYs was calculated as:

$$\boldsymbol{QY = QYref \times \frac{I_{sample}}{A_{sample}} x \frac{A_{standard}}{I_{sample}} x \frac{(n_{sample})^2}{(n_{standard})^2}}$$

QYref – represents the quantum yield

I – represents integrated PL emission intensity

A – represents the absorbance at excitation wavelength (at A < 0.1)

n – reflective index of solvents (n = 1.33 for deionized water, n = 1.36 for ethanol).

3.3. Results and discussion

3.3.1. Synthesis of AgInS core QDs using reflux method.

Effect of reaction time

Figure 3.1 (a) and (b) depict the optical properties of the as-synthesized AgInS core QDs at different time intervals for 60 minutes. The influence of refluxing time on PL intensities was studied, as shown in figure 3.1a. The PL intensities of the as-synthesized AgInS core QDs increased as the reaction time increased. This was accounted to the improvement in the crystallinity of the AgInS core QDs (Kiprotich *et al.,* 2018). The absorption spectra in Figure 3.1b demonstrate that the absorbance decreased as the reaction time increased, with 0 min denoting an aliquot of QDs obtained after adding Na_2S as a sulphur source, signalling burst nucleation. The absorption spectra depicted broad excitation peaks. Figure 3.1c and d depicts changes of intensity and absorbance over time at a wavelength of 555.5 nm and 290 nm, respectively. It was observed that the reaction followed classical

nucleation theory (Figure 3.1c), which is the process whereby the formation of a solid takes place in a single step and once the clusters reach a certain size, they become thermodynamically stable and continue to expand spontaneously (Wu *et al.,* 2022). While figure 3.1c showed that the reaction followed a two-step nucleation mechanism which is possible in the existence of a metastable phase whose thermodynamic stability is intermediate between that of an old supersaturated phase and that of the assumed crystal phase (Kashchiev, 2020). These two mechanisms observed might be due to variations in particle sizes during the synthesis.

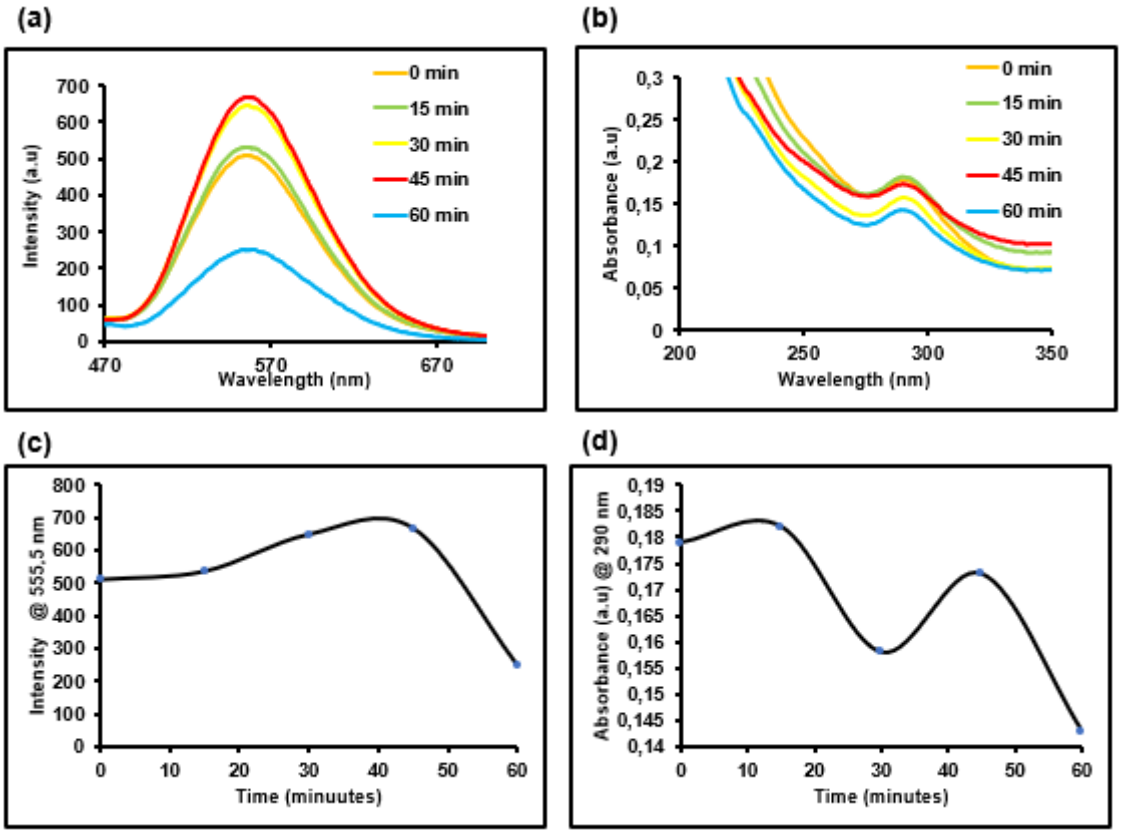

Figure 3.1: (a) Photoluminescence (PL) spectra of AgInS core QDs at different times, (b) UV-vis spectra of AgInS core QDs at different times and (c) Graph of intensity versus time (d) Graph of absorbance versus time.

Effect of pH.

The effect of pH on the optical properties of the as-synthesized AgInS core QDs was studied as shown in figure 3.2 (a) and (b). The PL intensity was significantly affected by the changes in pH of the as-synthesized AgInS core QDs as shown in figure 3.2a. The pH of the reaction solution before the addition of Na_2S was tuned at 3.58, 7.58, 9.58 and 11.58. Adjusting the pH of the mixture from 3.58 to 7.58 resulted in increased PL intensity and further adjustment in pH from 7.58 to 11.58 resulted in quenching of the PL intensity. Therefore, the maximum intensity was obtained at pH 7.58. This was probably due to GSH having a pKa value of 8.7, and between GSH and AgInS QDs show stronger bonding forces at this pH value (Xiong *et al.,* 2013). Figure 3.2b revealed a continuous blue-shift when the pH value was increased from 3.58 – 11.58. The blue-shift in the UV-vis absorption spectra due to an increase in pH value is also reported elsewhere (Soheyli *et al.,* 2019). Thus, pH 7.58 was selected for further experiments.

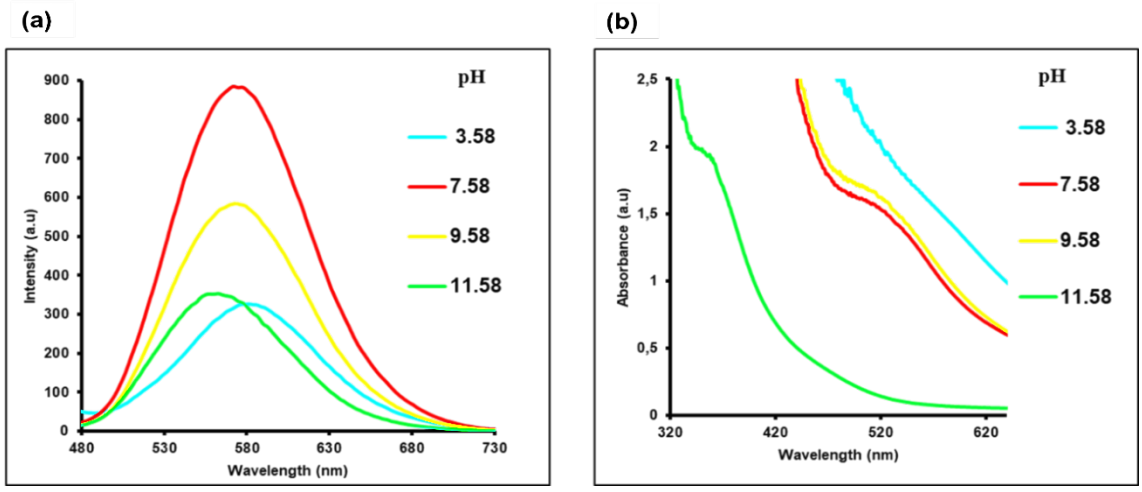

Figure 3.2: (a) Photoluminescence (PL) spectra of AgInS core QDs at different pH values and (b) UV-vis spectra of AgInS core QDs at different pH values.

Effect of molar ratio of precursors.

Figure 3.3a shows the PL intensity of the synthesized AgInS core QDs with nominal In: Ag ratios varied from 1:1 to 1:16. The PL intensity increased with an increase in Ag up to 1:8 with In: Ag (1:4) exhibiting maximum PL intensity. Then after 1:8 (In: Ag) the PL intensity decreased. Furthermore, increasing the Ag content caused a slight blue-shift in PL peaks. Suggesting that increasing Ag content caused repulsion between Ag d and S p orbitals in AgInS, leading to the rising of the valence band maximum (Kang *et al.,* 2015). UV-visible absorption spectra in figure 3.3b of the as-synthesized AgInS QDs revealed that increasing the In: Ag molar ratio was accompanied by a continuous redshift and decreasing the In:Ag ratio molar ratio causes a blue-shift. Thus, optimal results were obtained at a ratio of 1:4 due to the highest emission intensity and a broad excitonic peak observed on the PL and UV-vis spectra.

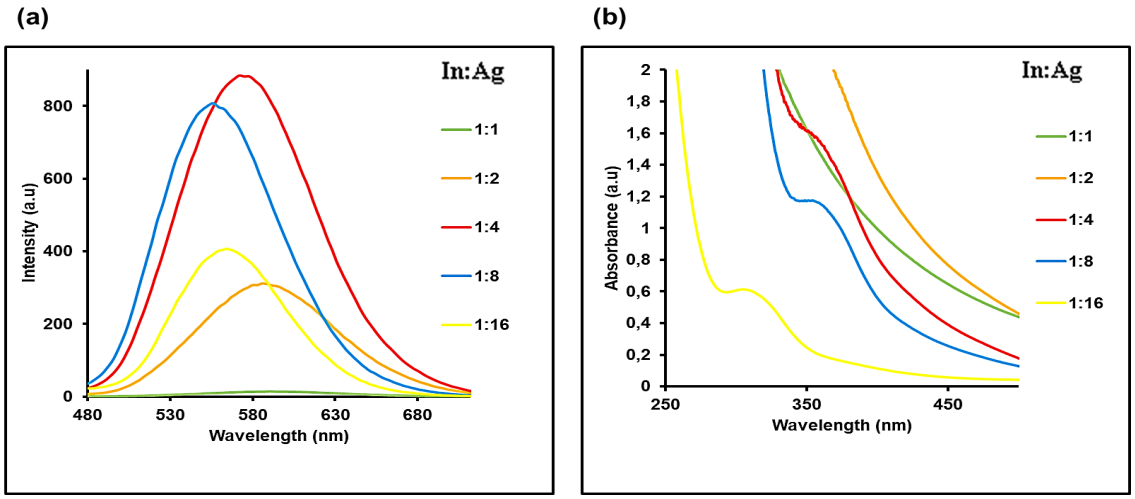

Figure 3.3: (a) Photoluminescence (PL) spectra and (b) UV-vis spectra of AgInS core QDs synthesized at different In: Ag ratios.

3.3.2. Synthesis and optimization of AgInS/ZnS core/shell QDs.

The UV-vis absorption and PL spectra of the as-synthesized AgInS/ZnS core/shell QDs are shown in figure 3.4 (a) and (b), respectively. In figure 3.4a injection of Zn/S precursor revealed an increase in PL intensity and a slight blue-shift in PL peak position was

observed, suggesting the formation of smaller particles. According to Delices *et al.,* 2020, the increase in PL intensity can be explained by the passivation of surface defects resulting in a reduction of non-radiative recombination pathways. In figure 3.4b a broad excitonc peak was observed in the core, the core/shell exhibits band-edge absorption.

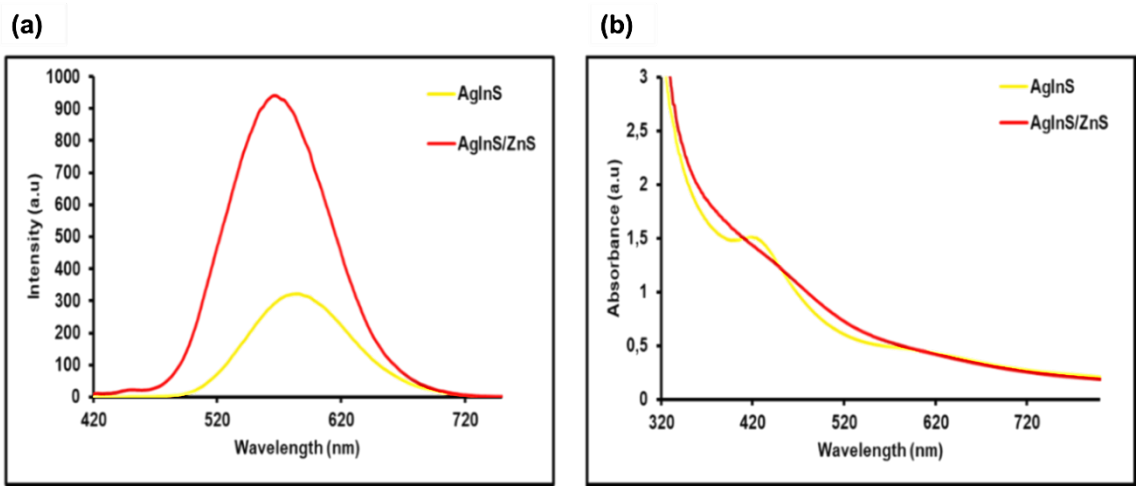

Figure 3.4: (a) Photoluminescence (PL) spectra and (b) UV-vis spectra of AgInS core QDs and AgInS/ZnS core/shell QDs.

Effect of capping agent.

Figure 3.5a shows the PL spectra of AgInS/ZnS QDs synthesized using GSH and Glycine as capping agents. GSH-capped AgInS/ZnS QDs PL intensities were higher than Glycine capped AgInS/ZnS QDs. According to Masab *et al.,* 2018, the difference in peaks of QDs capped with different capping agents is due to the complexation constants of different capping agents capable of modifying the growth kinetics of QDs. Figure 3.5b shows the corresponding UV-vis absorption spectra of the as-synthesized QDs. The absorption spectra of GSH-capped core QDs had an excitonic peak and after the addition of ZnS, the excitonic peak disappeared, confirming the elimination of surface defects on the QDs. The glycine capped QDs revealed a slight redshift following the addition of ZnS shell indicating the formation of bigger particles. GSH was selected as a capping agent due to its higher luminescent intensities and stability.

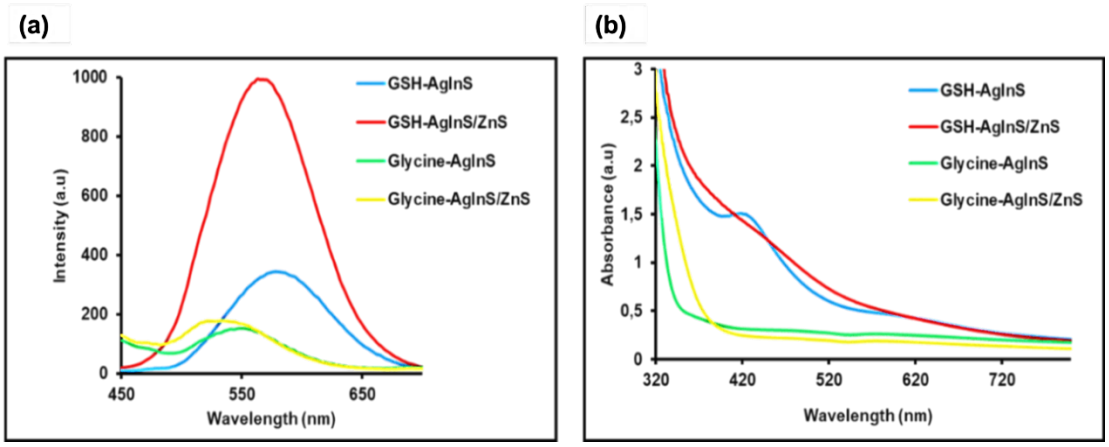

Figure 3.5: (a) Photoluminescence (PL) spectra and (b) UV-vis spectra of AgInS core and AgInS/ZnS core/shell QDs synthesized via different capping agents (i.e., GSH and Glycine).

Effect of stabilizing agent (dual source and single source)

Figure 3.6 (a) and (b) depict optical properties of the AgInS/ZnS QDs synthesized using various stabilizing agents, namely, (i) dual stabilizing agent (i.e., GSH and sodium citrate), (ii) single source consisting of GSH only (i.e., without the addition of sodium citrate). Figure 3.6a depicts the PL spectra of the as-synthesized QDs it was observed that lower PL intensity was observed on the QDs synthesized using a single source while a high PL intensity was observed for QDs synthesized using dual stabilizing agents. The UV-vis absorption spectra in figure 3.6b showed a lack of excitonic peak on the AgInS/ZnS QDs synthesized using a dual stabilizer and single source, respectively. AgInS/ZnS QDs synthesized using a dual stabilizing agent showed enhanced optical emission properties and thus were further used throughout this study.

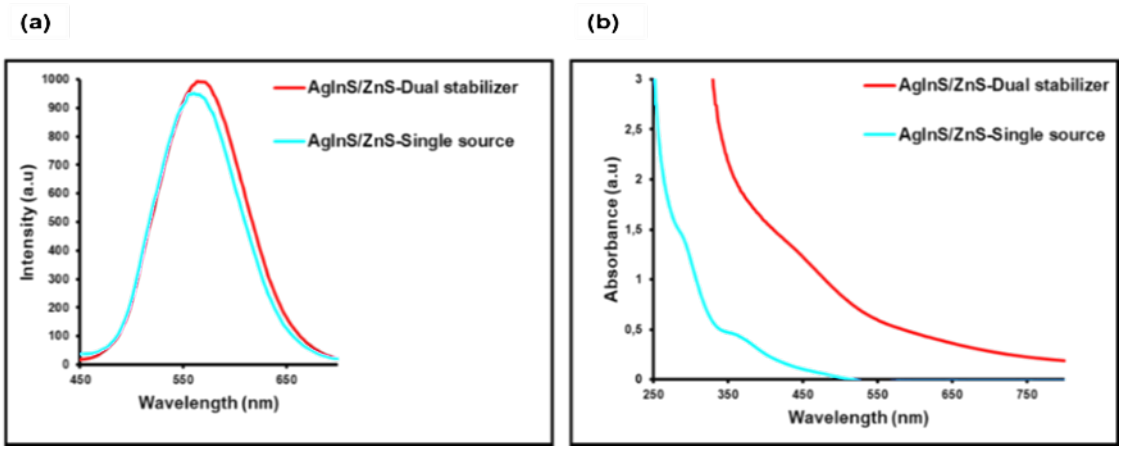

Figure 3.6: (a) Photoluminescence (PL) spectra and (b) UV-vis spectra of AgInS core and AgInS/ZnS core/shell QDs synthesized using dual stabilizing agents (GSH and sodium citrate) and a single source (i.e., removal of sodium citrate).

Effect of GSH concentration

To further improve the quality of GSH-capped AgInS/ZnS QDs, the amount of GSH was varied from 0.145 to 0.58 mmol, respectively. It was observed that with decrease in the concentration of GSH from 0.58 to 0.145 mmol increases the PL intensity. A slight blue-shift was observed as shown in figure 3.7a. The UV-vis absorption spectra show the presence of excitonic peaks at high concentrations with a decrease in GSH concentration. Low concentration of GSH resulted in the formation of more stable GSH-capped AgInS/ZnS QDs. Thus, 0.145 mmol was selected as the optimum for further analysis.

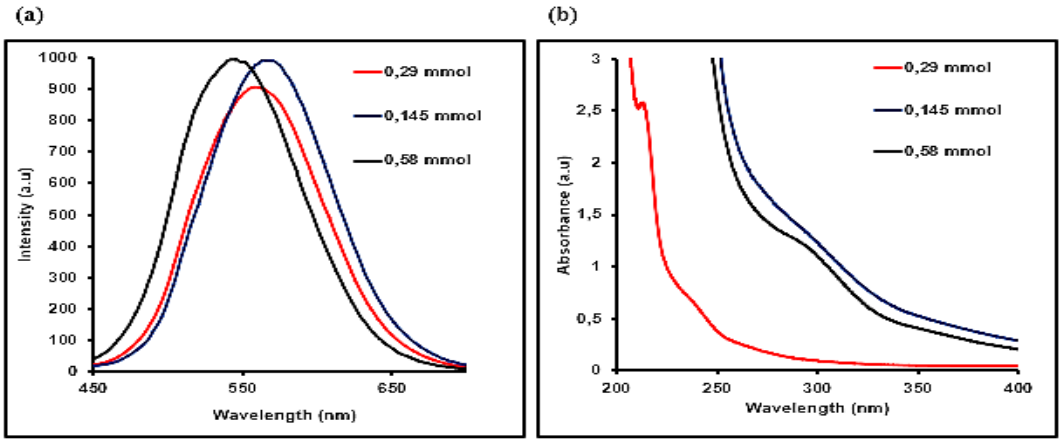

Figure 3.7: (a) Photoluminescence (PL) spectra and (b) UV-vis spectra of AgInS/ZnS core/shell QDs synthesized at different amounts of GSH.

Effect of ZnS shell layers

The effect of shell passivation on photo-physical properties of the synthesized QDs was investigated by adding three ZnS layers on the AgInS core QDs. Figure 3.8a shows the PL spectra of core and core-multi shell layers of AgInS/ZnS QDs. Increasing the number of ZnS shell monolayers resulted in a continuous blue-shift from 582 nm (AgInS core) to 564, 541 and 525 nm for ZnS shell monolayers 1, 2 and 3, respectively. In ternary QDs, the observed blue shift after ZnS passivation is a common phenomenon and is explained by the diffusion of Zn^{2+} ions into the core via partial cationic (Ag^{+} or In^{3+}) exchange with the Zn^{2+} in the core (Tsolekile *et al.,* 2020). The UV-vis absorption spectra in figure 3.8b show broad absorption peaks as the ZnS shell monolayer increases increase and a blue shift in the onset of the AgInS/ZnS QDs. This study used AgInS/ZnS core-shell QDs with one ZnS coating based on maximum wavelength and high intensity. Figure 3.8c and d shows digital photographs of AgInS core and AgInS/ZnS core/shell under day light (c) and under UV-lamp (d). Under the UV-lamp AgInS core showed a dark bright orange colour while AgInS/ZnS core/shell displayed a bright yellow colour. Colour change under the UV-lamp indicate the fluorescent nature of the QDs. Thus, it was observed that AgInS/ZnS core/shell QDs are brighter than AgInS core QDs under UV light, that can be ascribed to the growth of core-shell QDs. AgInS core QDs were estimated to have a PLQY of 31.6%, which increased to 35.4% for AgInS/ZnS core/shell QDs. This demonstrates that after ZnS passivation, the material's quality improved. In addition, compared to QDs synthesized using other ligands, such as 1-dodecanethiol (DDT), thioglycolic acid (TGA), and mercapto propionic acid (MPA), the luminescence and/or QY of the as-synthesized QDs appears to be superior (Miropoltsev *et al.,* 2020; May *et al.,* 2019 and Shi *et al.,* 2020).

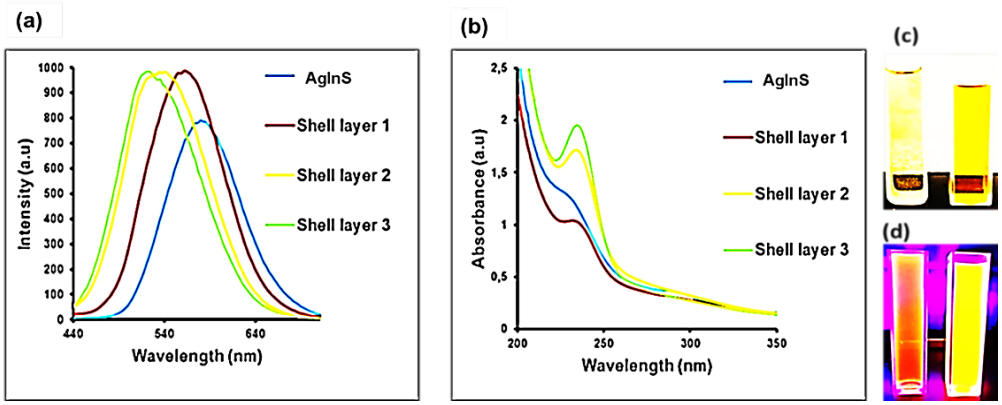

Figure 3.8: (a) Photoluminescence (PL) spectra, (b) UV-vis absorption spectra of AgInS core and AgInS/ZnS shell layers. (c) digital image day light and (d) digital image under UV-lamp of AgInS core and AgInS/ZnS core/shell.

3.3.3. Synthesis of AgInS core QDs using heat-up method

Open beaker

Figure 3.9a shows the photoluminescence spectra of the AgInS core QDs synthesized using the open-beaker heat-up method. The results revealed a decrease in the PL intensity as the reaction time increased. After 30 minutes, a precipitate was obtained; hence the synthesis was stopped. The UV-vis absorption spectra showed a continuous redshift as the reaction time increased, suggesting the formation of larger particles, as shown in figure 3.9b.

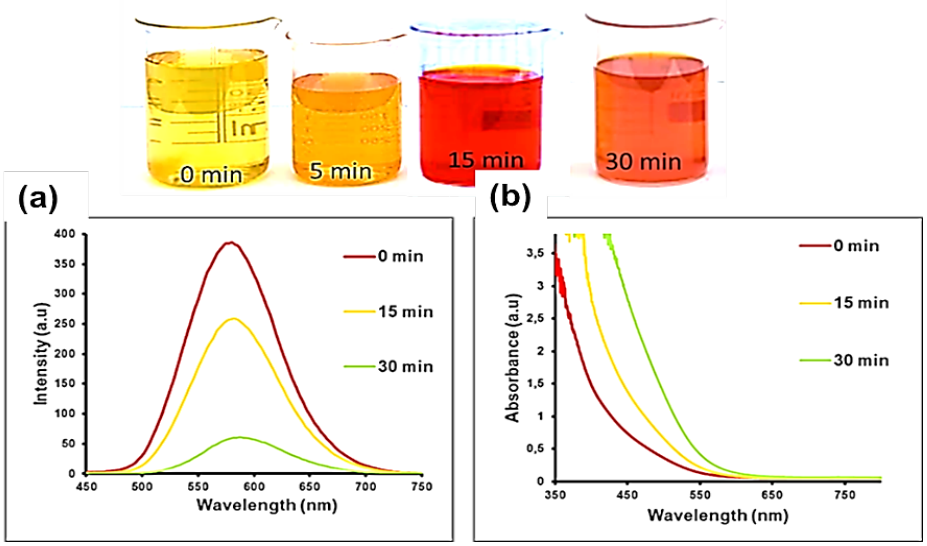

Figure 3.9: (a) Photoluminescence (PL) spectra of AgInS core QDs and (b) UV-vis spectra of AgInS core QDs synthesized using open beaker heat-up method at pH 7.58

Closed beaker heat up method.

Figure 3.10a shows the photoluminescence spectra of AgInS core QDs synthesized using closed beaker heat-up method. The results revealed a similar trend observed when using the reflux technique, i.e., as the reaction time increased the PL intensity also increased. The UV-vis absorption spectra showed a slightly broad excitonic peak and a slight redshift showing bigger particles were continuously formed as shown in figure 3.10b. Despite the PL peaks and UV-vis absorptions showing relatively similar results to the reflux method. The low PL intensities observed in these methods suggest the maximum separation of charge carriers.

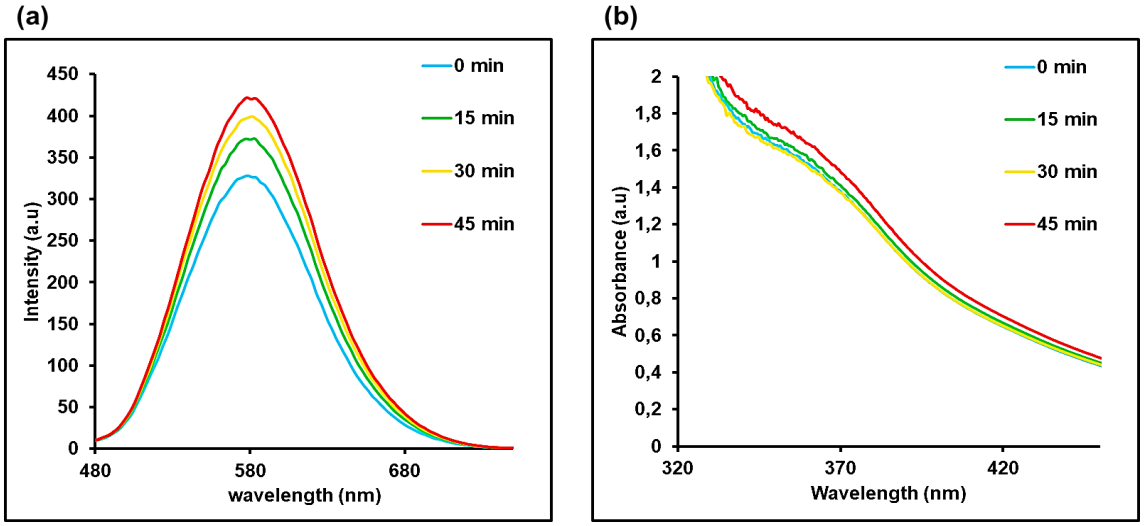

Figure 3.10: (a) Photoluminescence (PL) spectra of AgInS core QDs and (b) UV-vis spectra of AgInS core QDs synthesized using closed beaker heat-up method at pH 7.58.

3.3.4. Synthesis of AgInS/ZnS QDs via monowave 50 method

Effect of time

The temporal evolution of AgInS core QDs were monitored by synthesizing the material at different reaction times. Figure 3.11a depicts the influence of reaction time on PL intensities of the synthesized material. As expected, the PL intensities of the as-synthesized AgInS core QDs increased as the reaction time increased, reached its maximum after 45 min, and decreased after 60 min and 75 min. Furthermore, a blue shift with increasing time for 60 and 75 min proved that the In^{3+} and Ag^{+} cation exchange reaction on pre-grown AgInS core QDs effectively took place (Kim *et al.,* 2020; Parani, and Oluwafemi, 2022). The absorption spectra in figure 3.11b depict that as the reaction time reached 30min and 75 min no excitonic peaks were observed, while at 5 min and 15 min showed broad excitonic peaks centred around 234 nm. At 60 min a slightly narrow sharp excitonic peak centred around 236 nm was observed. Changes in fluorescence intensity and absorbance were confirmed by a calibration curve in figure 3.11c and d respectively. Figure 3.11c depicted a slow reaction rate occurring from 5 to 30 min. The reaction rate started to increase exponentially, which is depicted by increased intensity from 30 minutes to its maximum after 45 minutes. A slight decrease in intensity was observed after 60 min and 75 min and was constant. The absorbance versus time graph in figure 3.11d revealed that the absorbance decreased after 10 min and started to increase after 30 min reaching a maximum absorbance at 60 min and decreasing after 75 min. Both figure 3.11c and d resembled a classical nucleation theory similar to the Ostwald step rule (Kashchiev, 2020).

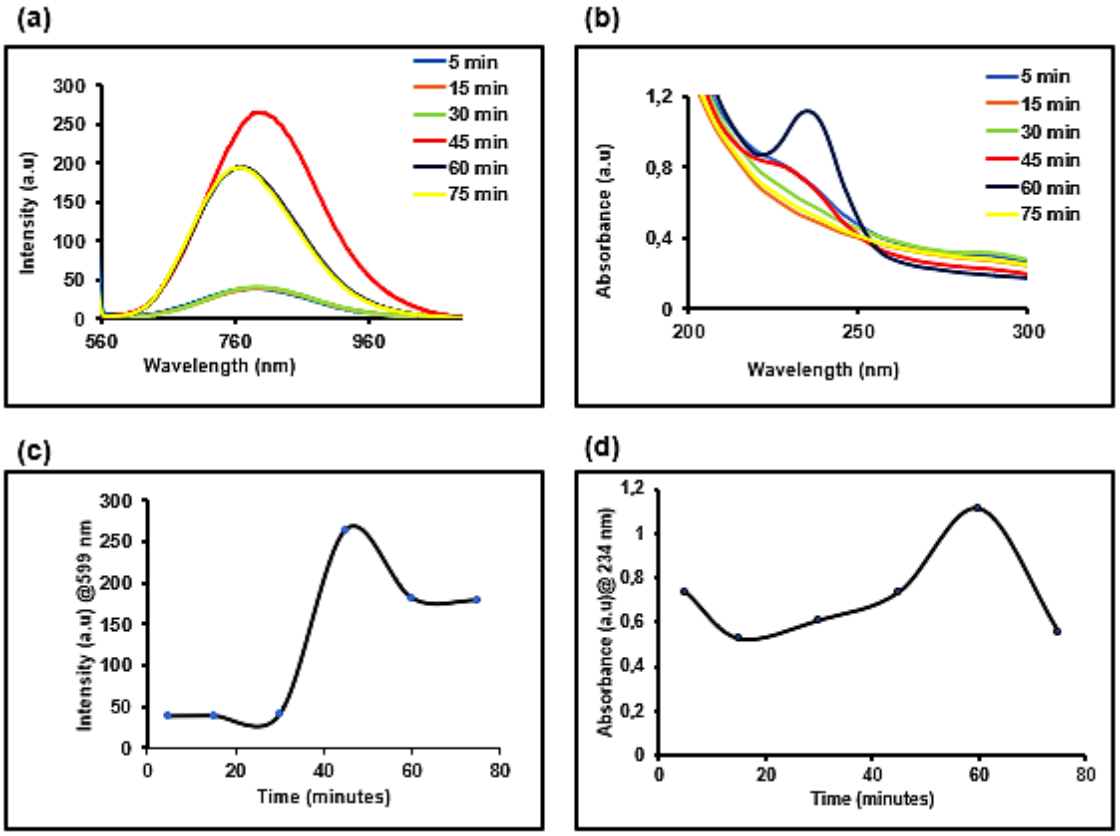

Figure 3.11**:** (a) Photoluminescence and (b) absorption spectra of AgInS core QDs at different reaction times, (c)&(d) graphs depicting intensity and absorbance changes overtime respectively

Effect of Ag:In ratio

The amount of indium was varied to achieve different Ag: In ratios. Figure 3.12a shows the PL intensity of the synthesized AgInS/ZnS core/shell QDs with nominal ratios varied from 1:4 to 1:16. It was observed that the PL intensity increased with increasing indium content up to 1:4. Following this the intensity quenched at 1:6. The PL peaks observed were broad compared to other synthetic techniques with full-width half maximum (FWHM) of 112 nm, while reflux and closed beaker heat-up method exhibited FWHM of 105 nm and 96 nm respectively. Figure 3.12b depicts the absorption spectra of AgInS/ZnS core/shell QDs at different Ag:In ratios. The absorption spectra of the as-synthesized AgInS/ZnS QDs revealed sharp excitonic peaks at high indium content with maximum absorbance obtained at 1:4. Hence 1:4 was the optimal ratio.

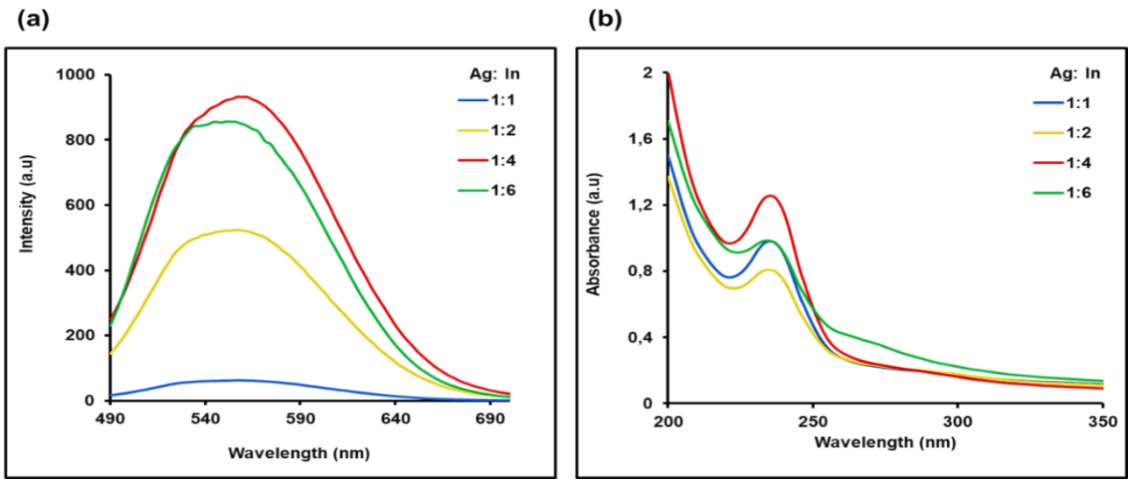

Figure 3.12: (a) Photoluminescence and (b) absorption spectra of AgInS/ZnS core/shell QDs synthesized at different Ag:In ratios.

Effect of reaction temperature

Reaction temperature controls the nucleation rate thus it's an important factor for the quality of QDs (Yu *et al.,* 2012). Figure 3.13a depicts the PL spectra of AgInS/ZnS core/shell QDs synthesized at different reaction temperatures. The PL intensity significantly increased with an increase in temperature. At a relatively moderate increase in temperature, the QDs started to grow, indicating that crystal growth requires higher temperatures. Thus, maximum PL intensity was obtained at a reaction temperature of 95 ˚C. The absorption spectra in Figure 3.13b depicts broad excitonic peaks with an increase in temperature from 50 to 60 ˚C and narrow sharp excitonic peaks with maximum absorbance at 95 ˚C.

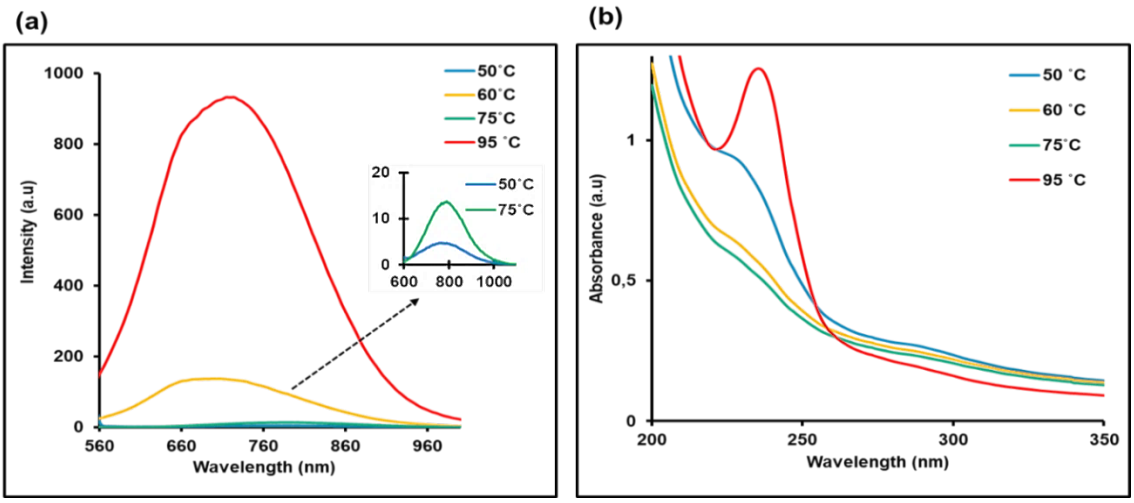

Figure 3.13: (a) Photoluminescence and (b) absorption spectra of AgInS core QDs at different temperatures.

Effect of capping agent

Thiol groups are appropriate ligands as capping agents because of their terminal functional groups (i.e., thiol, amines, or carboxylic acid). During synthesis and storage, the functional groups prevent agglomeration and enable surface binding to the surface of QDs (Wonci *et al.,* 2022). Figure 3.14 depicts the optical properties of AgInS/ZnS core/shell QDs capped with different capping agents such as Glycine, L-methionine, l-serine, GSH and amino acid mixture. Figure 3.14a shows the PL spectra of the QDs capped with different thiol groups. GSH exhibited the highest maximum intensity while the amino acid mixture (which contains Glycine, L-methionine, l-serine and GSH) showed a slight decrease in intensity. The absorption spectra showed broad excitonic peaks for all the different thiol groups (figure 3.14b) except for the amino acid mixture. Serine has only one additional functional group (CH_2OH) compared to Glycine hence it showed maximum absorptions. GSH has a thiol group that plays an essential role in its functions and is made up of three amino acids (i.e., cysteine, glutamic acid, and glycine), while L-methionine has thiol functional group and is a constituent of GSH; hence GSH showed high absorbance compared to L methionine. The figure 3.14c shows the structure of the various amino acids.

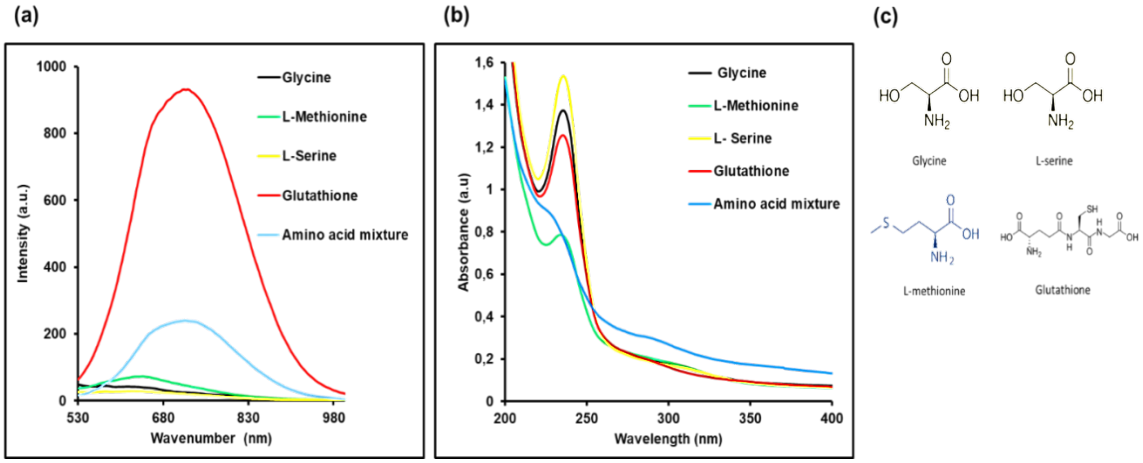

Figure 3.14: (a) Photoluminescence and (b) absorption spectra of AgInS/ZnS core/shell QDs synthesized using different capping agent and (c) Structures of amino acids.

3.3.5. Morphological and structural of as-synthesized QDs.

FTIR

Figure 3.15 shows the FTIR spectra of GSH (capping agent) and the as-synthesized AgInS/ZnS core/shell QDs. The GSH capping on the as-synthesised QDs was confirmed using the FTIR spectra. GSH exhibited peaks at 3340 cm^{-1} and 3251 cm^{-1} that were assigned to -OH and -NH functional groups respectively. The characteristic thiol (-SH) group stretching vibrations of GSH was observed at 2524 cm^{-1} and the peaks at 1595 - 1535 cm^{-1} were attributed C=O stretching band of the carboxylic group. Asymmetric and symmetric COO^- stretching were observed at 1595 cm^{-1} and 1535 cm^{-1}, respectively. The peak broadening and shift of the vOH and vC-H functional groups was observed in AgInS core QDs. The GSH thiol group (SH) disappearance in AgInS core QDs showed that the -SH group was involved in capping the AgInS core surface with GSH. The AgInS/ZnS QDs showed similar spectra to the AgInS core QDs after passivation with ZnS, but with a slight decrease in intensity and peak shift in the vOH and vC-H bands. Additionally, the AgInS/ZnS core/shell QDs displayed vC=O at 1560 cm^{-1} (asymmetrical) and 1358 cm^{-1} (symmetrical), indicating successful capping of the as-synthesised AgInS/ZnS QDs with GSH.

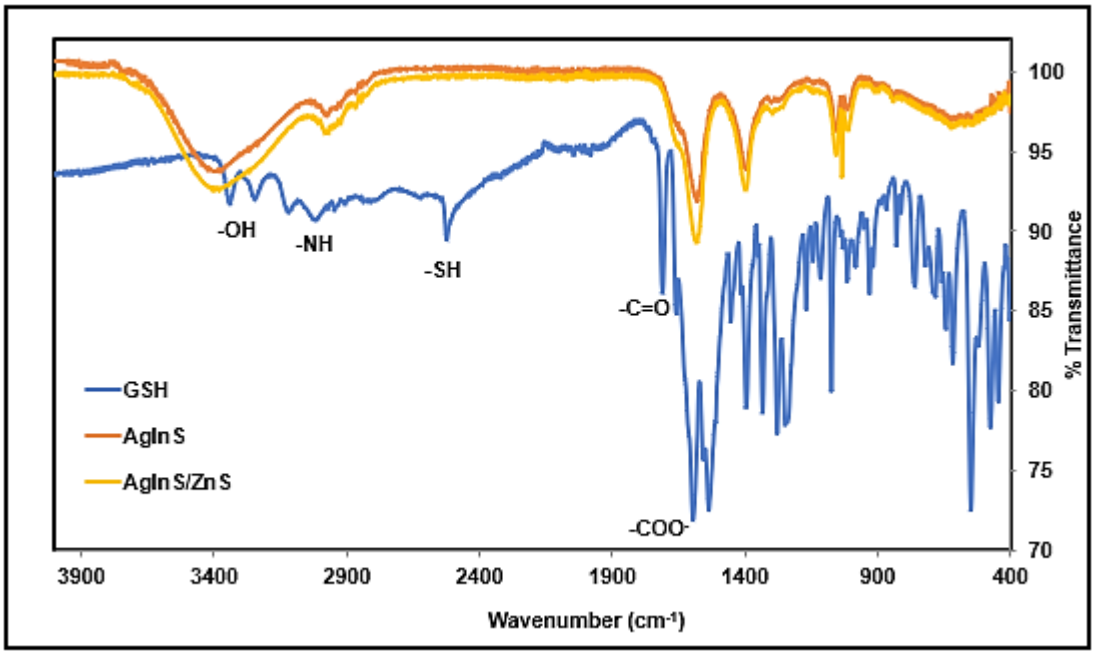

Figure 3.15: FTIR spectra of GSH and AgInS core AgInS/ZnS core/shell QDs.

XRD and EDX

To determine the crystalline structure and elemental composition of AgInS core QDs and AgInS/ZnS core/shell QDs XRD and EDX analysis were carried out. Figure 3.16a depict the XRD patterns of AgInS core and AgInS/ZnS core/shell QDs. The XRD patterns of AgInS core QDs showed major peaks at 2Θ values of 27.6◦, 45.4◦ and 52.5◦ corresponding to 112, 220 and 312 planes of tetragonal crystal structure, respectively. The shift of these peaks to higher angle for AgInS/ZnS QDs confirms the formation of core/shell QDs which match reference JCPDS: 25-1330 in-line with literature (Oluwafemi *et al.,* 2019). Figure 3.16b depicts the EDX profiles of the as-synthesized QDs. The presence of Silver, indium and sulphur characteristic peaks indicate the formation of AgInS core QDs, while in AgInS/ZnS core/shell QDs the passivation of ZnS shell is indicated by the presence of Zn peaks in the EDX profile.

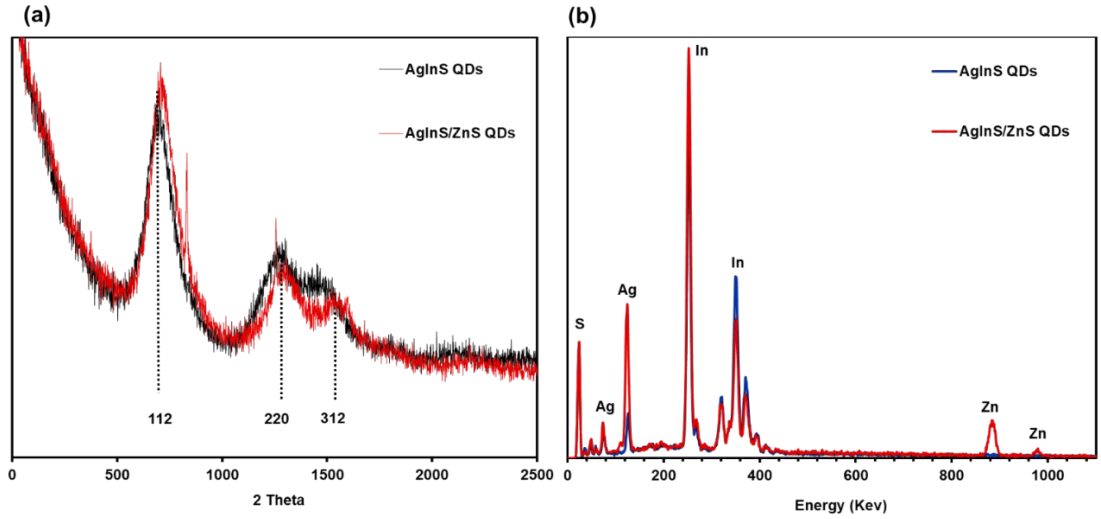

Figure 3.16: (a) XRD and (b) EDX spectra of AgInS core and AgInS/ZnS core/shell QDs.

TEM, SEM and size distribution

Transmission electron microscopy (TEM) and scanning electron microscopy (SEM) were used to analyse the size and morphology of the as-synthesized QDs. The AgInS core QDs and AgInS/ZnS core/shell QDs were small and spherical, as shown in Figure 3.17 and c. According to the size distribution curves, the AgInS core QDs have a size that is centred around 1.5 nm, while the AgInS/ZnS core/shell QDs have a particle size that is less than 2.5 nm (Figure 3.17 b, d). The SEM morphologies of AgInS/ZnS core/shell QDs are shown in Figure 3.17f. From figure 3.16e the shape of the AgInS core QDs are polydisperse with larger particle size. After adding the ZnS shell depicted in figure 3.17f the QDs are polydisperse with smaller particle size.

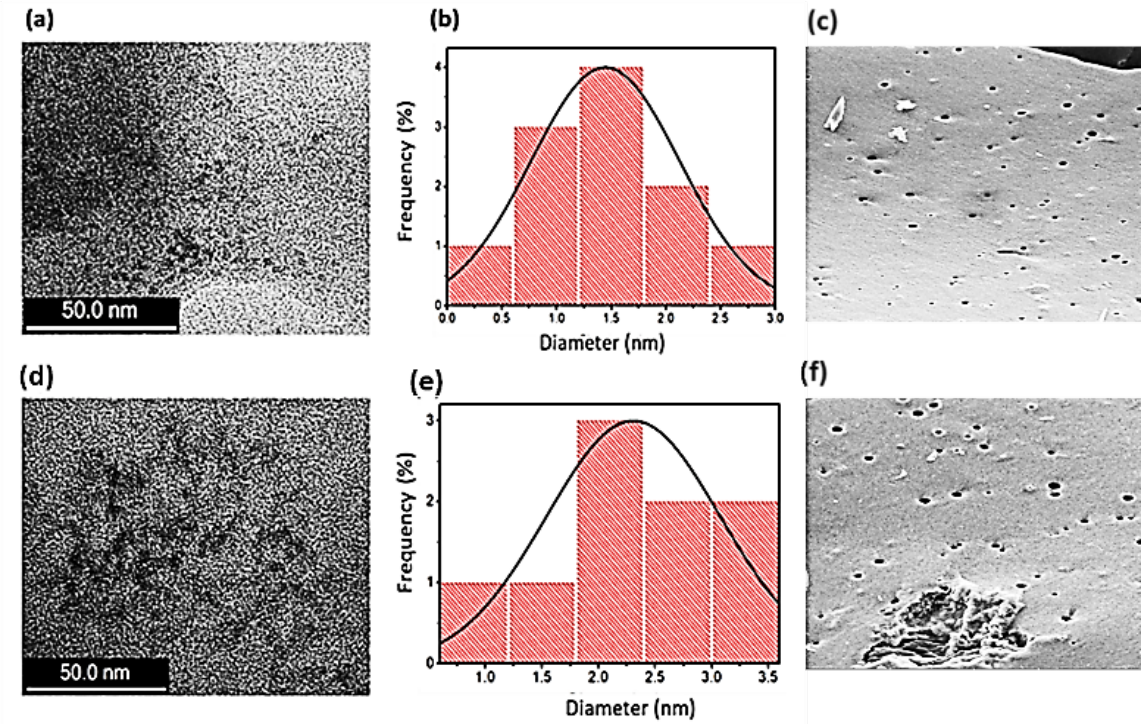

Figure 3.17: (a) TEM, (b) particle size distribution and (c) SEM of AgInS core QDs. (d) TEM, (e) particle size distribution and (f) SEM of AgInS/ZnS core/shell QDs.

Dynamic light scattering (DLS)

Figure 3.18 shows the zeta size distribution of (a) AgInS core, (b) AgInS/ZnS core/shell QDs and zeta potential of (c) AgInS core, (d) AgInS/ZnS core/shell QDs. AgInS core QDs exhibited narrow size distribution compared to AgInS/ZnS core/shell QDs. As expected, the size of the AgInS core QDs was higher than size AgInS/ZnS core/shell QDs with values 449.9 d.nm and 79.31 d.nm respectively. The reduction in particle size of the quantum dots confirms the improvement in quality of the as-synthesized QDs following ZnS passivation. The highly negative zeta potential of the AgInS core QDs and the AgInS/ZnS core/shell QDs (-51.4 mV and -26.4 mV, respectively) showed the remarkable colloidal stability of the synthesized material.

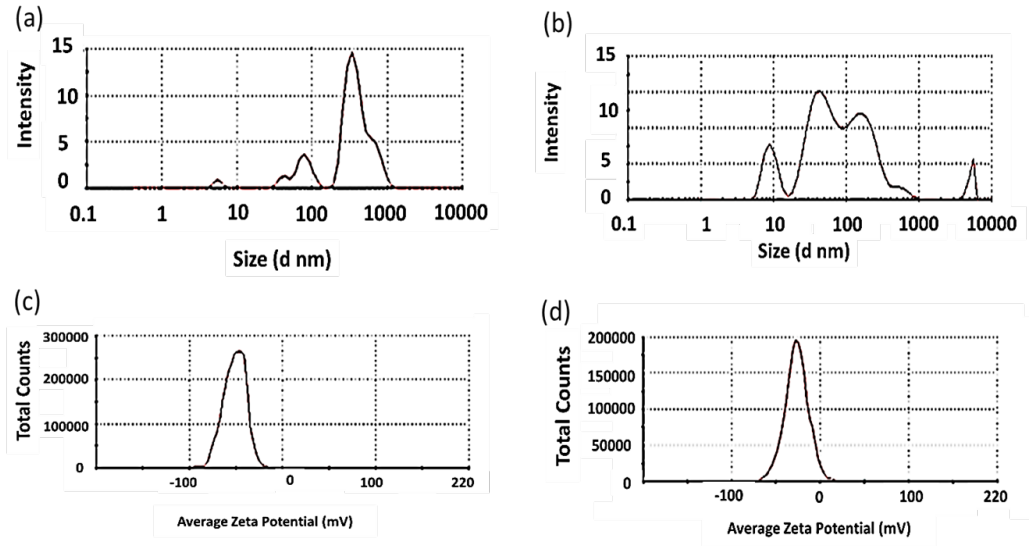

Figure 3.18: Zeta size of (a) AgInS core, (b) AgInS/ZnS core/shell and Zeta potential (c) AgInS core, (d) AgInS core/shell.

3.3.6. Optimization of conjugation/Functionalization of GSH capped AgInS/ZnS QDs with BSA.

According to Muñoz *et al.,* 2021 ternary QDs have become common practice for chemical evaluation of inorganic, organic and biological molecules depending on the binding affinity between the surface of QDs and the analyte. Furthermore, the electron-hole pair dispersion during the interaction between QDs and the analyte may quench or enhance the fluorescence signal. (Muñoz *et al.,* 2021). Herein, the interaction of bovine serum albumin (BSA) with GSH-capped AgInS/ZnS QDs was investigated and optimized using different conjugation and functionalization methods (i) concentration of BSA using two methods (ii) ratios of BSA: AgInS/ZnS QDs and (iii) use of activation agent (cross-linker) via carbonamide: EDC/NHS.

Effect of Concentration of BSA using two methods.

GSH-capped AgInS/ZnS core/shell QDs were conjugated with BSA at different concentrations of BSA (i.e., 0.2, 0.55, 0.7 and 0.9 mg/ml) respectively using two different methods; (i) addition of BSA with the ZnS shell denoted by AgInS/**BSA**ZnS and (ii)

addition of BSA with the core after the addition of $InCl_2$ precursor denoted by AgIn**BSA**S/ZnS. Figure 3.19 shows the fluorescence emission spectra of the AgInS/ZnS-BSA conjugate at different BSA concentrations. The as-synthesized AgInS/ZnS core/shell QDs have the maximum intensity at 681.71 a.u at a wavelength of 567.5 nm. The AgInS/ZnS-BSA conjugates synthesized using different methods resulted in either quenching or enhancement of fluorescence emission intensity. The first method, adding BSA with ZnS shell, resulted in quenching of fluorescence intensity for 0.9, 0.2 and 0.55 mg/ml with intensities of 584.36, 678.32 and 678.27 a.u respectively. While 0.7 mg/ml resulted in an enhanced intensity of 685.09 a.u. The second method, adding BSA after $InCl_2$ precursor, resulted in quenching of fluorescence intensity at 0.55 and 0.2 mg/ml with intensities of 678.57 and 678.32 a.um respectively. While at 0.9 and 0.7 mg/ml, fluorescence intensity was enhanced to 741.21 and 685.09 a.u respectively. The optimum fluorescence intensity thus was obtained at a concentration of 0.9 mg/ml.

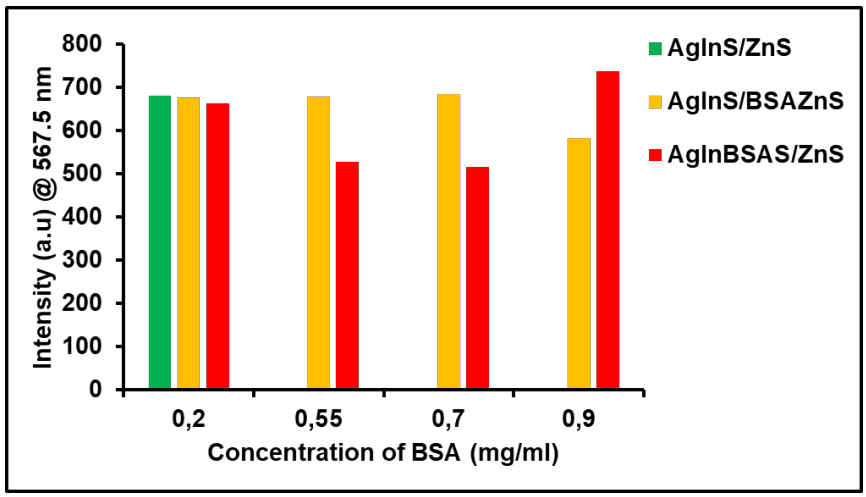

Figure 3.19: Bar graph of AgInS/ZnS QDs, and AgInS/ZnS-BSA conjugates synthesized using two methods at different concentrations.

Effect of AgInS/ZnS: BSA ratios.

To further improve the stability, optical properties, and biocompatibility of AgInS/ZnS-BSA conjugates, the fluorescence properties were optimized by varying AgInS/ZnS: BSA ratios. Whereby AgInS/ZnS was kept constant and BSA was varied (i.e., 0.9 mg/ml).

Figure 3.20 (a) and (b) depicts the optical properties of the as-synthesized material at different AgInS/ZnS: BSA ratios (1:1 to 1:5). It was discovered that the addition of BSA enhanced the fluorescence emission intensity with a slight blue-shift in PL peak position. Ratio 1:2 showed max fluorescence emission intensity at 559 nm. Further increase in BSA concentration (1:3 to 1:5) resulted in a reduction in fluorescence emission intensity. Thus, 1:2 was the optimum AgInS/ZnS: BSA ratio with a max intensity of 999.58 a.u. UV-vis absorption spectra revealed a slight blue shift and reduction in absorbance as concentration of BSA increased.

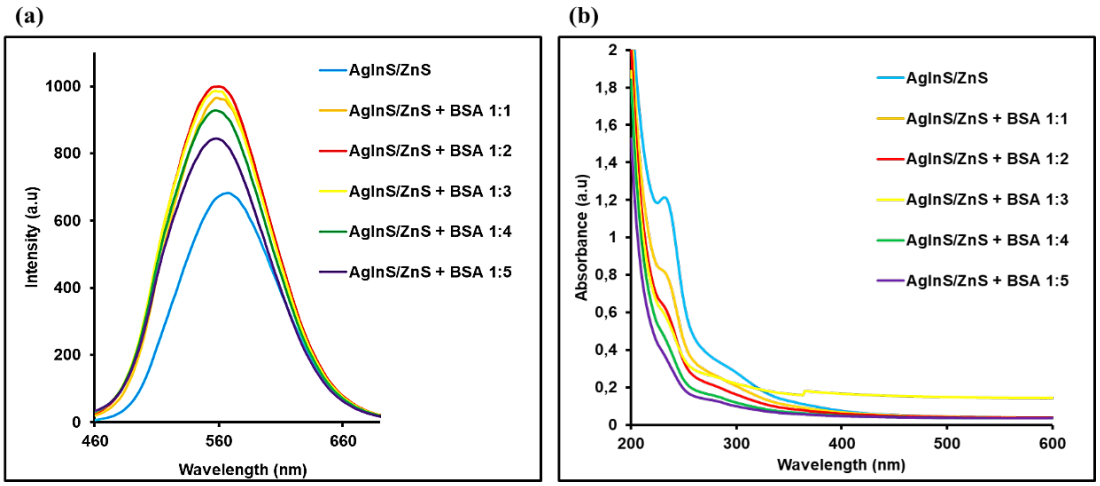

Figure 3.20: Photoluminescence (PL) spectra and (b) UV-vis spectra of AgInS/ZnS: BSA ratios.

Effect of cross-linker (EDC/NHS) on AgInS/ZnS-BSA conjugation

The cross-linking and conjugating biomolecules to various substrates are widely used in various fields such as chromatography, biomaterials, biosensors etc (Wang *et al.,* 2011). Cross-linking methods include chemical (glutaraldehyde, isocyanates, or carbodiimide-based), physical (de-hydrothermal) and enzymatic (Shepherd *et al.,* 2015) methods. Compared to other cross-linking reagents such as glutaraldehyde and formaldehyde, the EDC/NHS activation approach has advantages such as high conversion efficiency, mild reaction conditions, and excellent biocompatibility to influence the bioactivity of target

molecules. Due to these advantages, EDC/NHS activation of carboxylic acids and amidation reactions have been widely applied for biomolecule conjugation and immobilization of proteins, peptides, and DNA to many substrate polymers, silicon, nanotubes, and nanoparticles (Wang *et al.,* 2011). Figure 3.21 a and b, depicts the PL and UV-vis absorption spectra of AgInS/ZnS-BSA conjugate using activation agent EDC/HNS as a cross liker between the QDs and BSA with NHS and without NHS. In the presence of NHS, the results show quenching in PL intensity. In the absence of NHS the PL intensity slightly increased. The UV-vis absorption spectra disappearance of the excitonic peak of the AgInS/ZnS QDs after conjugation.

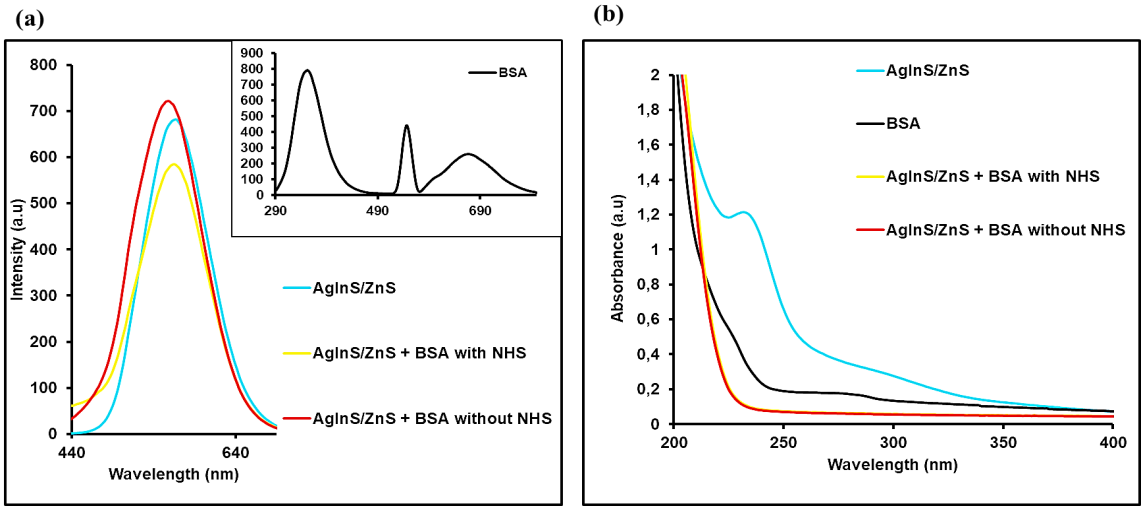

Figure 3.21: Photoluminescence (PL) spectra and (b) UV-vis spectra of AgInS/ZnS, BSA and AgInS/ZnS + BSA with NHS and without NHS (Insert: BSA).

3.3.7. Morphological and structural analysis of AgInS/ZnS-BSA conjugate and mechanism of AgInS/ZnS and BSA interaction

FTIR

To evaluate the nature of the binding, between AgInS/ZnS QDs and BSA and their interaction mechanism FTIR was studied. Figure 3.22 depicts the FTIR spectra of AgInS/ZnS QDS, pure BSA and AgInS/ZnS-BSA conjugate. The AgInS/ZnS QDs

exhibited peaks at 3384 cm^{-1}, 1560 cm^{-1} and 1358 cm^{-1} which were assigned to νOH group, asymmetrical and symmetrical stretches respectively (Vitshima *et al.,* 2022). The IR spectra of pure BSA at 3257 cm^{-1}, 1644 cm^{-1} and 1532 cm^{-1} were assigned to stretching vibrations of νOH, amide I band caused by stretching of νC=O group and amide II band comes from νNH_2 deformation of νNH bending and νC-N stretching in secondary amides respectively, which were observed by (Ye *et al.,* 2019) and (Ghosh *et al.,* 2012). Ranjan *et al.,* 2016, in proteins the amide I band contributes to exposed α-helix structure. In the absence of AgInS/ZnS QDs, pure BSA demonstrated an α-helix peak, the amide I band. While in the presence of AgInS/ZnS QDs a shift to 1618 in the exposed α-helix peak was observed. Furthermore, at 1532 cm^{-1} BSA demonstrated a β-sheet corresponding to the amide II band at 1532 cm^{-1}, in the presence of AgInS/ZnS QDs the peak shifted to 1579 cm^{-1}. The shifts observed in the α-helix and β-sheet peaks suggest that the secondary structure of BSA was distorted and the protein absorbs to the AgInS/ZnS QDs through exposed α-helix and β-sheets, thus forming the AgInS/ZnS-BSA conjugate.

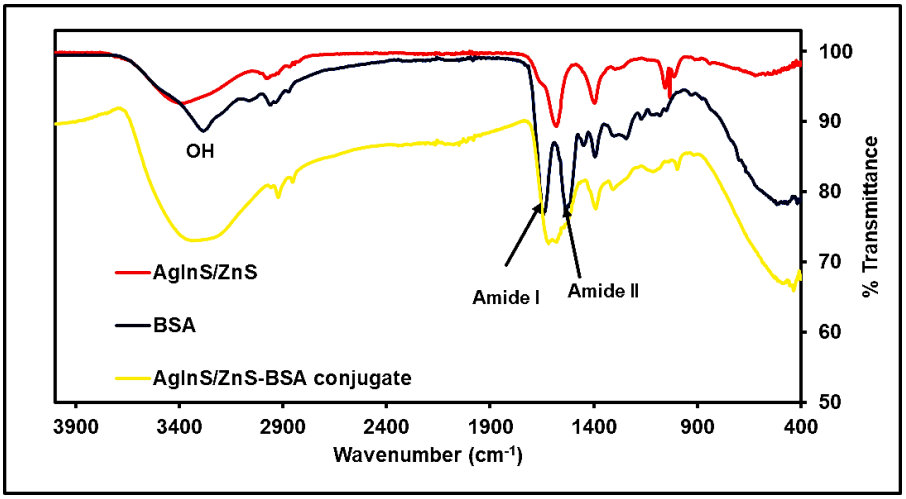

Figure 3.22: FTIR spectra of AgInS/ZnS QDs, BSA and AgInZnS-BSA conjugate.

EDX and SEM for QD-bioconjugate

The elemental composition and morphology were further evaluated for the AgInS-BSA core and AgInS/ZnS-BSA core/shell bioconjugate. Figure 3.23a depicts the EDX analysis

of QDs-bioconjugates. The spectra showed similar elemental composition to that of AgInS core and AgInS/ZnS core/shell QDs. However, the AgInS-BSA showed enhanced intensity on the peaks compared to AgInS core QDs, while the AgInS/ZnS-BSA showed a reduction in intensity compared to AgInS/ZnS QDs. This may be attributed to adsorption of BSA to the surface of the QDs. Figure 3.23b depicts the SEM morphologies of the as-synthesized material. For the AgInS-BSA the particles were more dispersed while for the AgInS/ZnS-BSA the particles were closely packed this might be due to the presence of BSA on the surface of the QDs.

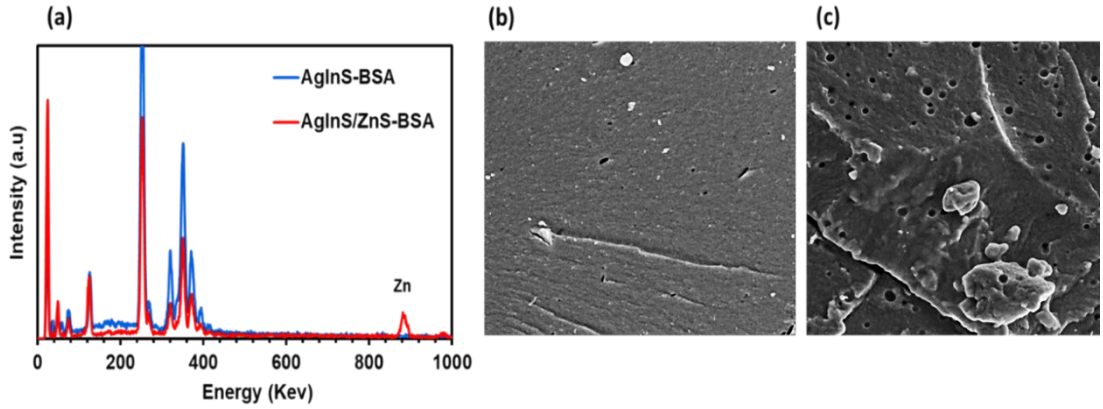

Figure 3.23: (a) EDX of AgInS-BSA and AgInS/ZnS-BSA, SEM (b) AgInS-BSA and (c) AgInS/ZnS-BSA.

3.4. Conclusion

The synthesis and optimization of AgInS/ZnS core/shell ternary QDs was done using three methods (i.e., reflux, heat-up methods and monowave 50 method). Various synthetic conditions such as reaction time, pH, Ag: In ratios, Zn/S shell layers, capping agent, GSH concentration and stabilizing agent on the fluorescence properties of the ternary AgInS/ZnS based QDs were examined. Optimal optical properties of the AgInS core QDs were obtained after 45 min synthesis at pH 7.58, Ag: In molar ratio of 1:4, GSH concentration of 0.145 mmol via reflux method. The addition of multiple ZnS shell

monolayers for the formation of AgInS/ZnS core-shell QDs resulted in a blue shift in PL peak position. FTIR analysis confirmed the formation of GSH capping on the QDs via S-metal bond. The highly negative zeta potential of the AgInS core QDs and the AgInS/ZnS core/shell QDs (-51.4 mV and -26.4 mV, respectively) showed the remarkable colloidal stability of the synthesized material. Furthermore, BSA conjugation with AgInS/ZnS QDs was confirmed using FTIR analysis. It was discovered that the as-synthesized AgInS/ZnS QDs were conjugated with BSA via the amide bonds. The AgInS/ZnS-BSA conjugate resulted in enhanced optical properties with enhanced stability. Thus, the as-synthesized materials can be useful in biological applications.

3.5. References

Aditha, S.K., Kurdekar, A.D., Chunduri, L.A., Patnaik, S. and Kamisetti, V., 2016. Aqueous based reflux method for green synthesis of nanostructures: Application in CZTS synthesis. MethodsX, 3, pp.35-42.

Aladesuyi, O.A. and Oluwafemi, O.S., 2020. Synthesis strategies and application of ternary quantum dots—in cancer therapy. Nano-Structures & Nano-Objects, 24, p.100568.

Chen, Y., Li, S., Huang, L. and Pan, D., 2013. Green and facile synthesis of water-soluble Cu–In–S/ZnS core/shell quantum dots. Inorganic chemistry, 52(14), pp.7819-7821.

Chen, Y., Wang, Q., Zha, T., Min, J., Gao, J., Zhou, C., Li, J., Zhao, M. and Li, S., 2018. Green and facile synthesis of high-quality water-soluble Ag-In-S/ZnS core/shell quantum dots with obvious bandgap and sub-bandgap excitations. Journal of Alloys and Compounds, 753, pp.364-370.

Delices, A., Moodelly, D., Hurot, C., Hou, Y., Ling, W.L., Saint-Pierre, C., Gasparutto, D., Nogues, G., Reiss, P. and Kheng, K., 2020. Aqueous Synthesis of DNA-Functionalized Near-Infrared AgInS2/ZnS Core/Shell Quantum Dots. ACS Applied Materials & Interfaces, 12(39), pp.44026-44038.

Ghosh, D., Mondal, S., Ghosh, S. and Saha, A., 2012. Protein conformation driven biomimetic synthesis of semiconductor nanoparticles. Journal of Materials Chemistry, 22(2), pp.699-706.

Girma, W.M., Fahmi, M.Z., Permadi, A., Abate, M.A. and Chang, J.Y., 2017. Synthetic strategies and biomedical applications of I–III–VI ternary quantum dots. Journal of Materials Chemistry B, 5(31), pp.6193-6216.

Hu, X., Chen, T., Xu, Y., Wang, M., Jiang, W. and Jiang, W., 2018. Hydrothermal synthesis of bright and stable AgInS2 quantum dots with tunable visible emission. Journal of Luminescence, 200, pp.189-195.

Kang, X., Huang, L., Yang, Y. and Pan, D., 2015. Scaling up the aqueous synthesis of visible light emitting multinary AgInS2/ZnS core/shell quantum dots. The Journal of Physical Chemistry C, 119(14), pp.7933-7940.

Kashchiev, D., 2020. Classical nucleation theory approach to two-step nucleation of crystals. Journal of Crystal Growth, 530, p.125300.

Kim, K.H., Jo, J.H., Jo, D.Y., Han, C.Y., Yoon, S.Y., Kim, Y., Kim, Y.H., Ko, Y.H., Kim, S.W., Lee, C. and Yang, H., 2020. Cation-exchange-derived InGaP alloy quantum dots toward blue emissivity. Chemistry of Materials, 32(8), pp.3537-3544.

Kiprotich, S., Onani, M.O. and Dejene, F.B., 2018. High luminescent L-cysteine capped CdTe quantum dots prepared at different reaction times. Physica B: Condensed Matter, 535, pp.202-210.

Leach, A.D. and Macdonald, J.E., 2016. Optoelectronic properties of CuInS2 nanocrystals and their origin. The journal of physical chemistry letters, 7(3), pp.572-583.

Masab, M., Muhammad, H., Shah, F., Yasir, M. and Hanif, M., 2018. Facile synthesis of CdZnS QDs: Effects of different capping agents on the photoluminescence properties. Materials Science in Semiconductor Processing, 81, pp.113-117.

May, B.M., Parani, S. and Oluwafemi, O.S., 2019. Detection of ascorbic acid using green synthesized AgInS2 quantum dots. Materials Letters, 236, pp.432-435.

McGown, A., Edmonds, A.K., Guest, D., Holmes, V.L., Dadswell, C., González-Méndez, R., Goodall, C.A., Bagley, M.C., Greenland, B.W. and Spencer, J., 2022. A Convenient, Rapid, Conventional Heating Route to MIDA Boronates. Molecules, 27(16), p.5052.

Miropoltsev, M., Kuznetsova, V., Tkach, A., Cherevkov, S., Sokolova, A., Osipova, V., Gromova, Y., Baranov, M., Fedorov, A., Gun'ko, Y. and Baranov, A., 2020. FRET-Based Analysis of AgInS2/ZnAgInS/ZnS Quantum Dot Recombination Dynamics. Nanomaterials, 10(12), p.2455.

Muñoz, R., Santos, E.M., Galan-Vidal, C.A., Miranda, J.M., Lopez-Santamarina, A. and Rodriguez, J.A., 2021. Ternary quantum dots in chemical analysis. Synthesis and detection mechanisms. Molecules, 26(9), p.2764.

Oluwafemi, O.S., May, B.M., Parani, S. and Rajendran, J.V., 2019. Cell viability assessments of green synthesized water-soluble AgInS2/ZnS core/shell quantum dots against different cancer cell lines. Journal of Materials Research, 34(24), pp.4037-4044.

Parani, S. and Oluwafemi, O.S., 2022. Synthesis, optical, structural and biocompatibility assessment of red-emitting CuInS2-ZnS quantum dots conjugated to folic acid. Nano-Structures & Nano-Objects, 32, p.100916.

Ranjan, S., Dasgupta, N., Srivastava, P. and Ramalingam, C., 2016. A spectroscopic study on interaction between bovine serum albumin and titanium dioxide nanoparticle synthesized from microwave-assisted hybrid chemical approach. Journal of Photochemistry and Photobiology B: Biology, 161, pp.472-481.

Ratnesh, R.K. and Mehata, M.S., 2017. Synthesis and optical properties of core-multi-shell CdSe/CdS/ZnS quantum dots: Surface modifications. Optical Materials, 64, pp.250-256.

Shepherd, D.V., Shepherd, J.H., Ghose, S., Kew, S.J., Cameron, R.E. and Best, S.M., 2015. The process of EDC-NHS cross-linking of reconstituted collagen fibres increases collagen fibrillar order and alignment. APL materials, 3(1), p.014902.

Shi, H., Jia, L., Wang, C., Liu, E., Ji, Z. and Fan, J., 2020. A high sensitive and selective fluorescent probe for dopamine detection based on water soluble AgInS2 quantum dots. Optical materials, 99, p.109549.

Soheyli, E., Azad, D., Sahraei, R., Hatamnia, A.A., Rostamzad, A. and Alinazari, M., 2019. Synthesis and optimization of emission characteristics of water-dispersible ag-in-s quantum dots and their bactericidal activity. Colloids and Surfaces B: Biointerfaces, 182, p.110389.

Tsolekile, N., Nahle, S., Zikalala, N., Parani, S., Sakho, E.H.M., Joubert, O., Matoetoe, M.C., Songca, S.P. and Oluwafemi, O.S., 2020. Cytotoxicity, fluorescence tagging and gene-expression study of CuInS/ZnS QDS-meso (hydroxyphenyl) porphyrin conjugate against human monocytic leukemia cells. Scientific reports, 10(1), pp.1-13.

Tsolekile, N., Parani, S., Vuyelwa, N., Maluleke, R., Matoetoe, M., Songca, S. and Oluwafemi, O.S., 2020. Synthesis, structural and fluorescence optimization of ternary Cu–In–S quantum dots passivated with ZnS. Journal of Luminescence, 227, p.117541.

Wang, C., Yan, Q., Liu, H.B., Zhou, X.H. and Xiao, S.J., 2011. Different EDC/NHS activation mechanisms between PAA and PMAA brushes and the following amidation reactions. Langmuir, 27(19), pp.12058-12068.

Wang, L., Kang, X. and Pan, D., 2017. Gram-scale synthesis of hydrophilic PEI-coated AgInS2 quantum dots and its application in hydrogen peroxide/glucose detection and cell imaging. Inorganic Chemistry, 56(11), pp.6122-6130.

Wu, K.J., Edmund, C.M., Shang, C. and Guo, Z., 2022. Nucleation and growth in solution synthesis of nanostructures–From fundamentals to advanced applications. Progress in Materials Science, 123, p.100821.

Xiong, W.W., Yang, G.H., Wu, X.C. and Zhu, J.J., 2013. Microwave-assisted synthesis of highly luminescent AgInS 2/ZnS nanocrystals for dynamic intracellular Cu (ii) detection. Journal of Materials Chemistry B, 1(33), pp.4160-4165.

Xiong, W.W., Yang, G.H., Wu, X.C. and Zhu, J.J., 2013. Microwave-assisted synthesis of highly luminescent AgInS 2/ZnS nanocrystals for dynamic intracellular Cu (ii) detection. Journal of Materials Chemistry B, 1(33), pp.4160-4165.

Xu, L., Sithambaram, S., Zhang, Y., Chen, C.H., Jin, L., Joesten, R. and Suib, S.L., 2009. Novel urchin-like CuO synthesized by a facile reflux method with efficient olefin epoxidation catalytic performance. Chemistry of materials, 21(7), pp.1253-1259.

Ye, Q., Guo, L., Wu, D., Yang, B., Tao, Y., Deng, L. and Kong, Y., 2019. Covalent functionalization of bovine serum albumin with graphene quantum dots for stereospecific molecular recognition. Analytical Chemistry, 91(18), pp.11864-11871.

Chapter 4

Sensing of Vascular endothelial growth factor using AgInS/ZnS QDs

4.1. Introduction

Electrochemical sensors are a highly effective subclass of chemical sensors that use an electrode as the transduction element and are highly qualified for meeting the size, cost, and power requirements of on-site environmental monitoring. Characteristics of electrochemical sensing systems include high sensitivity and selectivity, a broad linear range, and inexpensive instrumentation (Hanrahan *et al.,* 2004). The incorporation of nanomaterials for electrochemical sensors has been of great benefit, with recent improvements in sensitivity, selectivity, and biocompatibility in electrochemical sensors (Jackowska and Krysinski, 2013). For the developed electrochemical sensors and biosensors to reach their maximum potential, it is crucial to use electrochemical techniques suitable for the sensor and target analytes (Qian *et al.,* 2021). Electrochemical techniques have been used to analyze a variety of drug molecules because they offer very low detection limits for electroactive molecules (Okumu *et al.,* 2020).

Electrochemical techniques play an essential role in studying metal nanoparticles as electrons may undergo quantum confinement effects reflected in their electrochemical behaviour. Quantum dots are receiving considerable attention due to their high fluorescence, making them suitable for biological and medical applications. Studying these materials in electrochemistry and electron-conducting electrodes is of great importance in finding relevant information on the structure and composition of nanoparticulate entities and their application in catalysis and sensing (Aliofkhazraei, 2016). This chapter focuses on evaluating the electrochemical properties of AgInS core QDs, AgInS/ZnS core/shell QDs and AgInS/ZnS-BSA QD-bioconjugates for sensing of vascular endothelial growth factor using electrochemical techniques such as cyclic voltammetry (CV), differential pulse voltammetry (DPV), square wave voltammetry (SWV) and electrochemical impedance spectroscopy (EIS).

CV has been shown as the most popular characterization method for analyzing analytes. It is useful for determining reaction kinetics, including the number of electrons transferred, stoichiometry, reversibility, and the reaction type. DPV and SWV are frequently used for electrochemical detection because of their higher sensitivity compared to CV. The detection limits that DPV can reach are 10^{-8} M or less (Qian *et al.,* 2021). While EIS is one of the most attractive diagnostic methods because of its applicability, quickness, precision, and low cost. It can isolate and measure the cell resistance of the bulk (Rb), charge transfer reaction (Rct) and diffusion process (Choi et al., 2020).

4.2. Experimental

4.2.1. Materials and reagents

The materials and chemicals for the fabrication of the sensor, AgInS QDs, AgInS/ZnS QDs, AgInS-BSA core and AgInS/ZnS-BSA core/shell QDs bioconjugates were used as mentioned in the previous chapter. As mentioned in the previous chapter, NaCl, KCl, Na2HPO4·12H2O, KH2PO4 and NaOH were used for PBS preparation. Hydrochloric acid (HCl) and vascular endothelial growth factor (VEGF) were obtained from Sigma Aldrich.

Apparatus

A typical conventional one-compartment, three-electrode setup connected to a potentiostat Autolab PGSTAT 101 (Metrohm, SA) operating software NOVA 2.1 was used to conduct electrochemical experiments (CV, DPV, and SWV). Glassy carbon (GC) was used as the working electrode, together with a platinum auxiliary electrode and an Ag/AgCl reference electrode. The GCE was polished with different concentrations of alumina powder between the experiments to remove any residue deposits on the surface. Unless stated otherwise, all experiments were run using HCl (0.01 M) and PBS (0.10 M)

solution over a potential range -1.5 to +1.5 V. The synthetic metal quantum dots solution was dissolved in electrolyte solution. The blank solution of 0.01M HCl and 0.1M PBS was first analyzed to determine the background signal and the solution AgInS QDs, AgInS/ZnS QDs, AgInS-BSA core and AgInS/ZnS-BSA core/shell QDs bioconjugates were investigated. All electrochemical experiments were carried out in solutions purged with high-purity nitrogen gas for 5 min. CV voltammograms for kinetic studies were obtained at scan rates by varying potential ranges against (Ag/AgCl).

Optimisation; effect of concentration of BSA and AgInS/ZnS: BSA ratio

GCE was modified with different concentrations of BSA for AgInS/ZnS-BSA bioconjugates (i.e., 0.2, 0.5, 0.7 and 0.9 mg/ml) and different AgInS/ZnS: BSA ratios (i.e., 1:1, 1:2, 1:3, 1:4 and 1:5) via drop coating method. Then, the electrodes were left to dry at room temperature before use. EIS and DPV was used for electrochemical studies.

VGEF preparation and detection

Under the optimized conditions, the fabricated immunosensor was used for detecting VEGF.

VEGF was prepared by diluting 10 μg in 1 ml of PBS. The sensor was incubated with various

concentrations of VEGF (3.33×10^{-3} – 1.70×10^{-2} μg/ml) in an electrochemical cell containing 3 mL of 0.1 M PBS buffer at pH 7.4. CV, DPV, SWV was used to measure the current response. The parameters used technique were potential of -1.5 to +1.5 V, scan rate of 30 to 270 mV/s, amplitude of 20 mV and frequency of 25 Hz.

Stability studies

The stability of the biosensor was studied using DPV for over 5 weeks.

4.3. Results and Discussion

4.3.1. Electrochemical Characterisation of AgInS core and AgInS/ZnS core/shell QDs

Figure 4.1 A and B represent the characterization of AgInS core QDs and AgInS/ZnS core/shell QDs. In figure 4.1A and B, typical CVs and DPVs were evaluated and compared in 0.01M HCl.

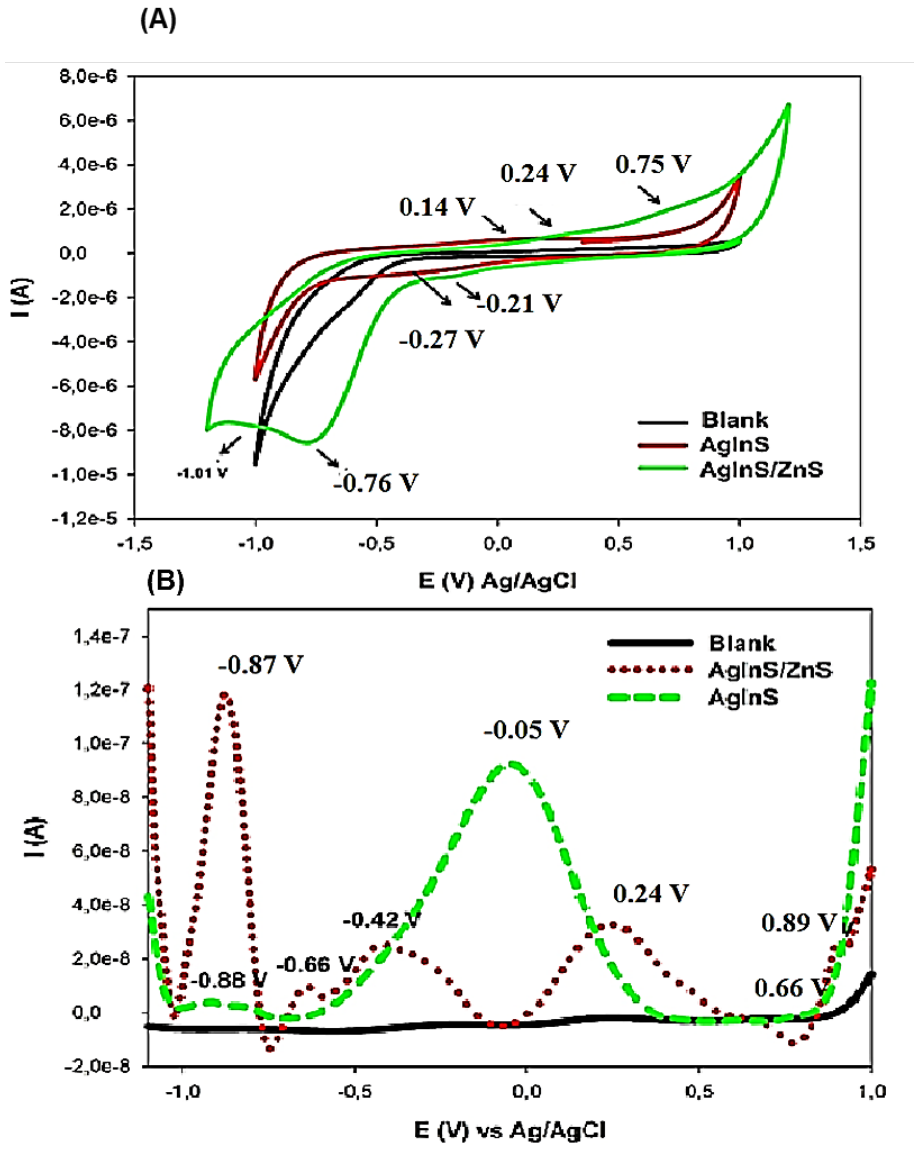

Figure 4.1: CVs a) and DPVs b) obtained at GCE, blank, AgInS core QD, and AgInS/ZnS Core/shell QD in 0.01 M HCl at scan rate 0.1 V/s.

Comparative cyclic voltammograms (CV) and differential pulse voltammograms (DPV) of AgInS core QDs and AgInS/ZnS core/shell QDs at the Glassy carbon electrode (GCE) in 0.01 M HCl solution are shown in Figure 4.1 at a scan rate of 0.1 V/s. In the absence of the QDs, there was no response observed at the GCE in 0.01 M HCl in either CV or DPV. A pair of weak redox peaks were observed in a CV of AgInS core QDs at (Epa) = 0.14 and Epc = -0.27 V with a formal potential of -0.065 V vs Ag/AgCl when comparing the electrochemical behaviour of AgInS core QDs with AgInS/ZnS core/shell QDs.

Ag ions produced by AgInS core QDs are responsible for the oxidation peak at 0.14 V, and the reduction peak at -0.27 V is linked to the reduction of Ag^{+} to Ag^{0}. This observation and related behaviour have previously been described (Okumu *et al.,* 2020; van der Horst *et al.,* 2016, Choi *et al.,* 2011). An interesting finding was discovered in the CV of the AgInS/ZnS core/shell QDs about the formation of a small cathodic peak at (Epc) = -1.01 V versus Ag/Cl and two sets of redox signals that appeared at (Epa) = 0.24 and 0.75 V and (Epc) = -0.21 and -0.76 V and correspond to the following reactions:

$$Ag^{0} \longrightarrow Ag^{+} + e \qquad \text{Equa 1}$$

$$Ag + e \longrightarrow Ag^{0} \qquad \text{Equa 2}$$

$$In^{0} \longrightarrow In^{3+} + 3e \qquad \text{Equa 3}$$

$$In^{3+} + 3e \longrightarrow In^{0} \qquad \text{Equa 4}$$

Further investigations were done to characterize the electrochemical properties of AgInS core QDs and AgInS/ZnS core/shell QDs (Figure 4.1B). DPV was used as a fast, effective, and more sensitive electrochemical technique compared to CV *(Wang et al., 2015).* Figure 4.1B shows that the AgInS core QDs DPV showed distinct oxidation peaks centred at potentials of -0.05 and -0.88 V versus Ag/AgCl for Ag and In ions, respectively, while the AgInS/ZnS core/shell QDs displayed three symmetrically spaced oxidation peaks at

potentials of -0.87, -0.66, and -0.42 V for Zn, In, and Ag The CV data and DPV data are in agreement. But compared to DPV, the current response of AgInS/ZnS core/shell QDs in the case of CV is higher. This might be because of the effective elimination of capacitance current.

4.3.2 Electrochemical Kinetics Studies

To examine the rate-limiting step on AgInS QDs core and AgInS/ZnS core shell QDs in Figure 4.2 A and B involved investigations on scan rates (10 mV/s to a maximum scan rate of 200 mV/s). According to the Randles-Sevcik equation: (Equation 4.1) (Kissinger, 1996), the total number of electrons, electron transport diffusion coefficient, De (in cm^2 s^1), and surface concentration of soluble species that react on the electrode surface with the formation of insoluble product, can all be calculated.

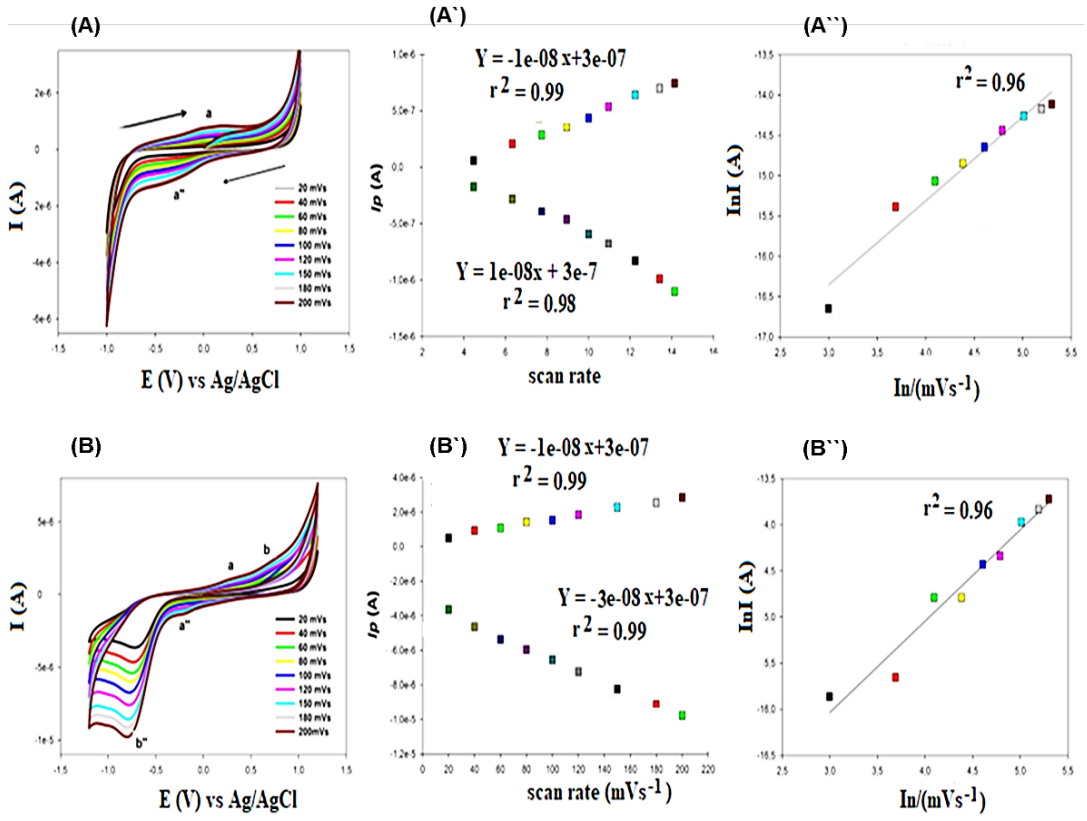

Figure 4.2: Cyclic voltammetry for the effect of variation of scan rates (20mV/s to 200 mV/s) of AgInS/ZnS core(A) and AgInS/ZnS core/shell (B)l from 1.0 to 1.0 V/s on a GCE in 0.01M HCl, (A` and B`) graph of the dependence of the anodic and cathodic peak current with square root scan rate (A`` and B``) graph of In anodic peak current vs In scan rate c).

$$Ip = 2.69\ x\ 10^5\ n^{2/3}\ .A\ .D_{OX}^{1/2}\ .C_{OX}^{*}\ .V^{1/2} \qquad Equa\ 4.1$$

Where Ip is the peak current, n is the total number of electrons transported, A is the working area, 0.0707 cm^2, and C is the concentration. These findings determined the number of electrons for AgInS QDs and AgInS/ZnS QDs, respectively, to be 1.08 and 0.75 utilizing the Ag peak. This demonstrates that a one-electron reaction occurs at the GCE in 0.01M HCl for both AgInS core QDs and AgInS/ZnS core/shell QDs. The value of De was found to decrease in the order AgInS core QDs > AgInS/ZnS core/shell QDs. This indicates that the electron diffusion was the slowest in the AgInS/ZnS QDs. The surface concentration of the AgInS QDs and AgInS/ZnS QDs on a GCE was also calculated by applying Equation 4.2 (Akinyeye *et al.,* 2007; Brown, 1977) and using the slope for the plot of Ip vs square root scan rate.

$$Slope = \frac{n^2.F^2\ .A.\Gamma}{4RT} \qquad Equa\ 4.2$$

Where Ip is the peak current at a given scan rate V, n is the number of electrons transferred, F is the Faraday constant and A is the geometric area of the electrode. The electroactive surface concentration of AgInS QDs was greater than that of AgInS/ZnS QDs.

Furthermore, two ways widely employed to study a reaction's reversibility and assess whether a reaction is adsorption or diffusion consist of the dependencies: Ip vs v½ and In Ip vs In v (Bard and Faulkner, 2001, Kessinger 1996). According to the Randles-Sevcik equation, the square root of the scan rate and the peak current (Ip) of a freely diffusing reversible electrochemical species have a linear relationship. Deviation from this equation can indicate surface adsorption or quasi-reversible adsorption. The peak current (Ipa) in Figure 4.2 (A') increases linearly with the scan rate's square root, while the peak current (Ipc) for scan rates less than 0.1 V/s increases linearly with the square root (Figure 4.2B').

At a scan rate greater than 0.1V/s deviates exhibiting values lower than those expected, a feature typical observed when an electrochemical reaction involves a nucleation step (Hills *et al.,* 1974). As the Randles-Sevcik equation suggests, the relationship between Ip and square root scan rate deviates, showing values lower than expected, a feature of a quasi-reversible and adsorption control system. In contrast, the slope of the In Ip vs Inv plot was 0.8739, which is quite close to 1 and indicates an adsorption-controlled system. A slope of 1 or close to one is expected for the adsorption process. Figure 4.2 (B) shows the scan rate influence for AgInS/ZnS core/ shell QDs. The values of the oxidation and reduction peak currents plotted against square root scan rates (Figure 4.2 B') were both linear, but they did not pass the origin, which is a sign of a quasi-reversible and adsorption control system. In Figure 4.2 B"' the plot of In Ip vs Inv gave a slope of 1.0386, indicating an adsorption-controlled system. The summary of kinetics parameters is shown in Table 4.1.

Table 4.1: Diagnostic kinetics parameters of AgInS core and AgInS/ZnS core/shell QDs.

GCE	**E^0(V)**	**N**	**De (cm^2 s^{-1})**	**Γ(mol. cm^{-1})**
AgInS QDs	-0.065	1.08	$1.33x10^{-18}$	$3.18x10^{-6}$
AgInS/ZnS QDs	0.015	0.75	$8.11x10^{-20}$	$9.42x10^{-7}$

4.4. Electrochemical characterization of AgInS/ZnS-BSA bioconjugates

4.4.1. CV and EIS Characterisation of AgInS/ZnS, AgInS-BSA core and AgInS/ZnS-BSA core/shell bioconjugates.

CV and EIS were also used to study the chemical and physical processes occurring at AgInS/ZnS core/shell, AgInS-BSA and AgInS/ZnS-BSA. In this study CV, was used as a qualitative technique as the sensitivity is limited by charging current. Therefore, for quantification of the analyte of interest, DPV was used.

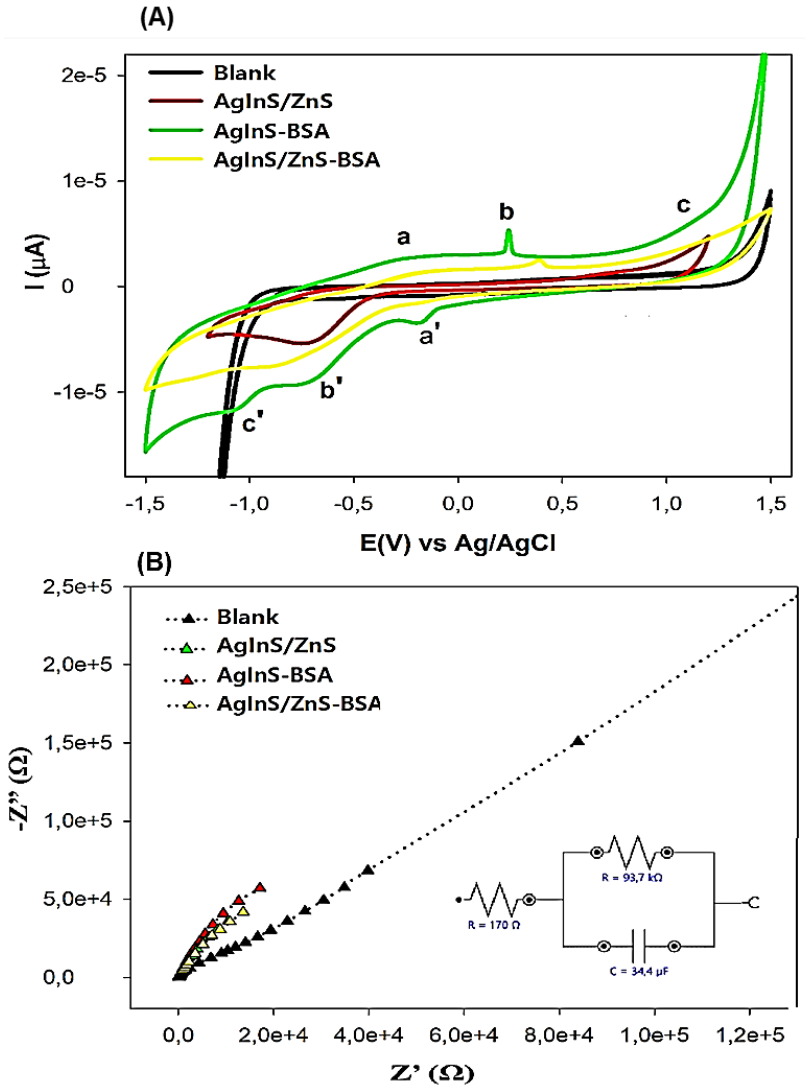

Figure 4.3: CV (A), and Nyquist plots (B) of a Bare GCE, AgInS/ZnS, AgInS-BSA core and AgInS/ZnS-BSA core/shell bioconjugates at 0.1M PBS buffer solution (pH 7.4).

The cyclic voltammetry results of the AgInS/ZnS core/shell QDs, AgInS-BSA core QDs and AgInS/ZnS-BSA core/shell QDs. AgInS/ZnS core/shell QDs without BSA has shown oxidation peaks at potentials 0.25, and 0.77V, while reduction peaks appeared at potentials -0.15 V, -0.72 V., and -1.03 denoted as (A/A', B/B' and C/C'). AgInS/ZnS-BSA has shown oxidation peaks at potentials -0.23 and 1.14 V with the reduction peaks at -0.11 and -0.72 V. Similarly, AgInS-BSA core QDs core showed a pair of redox peaks at potentials -0.23/-0.15 V, 0.25/0.68 V and 1.14/1.05 V. The readers referred to 4.1 for the

detailed origin of these peaks and the values of anodic and cathodic potentials are shown in Table 4.5.

To further study the interaction of BSA with AgInS/ZnS core/shell QDs, Electrochemical impedance spectroscopy (EIS) was used as an effective technique to determine the electron transfer kinetics for AgInS/ZnS core/shell QDs in the absence and presence of BSA. The Nyquist plots in Figure 4.3B were studied to determine the Rct (charge transfer resistance) value that controls the electron transfer kinetics. According to Nxele *et al.,* 2022, a Rct value indicates improved charge transfer. Various values of circuit parameters calculated by fitting spectra are displayed in Table 4.2. The data shows that bare GCE (blank) has the highest Rct value of 1710 KΩ. Upon the addition of AgInS/ZnS core/shell QDs on the electrode surface, the Rct decreased to 83.1 KΩ. This confirmed the existence of lower diffusion resistance and excellent conductivity at electrode/electrolyte surface due to the accessibility of electrolyte ions within the electrode (Sankar *et al.,* 2015). From Table 4.2, the sequence of the Rct values is in order, blank electrolyte > AgInS BSA core QDs > AgInS/ZnS-BSA core/shell QDs.

Table 4.2: Summary of results for Bare GCE, AgInS/ZnS, AgInS-BSA core and AgInS/ZnS-BSA core/shell bioconjugates determined using EIS.

Material	**Rs (Ω)**	**Rct (KΩ)**	**C (µF)**
Blank	3260	1710	1.54
AgInS/ZnS core/shell QD	169	83.1	49.4
AgInS-BSA core QD	164	172	19.8
AgInS/ZnS-BSA core/shell QDs	170	93.7	34.4

4.4.2. Electrochemical Kinetics of AgInS-BSA and AgInS/ZnS-BSA bioconjugates.

The effect of various scan rates on the electroactivity and electron transfer processes of AgInS-BSA core and AgInS/ZnS-BSA core/shell bioconjugates was investigated from scan rates (20mV/s to 280mV/s) as can be seen in Figure 4.4A and B.

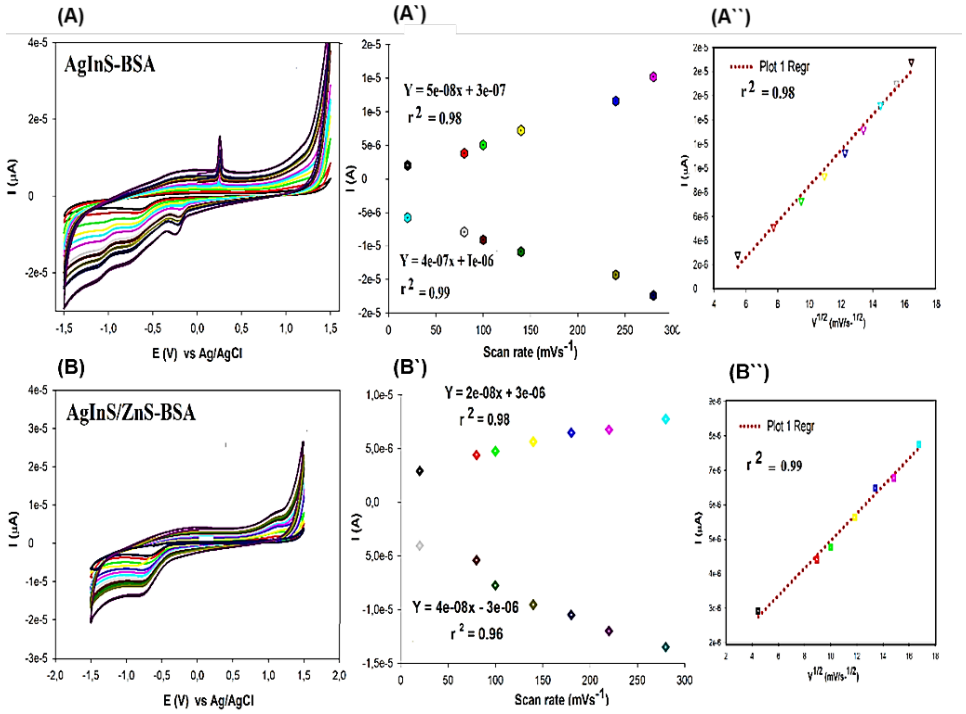

Figure 4.4: The Cyclic voltammetry for the effect of variation of scan rates (20 mV/s to 280 mV/s) of (A) AgInS-BSA core, (A') Randle`s plot insets square root scan rate, (B) AgInS/ZnS-BSA core/shell, B' AgInS/ZnS-BSA bioconjugates from -1.5 to 1.5 V/s on a GCE in pH 7.4 PBS buffer.

The observation obtained for AgInS-BSA core/shell QDs and AgInS/ZnS-BSA core/shell QDs resulted in increased peak current as the scan rate increased for both anodic and cathodic peaks with peak current ratio of close to1.00 for both materials. The reduction peaks shifted towards more negative potentials. This is an indication of reversibility to quasi-reversible behaviour. Change in potentials (ΔEp) values agree with standard

difference for one electron reaction, that is 0.059 for fast electron transfer process. However, the largest increase in peak current was observed in the AgInS-BSA core bioconjugate compared to the AgInS/ZnS-BSA core/shell. According to Timakwe *et al.,* 2022, as the size of nanoparticles decrease the peak potential shift to less negative potentials. This was also reflected in PL spectra and UV-vis absorption for the QD-BSA core/shell bioconjugate with narrow peaks, indicating the formation of smaller particles suitable for biological applications.

4.4.3. Optimization conditions of AgInS/ZnS-BSA conjugate.

Effect of BSA concentration

Figure 4.5 shows the influence of BSA concentrations on AgInS/ZnS core/shell QDs. Four concentrations (0.2, 0.5, 0.7 and 0.9 mg/ml were evaluated and their effect on peak shape and peak current density were observed using DPV and EIS.

To obtain high response signals and improve the detection sensitivity the effect of BSA concentrations were studied using differential pulse voltammetry (DPV) and EIS. The DPV results revealed that as the concentration of BSA increased from 0.2 to 0.9 mg/ml the was an increase in current density. High concentrations of 0.7 and 0. 9 mg/ml of BSA were found to produce the best voltammograms with more symmetrical, narrow and sharp peaks which shifted in cathodic direction. The optimum conditions were obtained in 0.9 mg/ml, thus indicating the improved interaction of quantum dots.

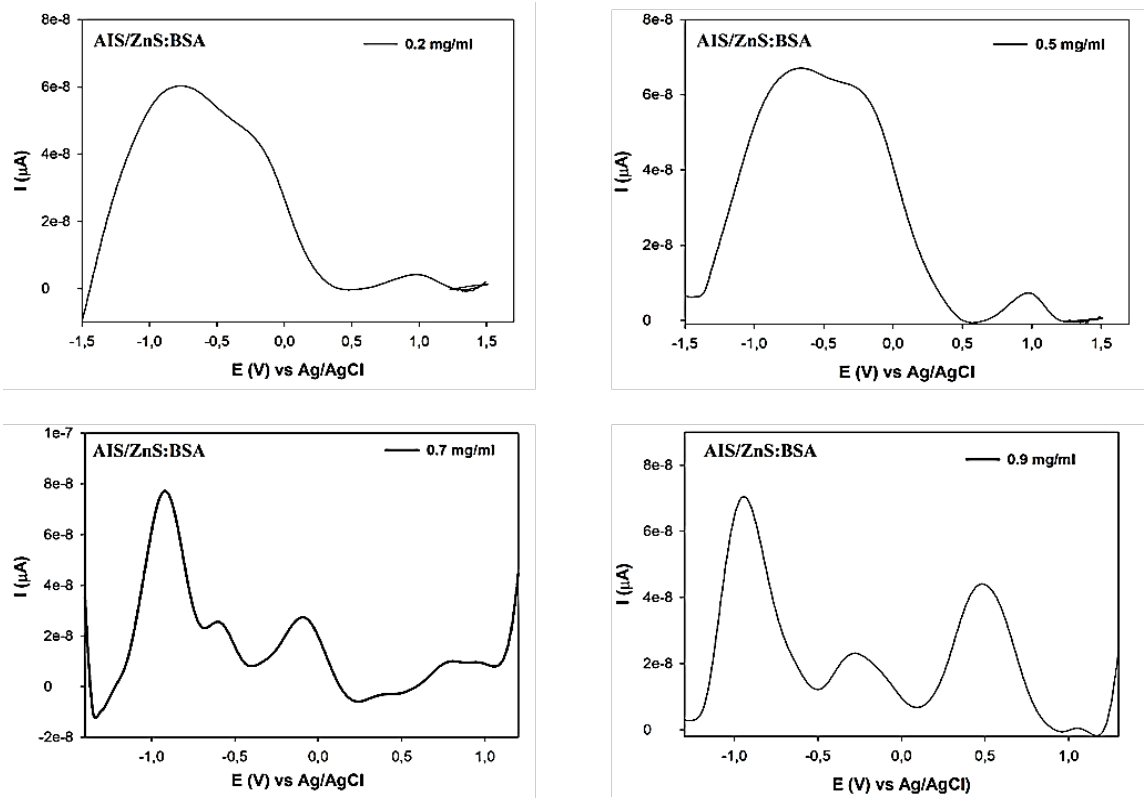

Figure 4.5: DPVs obtained at GCE, AgInS/ZnS-BSA core/shell bioconjugate at different BSA concentrations in pH 7.4 PBS buffer solution

Further investigation was done on the effect of BSA concentration using EIS. The Nyquist plots in Figure 4.6 obtained at different concentrations of BSA was studied to determine charge transfer (Rct) values. The Rct values are summarized in table 4.2. Low Rct values were observed for the AgInS/ZnS-BSA bioconjugate at 0.2 and 0.5 mg/ml (93.70 KΩ), followed by 0.9 mg/ml (99.60) and 105.00 mg/ml of BSA concentration. The highest Rct values were observed at 0.2 and 0.5 mg/ml suggesting improvement in charge tranfer. However, due to the highly distinct peaks observed in DPV analysis, 0.9 mg/ml of BSA was subsequently chosen for further analysis.

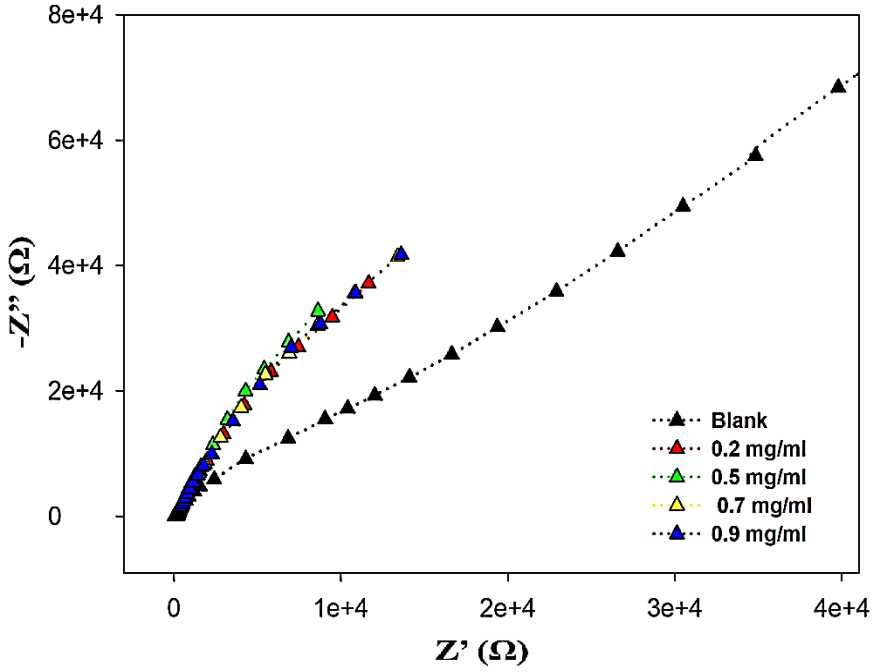

Figure 4.6: Nyquist plots of a Bare GCE and AgInS/ZnS-BSA core/shell bioconjugates at different BSA concentrations in pH 7.4 PBS buffer solution.

Table 4.3: Summary of results for Bare GCE and different concentrations of BSA for AgInS/ZnS-BSA core/shell bioconjugates determined using EIS.

Concentration (mg/ml)	**Rs (Ω)**	**Rct (kΩ)**	**C (µF)**
Blank	3260	1710	1.54
0.2	170	93.70	34.4
0.5	157	93.70	40.0
0.7	188	105.0	29.1
0.9	191	99.60	35.9

Effect of AgInS/ZnS: BSA ratios

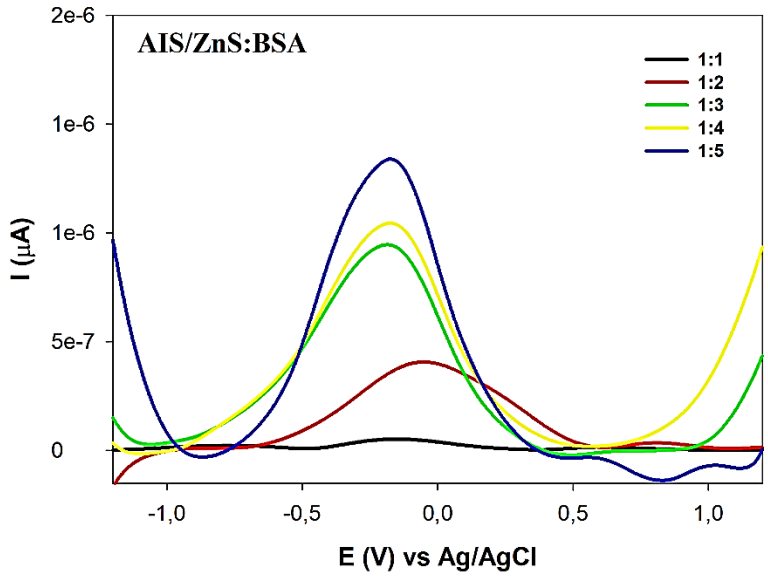

Figure 4.7: DPVs obtained at GCE, AgInS/ZnS-BSA core/shell bioconjugate at different ratios in 0.1M PBS (pH, 7.4) buffer solution.

Figure 4.7 depicts the DPV voltammograms at different AgInS/ZnS: BSA ratios. By analysing the DPV voltammograms the peak current increased with increasing ratio of BSA. Highly distinct peak current was observed at 1:5 ratio, while the least signal was observed at 1:1 ratio.

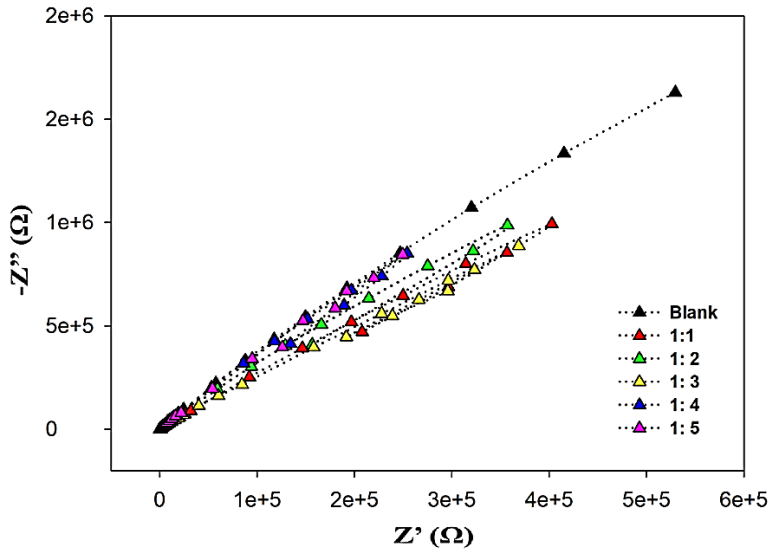

Figure 4.8: Nyquist plots of a Bare GCE and AgInS/ZnS-BSA core/shell bioconjugates at different BSA ratios in 0.1 MPBS pH 7.4 buffer solution.

EIS was further used to determine the electron kinetics for the AgInS/ZnS: BSA ratios. The Nyquist plots in Figure 4.8 were used to determine the Rct values which are summarized in Table 4.4. It is worth noting the lowest charge transfer (Rct) was at ratio 1:3 followed by 1:1 and 1:2 with very close values, while 1:4 and 1:5 also gave the very close value of Rct suggesting high conductivity (Nxele *et al.,* 2021).

Table 4.4: Summary of results for Bare GCE and different ratios of BSA for AgInS/ZnS-BSA core/shell bioconjugates determined using EIS.

Ratio	**Rs (Ω)**	**Rct (kΩ)**	**C (µF)**
Blank	3180	2240	0.65
1:1	139	886	0.89
1:2	138	893	1.25
1:3	122	693	0.54
1:4	124	936	1.35
1:5	98.2	931	1.52

4.5. Electrochemical sensing of VEGF at AgInS/ZnS-BSA core/shell QDs bioconjugate

Substantial information on the electrochemical processes that occur on AgInS/ZnS core/shell QDs for the detection of VEGF was studied using various electrochemical techniques such as CV, DPV and SWV. Generally, CV is usually used as a tool for determination of redox mechanisms, electron transfer kinetics and formal potentials. While DPV and square wave are used for electroanalysis and considered more sensitive compared to CV (Hussain and Silvester, 2018).

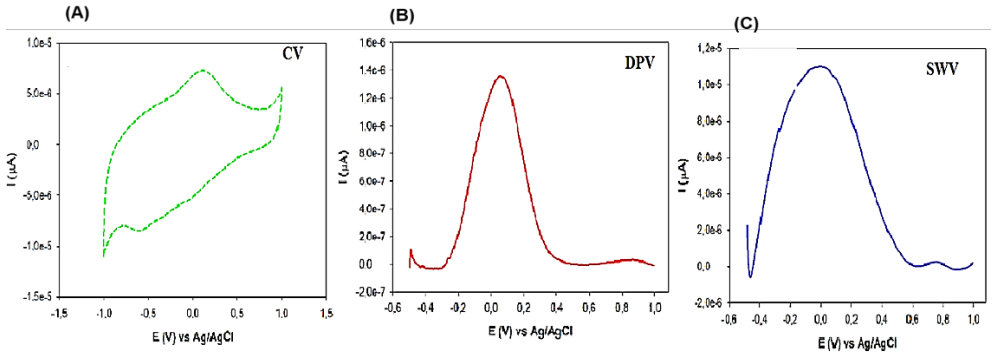

Figure 4.9: CV (A), DPV (B) and SW (C) voltammograms of AgInS/ZnS-BSA in the presence of EVGF at 0.06 V/s in 0.1M PBS (pH 7.4).

Figure 4.9 shows the comparative voltammograms of CV, DPV and square wave. DPV was observed to be more sensitive compared to square wave due to its narrow distinct peak compared to broad peak in square wave. Therefore, DPV were used for further detection.

4.5.1. Effects of scan rates on the determination of VEGF at AgInS/ZnS-BSA core/shell QDs.

The effects on the electrochemical behaviour of VEGF at AgInS/ZnS-BSA core/shell QDs were investigated by varying scan rates using cyclic voltammetry. The scan rate studies were conducted using CV with scan rates from 30 to 270 mV/s. With the increase in scan rate the peak current also increased as shown in Figure 4.12. The increase in peak current with increase in scan rate was also observed by van der Horst *et al.,* 2017.

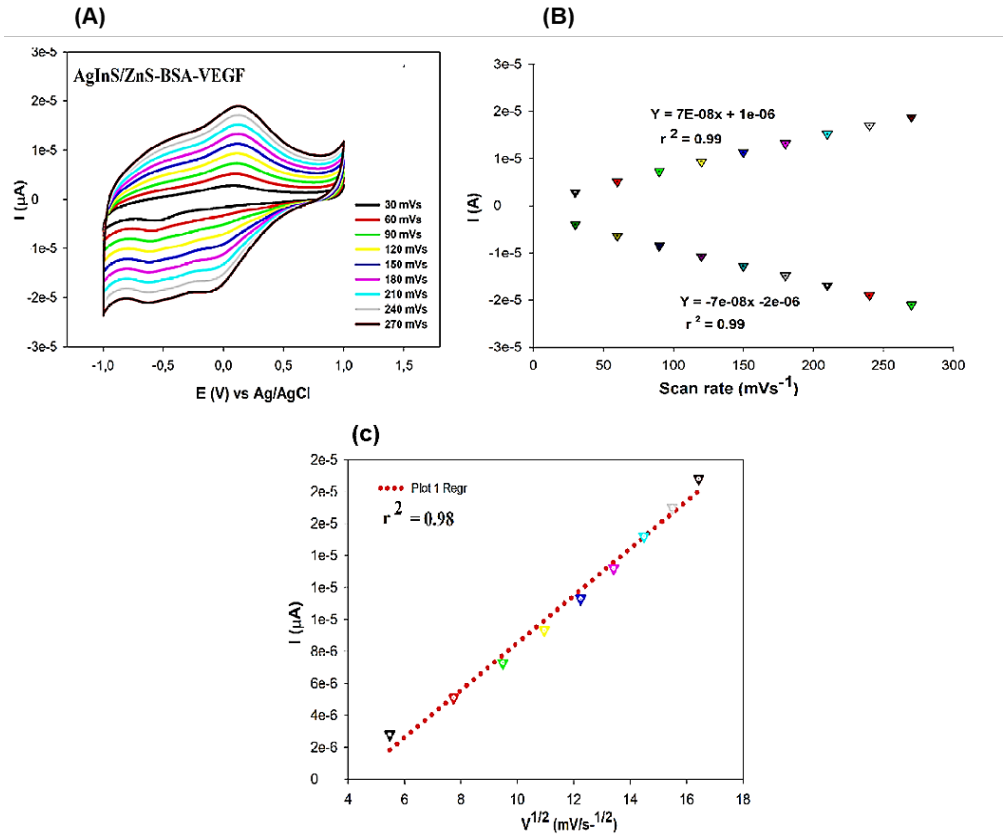

Figure 4.10: The Cyclic voltammetry for the effect of variation of scan rates (30 mV/s to 270 mV/s) of VEGF from -1.5 to 1.5 V/s on a GCE in pH 7.4 PBS buffer.

Figure 4.10 shows that the peak current increases by increasing the scan rate**.** It was also observed that the peaks of interest were not affected by changes in scan rate. The oxidation and reduction peaks tend to be stable. The plot of peak current vs scan rate resulted in a straight line for both oxidation and reduction peaks (Figure 4.10B) suggesting interaction of AgInS/ZnS-BSA was an adsorption-controlled process. The plot of peak current vs square root of scan rate (Figure 4.10 C) also gave linear relationship. Table 4.5 shows the summary of all cyclic voltammetry data of the conjugates. The most intense peaks were used to calculate the value of n (number of electrons transferred).

Table 4.5: Summary of all cyclic voltammetry data for all the studied materials with BSA and without BSA and in the presence of VEGF at 60mVs^{-1}.

Material	**Epa (V)**	**Epc (V)**	**Ipa/Ipc**	**N**	**∆Ep (V)**
AgInS/ZnS-BSA	-0.23	-0.11	0.34	-	
	1.14	-0.72	0.93	0.99	0.0596
AgInS-BSA	-0.24	-0.15	0.91		
	0.24	-0.67	0.50		
	1.15	-1.05	1.10	0.98	0.060
AgInS/ZnS-BSA-VEGF	-0.52	-0.38	0.50		
	0.12	-0.56	0.34	0.94	0.063

4.5.2. Effects of VEGF concentrations on AgInS/ZnS-BSA core/shell QDs bioconjugate electrode surface

Figure 4.11 shows the relationship in response of AgInS/ZnS-BSA core/shell sensor to VEGF antibody using DPV in 0.1 M, PBS, pH 7.4.

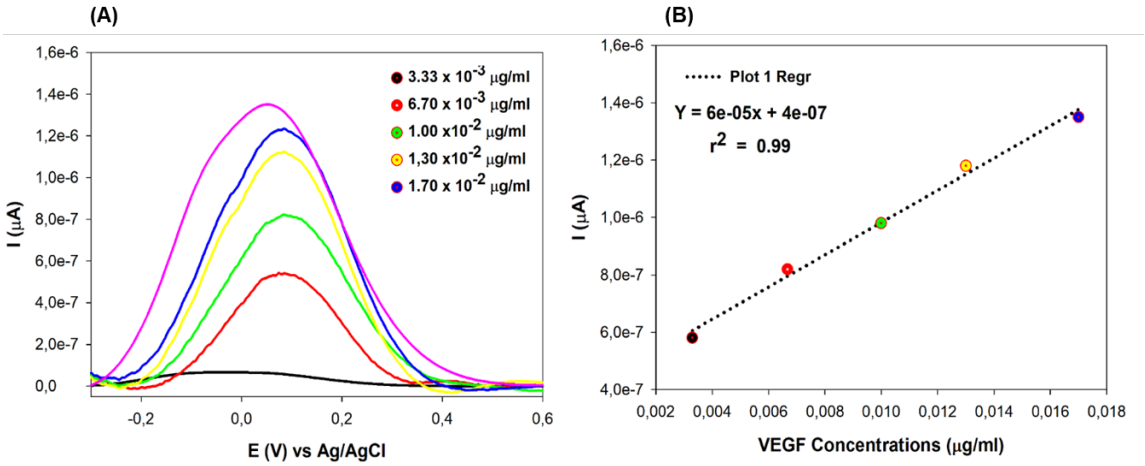

Figure 4.11: The DPV for the effect of variation of VEFG volumes from -1.5 to 1.5 V/s on a GCE in pH 7.4 PBS buffer.

It was observed that increasing the concentration of VEGF antibody resulted in increased peak currents at potential 0.10 V. The increasing concentrations of VEGF were studied in the range 3.30 x 10^{-3} – 1.70 x 10^{-2} µg/ml and the correlation in peak current was observed. The peak potential shows a negative shift compared to the peak potentials that are represented by CV, attributed to the sensitivity of DPV than CV (Chireke et al. 2019). This peak was used for the calibration curve, as seen in Figure 4.11 B. The linear range was obtained from 0.003 to 0.017 µg/ml. A detection limit (LOD) and limit of quantification (LOQ) were found to be

1.50 x 10^{-3} and 5 x 10^{-3}, respectively.

4.5.3. Stability of the biosensor

Figure 4.12 shows the curve obtained from the DPV profile carried out to evaluate stability of AgInS/ZnS-BSA core/shell.

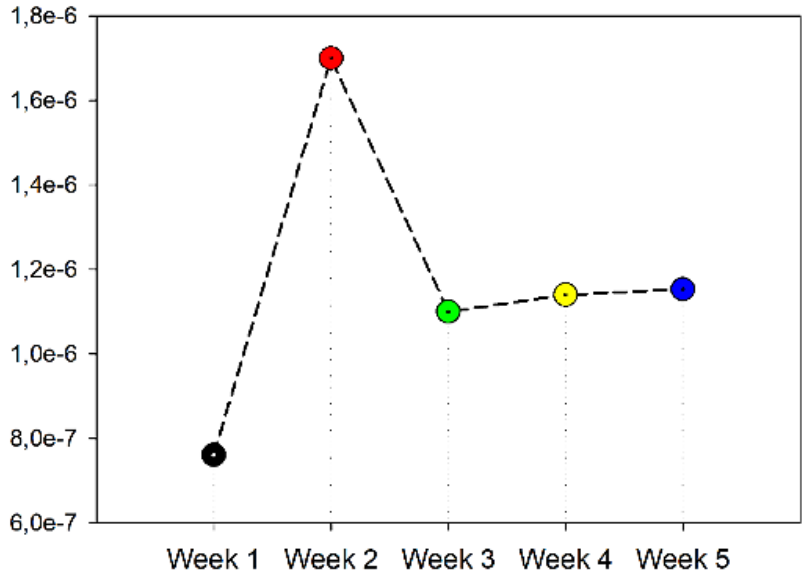

Figure 4.12: The stability of AgInS/ZnS-BSA core/shell QDs on a GCE for detection of VEGF in 0.1M PBS pH 7.4 buffer for five weeks.

The stability of the AgInS/ZnS- BSA core/shell QDs on a GCE surface was investigated by DPV using freshly 40 µl of VEGF in 0.1 M PBS buffer solution of pH 7.4 for five weeks as show in figure 4.12. As shown on the graph, an increase in peak current from week 1 to week 2 was observed, due to population of active sites on the AgInS/ZnS-BSA core/shell QD on the electrode. The decrease from week 2 to week 3 might be due to surface passivation. As from week 3 to 5, it levels off. This investigation portrayed good stability of AgInS/ZnS-BSA core/shell QDs.

4.6. Conclusion

This chapter reported on the development of an electrochemical biosensor using AgInS/ZnS-BSA bioconjugate for detection of VEGF biomarker. Electrochemical techniques such as CV, DPV and SWV were applied for the detection of VEGF. DPV results showed increased current and better resolution. The biosensor's linearity towards VEGF was from 0.003 to 0.017 µg/ml with LOD and LOQ of 1.5×10^{-3} and 5×10^{-3} respectively. The biosensor showed good stability of AgInS/ZnS-BSA bioconjugate for detection of VEGF for over five weeks. This showed potential for biological application.

4.7. References

Aydın, E.B. and Sezgintürk, M.K., 2017. A sensitive and disposable electrochemical immunosensor for detection of SOX2, a biomarker of cancer. Talanta, 172, pp.162-170.

Chikere, C.O., Faisal, N.H., Kong Thoo Lin, P. and Fernandez, C., 2019. The synergistic effect between graphene oxide nanocolloids and silicon dioxide nanoparticles for gallic acid sensing. Journal of solid-state electrochemistry, 23(6), pp.1795-1809.

Choi, W., Shin, H.C., Kim, J.M., Choi, J.Y. and Yoon, W.S., 2020. Modeling and applications of electrochemical impedance spectroscopy (EIS) for lithium-ion batteries. Journal of Electrochemical Science and Technology, 11(1), pp.1-13.

Hanrahan, G., Patil, D.G. and Wang, J., 2004. Electrochemical sensors for environmental monitoring: design, development and applications. Journal of environmental monitoring, 6(8), pp.657-664.

Hussain, G. and Silvester, D.S., 2018. Comparison of voltammetric techniques for ammonia sensing in ionic liquids. Electroanalysis, 30(1), pp.75-83.

Jackowska, K. and Krysinski, P., 2013. New trends in the electrochemical sensing of dopamine. Analytical and bioanalytical chemistry, 405(11), pp.3753-3771.

Nxele, S.R., Nkhahle, R. and Nyokong, T., 2021. The composites of asymmetric Co phthalocyanines-graphitic carbon nitride quantum dots-aptamer as specific electrochemical sensors for the detection of prostate specific antigen: Effects of ring substituents. Journal of Electroanalytical Chemistry, 900, p.115730.

Nxele, S.R., Nkhahle, R. and Nyokong, T., 2022. The synergistic effects of coupling Au nanoparticles with an alkynyl Co (II) phthalocyanine on the detection of prostate specific antigen. Talanta, 237, p.122948.

Okumu, F.O., Silwana, B. and Matoetoe, M.C., 2020. Application of MWCNT/Ag-Pt Nanocomposite Modified GCE for the Detection of Nevirapine in Pharmaceutical Formulation and Biological Samples. Electroanalysis, 32(12), pp.3000-3008.

Pinto, E.M., Soares, D.M. and Brett, C.M., 2008. Interaction of BSA protein with copper evaluated by electrochemical impedance spectroscopy and quartz crystal microbalance. Electrochimica Acta, 53(25), pp.7460-7466.

Qian, L., Durairaj, S., Prins, S. and Chen, A., 2021. Nanomaterial-based electrochemical sensors and biosensors for the detection of pharmaceutical compounds. Biosensors and Bioelectronics, 175, p.112836.

Rebelo, T.S., Ribeiro, J.A., Sales, M.G.F. and Pereira, C.M., 2021. Electrochemical immunosensor for detection of CA 15-3 biomarker in point-of-care. Sensing and Bio-Sensing Research, 33, p.100445.

Sankar, K.V., Selvan, R.K. and Meyrick, D., 2015. Electrochemical performances of CoFe 2 O 4 nanoparticles and a rGO based asymmetric supercapacitor. Rsc Advances, 5(121), pp.99959-99967.

Timakwe, S., Silwana, B. and Matoetoe, M.C., 2022. Electrochemistry as a Complementary Technique for Revealing the Influence of Reducing Agent Concentration on AgNPs. ACS omega, 7(6), pp.4921-4931.

van der Horst, C., Silwana, B., Iwuoha, E. and Somerset, V., 2017. Electrocatalytic evaluation of a horseradish peroxidase biosensor based on a novel Bi-Ag bimetallic nanocomposite. Procedia technology, 27, pp.179-182.

Zhu, C., Yang, G., Li, H., Du, D. and Lin, Y., 2015. Electrochemical sensors and biosensors based on nanomaterials and nanostructures. Analytical chemistry, 87(1), pp.230-249.

Chapter 5

Conclusion and recommendations

Conclusion

The research work described in this thesis focuses on the facile synthesis of GSH-capped AgInS core and AgInS/ZnS core/shell QDs. The AgInS core QDs was synthesized via the reflux, heat-up and mono-wave 50 synthesis methods. Broad emission PL peaks were observed for the synthetic methods with full-width half maximum (FWHM) of 112 nm for mono wave 50, while reflux and closed beaker heat-up methods exhibited FWHM of 105 nm and 96 nm, respectively. The open beaker method showed a reduction in fluorescence intensity with an increase in time and formed a precipitate. The reflux method was therefore selected as a synthetic method for the study because it gave the desired fluorescence optical properties with precise control over reaction parameters. Following the synthesis, the QDs were bio-conjugated with BSA. This showed enhanced optical properties and improvement in the quality of the QDs. The electrochemical properties of AgInS core QDs and AgInS/ZnS core/shell QDs were evaluated using CV and DPV. While electrochemical properties of AgInS-BSA core and AgInS/ZnS-BSA core/shell bioconjugates were evaluated using CV, DPV, SWV and EIS.

The sub-objective to synthesize core AgInS QDs and core/shell AgInS/ZnS QDs was executed successfully as discussed in chapter 4. Both the synthesis of AgInS/ZnS core/shell ternary QDs and factors affecting their synthesis are detailed. Furthermore, it was observed that various synthetic routes, with conjugation and encapsulation of QDs could produce less toxic materials used for biomedical applications. Detailed background on VEGF focuses on its detection methods and the importance of developing user-friendly, cost-effective and quick methods for detecting VEGF.

The other sub-objectives of optimization of the synthetic methods used for the QDs and the bio-conjugation of quantum dots to antibodies were discussed in Chapter 3. Evaluation of eco-friendly synthetic methods to produce ternary AgInS/ZnS core/shell QDs was

achieved through comparison of various synthesis methods and synthetic optimization of selected parameters such as time, ratio, capping and concentration. Best synthesized QDs optical properties gave optical properties of the AgInS core QDs after 45 min synthesis at pH 7.58, Ag: In molar ratio of 1:4, and GSH concentration of 0.145 mmol via reflux method. Successful passivation of AgInS core QDs by ZnS shell was confirmed by FTIR and resulted in a PLQY increase from 31.6 to 35.4% for AgInS core and AgInS/ZnS core/shell QDs, respectively. This further demonstrated improvement in the quality of material following the ZnS passivation. XRD and EDX also confirmed the passivation by ZnS shell. Conjugation of AgInS/ZnS QDs to BSA showed enhanced optical properties of the QDs. FTIR confirmed the conjugation via the formation of amide bonds. EDX and SEM results showed changes in particle size in the presence of BSA, demonstrating the interaction of BSA with AgInS/ZnS core/shell QDs.

Synthesized QDs were characterized using spectroscopy as described above as well as using various electroanalytical techniques. All the synthesized QDs were of electroactive as indicated in Chapter 4. It was revealed that the as-synthesized QDs exhibited chemical composition-dependent properties enabling the use of the materials in both electronic and bio-applications. The results also revealed that AgInS core and AgInS/ZnS core/shell QDs are adsorptions controlled with Ag^{+} showing a one-electron system. Studies of the electrochemical properties of AgInS-BSA and AgInS/ZnS-BSA bioconjugates showed enhanced peak currents suggesting higher conductivity and electrical properties. EIS confirmed improved charge transfer resistance for AgInS/ZnS-BSA core/shell bioconjugate.

An immunosensor for VEGF using GCE modified with AgInS/ZnS-BSA core/shell bioconjugates was fabricated and characterized using CV, DPV and SWV for its sensitivity. The developed VEGF biomarker sensor analytical applicability was assessed

through signal measurement of varying VEGF concentrations using DPV. A linear response, with good R^2 was obtained and used to determine the sensors analytical parameters. The method's linear range was 0.003 to 0.017 µg/ml. The LOD and LOQ were determined to be 1.5 x 10^{-3} µg/ml and 5 x 10^{-3} µg/ml, respectively. The developed immunosensor showed enhanced stability over a period of five weeks.

Recommendations

- Electrochemical sensors using real-life biological applications such as blood serum to detect VEGF would further confirm the success of the developed sensor.
- Analysis of the electrochemical sensor for detecting another disease would be great work.